



MISSOURI
S&T

CENTER FOR TRANSPORTATION INFRASTRUCTURE AND SAFETY



Recycled Concrete Aggregate: Field Implementation at the Stan Musial Veterans Memorial Bridge

by

Kamal H. Khayat, Ph.D., P.Eng.
Seyedhamed Sadati, Ph.D. Candidate

August 2014

**NUTC
R332**

**A National University Transportation Center
at Missouri University of Science and Technology**

Disclaimer

The contents of this report reflect the views of the author(s), who are responsible for the facts and the accuracy of information presented herein. This document is disseminated under the sponsorship of the Department of Transportation, University Transportation Centers Program and the Center for Transportation Infrastructure and Safety NUTC program at the Missouri University of Science and Technology, in the interest of information exchange. The U.S. Government and Center for Transportation Infrastructure and Safety assumes no liability for the contents or use thereof.

Technical Report Documentation Page

1. Report No. NUTC R332	2. Government Accession No.	3. Recipient's Catalog No.	
4. Title and Subtitle Recycled Concrete Aggregate: Field Implementation at the Stan Musial Veterans Memorial Bridge		5. Report Date August 2014	
		6. Performing Organization Code	
7. Author/s Kamal H. Khayat, Ph.D., P.Eng., Seyedhamed Sadati, Ph.D. Candidate		8. Performing Organization Report No. Project #00042239	
		10. Work Unit No. (TRAIS)	
9. Performing Organization Name and Address Center for Transportation Infrastructure and Safety/NUTC program Missouri University of Science and Technology 220 Engineering Research Lab Rolla, MO 65409		11. Contract or Grant No. DTRT06-G-0014	
		13. Type of Report and Period Covered Final	
12. Sponsoring Organization Name and Address U.S. Department of Transportation Research and Innovative Technology Administration 1200 New Jersey Avenue, SE Washington, DC 20590		14. Sponsoring Agency Code	
		15. Supplementary Notes	
16. Abstract The main objective of this research is to evaluate the feasibility of using RCA for concrete production in rigid pavement applications. The experimental program was undertaken to investigate the performance of different concrete made with different amounts of RCA, water-to-cementitious materials ratios (w/cm), and Class C fly ash contents to develop sustainable concrete designated for rigid pavement. The scope of work was implemented to achieve the objective of the research study is presented below: Task #1: The purpose of this task is to conduct a literature review of past experience and previous research on RCA. RCA properties as well as the behavior of concrete containing RCA, including the fresh and hardened properties (e.g., workability, compressive strength, flexural strength, shrinkage), and durability (e.g., freeze-thaw resistance, permeability, scaling). Specifically, the literature review focuses on studies that investigated performance of rigid pavement made with partial or full replacement of RCA. Task #2: The purpose of this task is to optimize concrete mixtures incorporating various levels of RCA. Various amounts of coarse and fine RCA were used as replacements of virgin aggregate. Alternative mixing procedures are used to develop concrete with RCA. Task #3: The performance of the optimized concrete mixtures is evaluated in terms of: fresh properties: slump, air content, and bleeding; mechanical properties: compressive strength, splitting tensile strength, flexural strength, modulus of elasticity, and shrinkage; as well as durability: permeable void volume, absorption, surface electrical resistivity, bulk electrical resistivity, freeze/thaw durability, and de-icing salt scaling. Task #4: The proven RCA-made concrete mixtures are then employed into the construction of pavement sections of the approach towards the Stan Musial Veterans Memorial Bridge in St. Louis, Missouri. Fresh properties of the concrete mixtures are investigated at the job site. In addition, samples are taken to further evaluation of mechanical properties and durability of the employed mixtures. Field instrumentation is carried out to monitor the long-term deformation characteristics of the pavement sections. Detailed information about the field implementation is presented in Chapter 5 of this report. Pavement structure is described in detail in Chapter 6. Task #5: Truck load testing is carried out to evaluate the in-situ performance of the pavement sections. Various loading scenarios are considered to monitor the deformation characteristics of the instrumented sections under controlled traffic loading.			
17. Key Words Recycled concrete aggregate, field performance, durability, sustainability, pavement construction		18. Distribution Statement No restrictions. This document is available to the public through the National Technical Information Service, Springfield, Virginia 22161.	
19. Security Classification (of this report) unclassified	20. Security Classification (of this page) unclassified	21. No. Of Pages 180	22. Price



Missouri University of Science and Technology

Final Report

August 2014

Recycled Concrete Aggregate

Field Implementation at the Stan Musial Veterans Memorial Bridge project

Prepared by:

Kamal H. Khayat, Ph.D., P.Eng.

Syedhamed Sadati, Ph.D. Candidate

Table of Contents

Table of Contents	i
List of Figures	v
List of Tables	ix
Executive summary	xi
Acknowledgement	xiv
1. Introduction	1
1.1. Background	1
1.2. Objective	2
1.3. Outline of report	3
2. Literature review on recycled concrete aggregate	5
2.1. General	5
2.2. Use of recycled concrete aggregate in concrete production	6
2.2.1. Background	6
2.2.2. Engineering properties of RCA	9
2.3. Properties of concrete made with RCA	11
2.3.1. Fresh properties	14
2.3.2. Mechanical properties	14
Compressive strength.	14
Splitting tensile strength.	15
Flexural strength.	15
Modulus of elasticity.	16
Shrinkage.	16
2.3.3. Durability	17
Chloride ion permeability.	17
Freeze/thaw resistance.	17
De-icing salt scaling.	18
Carbonation depth.	18
Absorption.	18
2.4. Use of RCA in rigid pavement construction	18

2.5.	Concluding remarks	20
3.	Experimental program	22
3.1.	Material properties	22
3.2.	Mixture proportions.....	26
3.2.1.	Conventionally proportioned mixtures	26
3.2.2.	Two stage mixing approach	27
3.2.3.	Equivalent mortar volume mixture proportioning method	27
3.3.	Experimental program.....	34
3.4.	Sampling and testing	38
4.	Results and discussion	39
4.1.	Step one, initial investigations	39
4.1.1.	General.....	39
4.1.2.	Compressive strength.....	40
4.1.3.	Splitting tensile strength	41
4.1.4.	Drying shrinkage.....	42
4.1.5.	Permeable void volume.....	46
4.2.	Mechanical properties and durability of selected mixtures.....	47
4.2.1.	General.....	47
4.2.2.	Fresh properties.....	49
4.2.3.	Mechanical properties.....	49
	Compressive strength.	49
	Splitting tensile strength.	51
	Flexural strength.	52
	Modulus of elasticity.	54
4.2.4.	DURABILITY	56
	Surface electrical resistivity.....	57
	Bulk electrical resistivity.....	61
	Permeable void volume.	63
	Freeze and thaw resistance.	63
	De-icing salt scaling.	65
4.3.	Summary and conclusion	70

5.	Field implementation.....	72
5.1.	Project overview and objectives.....	72
5.2.	Concrete mixture and material properties.....	73
5.3.	Experimental program of the field evaluation.....	74
5.3.1.	Fresh properties.....	74
	Batching plant sampling.....	74
	Work at the job site.....	78
5.3.2.	Sampling for laboratory investigation.....	79
	Compressive strength.....	81
	Splitting tensile strength.....	83
	Flexural strength.....	84
	Drying shrinkage.....	86
	Modulus of elasticity.....	87
	Chloride-ion permeability.....	90
	Permeable void volume.....	91
	Freeze/thaw resistance.....	93
	Coefficient of thermal expansion.....	94
5.3.3.	Core sampling.....	95
5.3.4.	Field instrumentation and monitoring of deformation.....	99
	Data acquisition systems.....	100
	Sensor placement.....	101
	Iso-thermal deformation.....	103
	Pavement deformation behavior.....	106
	Deformation analysis.....	108
6.	Truck loading testing.....	129
6.1.	Introduction.....	129
6.2.	Pavement structure.....	129
6.3.	Re-examing the sensor locations.....	129
6.4.	Data acquisition.....	131
6.5.	Truck and loading configuration.....	133
6.6.	Results and discussion.....	135

6.6.1.	General observations.....	135
6.6.2.	Peak deformation	136
6.6.3.	Verification of peak deformation.....	138
6.6.4.	Statistical data analysis	142
	Effect of concrete mixture and axle type on deformation.	143
	Effect of speed on deformation.	144
6.7.	Conclusion.....	146
7.	Summary and Conclusion.....	148
	References.....	151

List of Figures

Figure 2-1. States recycling concrete as aggregate (FHWA 2004)	8
Figure 2-2. States recycling concrete as aggregate base (FHWA 2004)	9
Figure 2-3. States recycling concrete as aggregate for new concrete production (FHWA 2004) ..	9
Figure 2-4. Scanning electron microscope (SEM) of old ITZ in RCA particle (Xiao et al., 2012)	10
Figure 3-1. RCA particles before separating the mortar (left) and after separating the residual mortar (right).....	24
Figure 3-2. Particle size distribution of the fine aggregate.....	25
Figure 3-3. Particle size distribution of the coarse aggregate.....	26
Figure 3-4. Individual percentages retained on each sieve.....	26
Figure 4-1. Photo of length measurement for drying shrinkage.....	43
Figure 4-2. Variation of drying shrinkage with respect to time for mixtures made with w/cm of 0.37.....	44
Figure 4-3. Variation of drying shrinkage with respect to time for mixtures made with w/cm of 0.40 and 0.42.....	45
Figure 4-4. Variation of drying shrinkage with respect to time for mixtures made with the two- stage mixing approach and the equivalent mortar volume methods.....	46
Figure 4-5. Compressive strength results.....	50
Figure 4-6. Splitting tensile strength results	52
Figure 4-7. Simply supported beam for determining the flexural strength (ASTM C78)	53
Figure 4-8. Flexural strength results	54
Figure 4-9. Modulus of elasticity test setup.....	55
Figure 4-10. Modulus of elasticity results	56
Figure 4-11. Schematic view of the surface resistivity measurement principles (Proseq SA 2013)	58
Figure 4-12. Surface resistivity measurement	59
Figure 4-13. Surface resistivity results	60
Figure 4-14. Measuring bulk electrical resistivity	62
Figure 4-15. Freezing and thawing cabinet (left); measurement of pulse velocity (right).....	64
Figure 4-16. Variation of durability factor as a function of freeze/thaw cycles.....	64
Figure 4-17. Rating scale for scaling resistance	68
Figure 4-18. Appearance of the top surfaces after 50 cycles of deicing salt scling test	69
Figure 5-1. General view of the ramp approach with the reference section already in place.....	73
Figure 5-2. Photos of fresh property tests at the batching plant	76
Figure 5-3. Variation in slump during the simulated transport period at the concrete batching plant.....	77
Figure 5-4. Variation in air content during the simulated transport period at the concrete batching plant.....	77

Figure 5-5. Photos of fresh property testing at job site.....	79
Figure 5-6. Sampling at the job site.....	81
Figure 5-7. Variation of compressive strength with respect to time.....	82
Figure 5-8. Splitting tensile strength results.....	84
Figure 5-9. Flexural strength results.....	86
Figure 5-10. Variation of drying shrinkage with time.....	87
Figure 5-11. Comparison of the MOE results at 28 days.....	88
Figure 5-12. Comparison of the MOE results at 56 days.....	89
Figure 5-13. Rapid chloride-ion permeability results (Coulomb).....	90
Figure 5-14. Correlation between the RCPT and the permeable void volume results.....	92
Figure 5-15. Variations in durability factor – Procedure A.....	94
Figure 5-16. Photos of core sampling at the job site (left) and grinding the test surface of the specimens (right).....	96
Figure 5-17 Cracks detected within the residual mortar attached to the RCA particles.....	98
Figure 5-18. SEM image for the crack propagation trough the old ITZ in RCA particles.....	98
Figure 5-19. SEM image of the interface between the virgin aggregate and surrounding new mortar.....	99
Figure 5-20. Vibrating wire strain gauge used to monitor temperature and strain in pavement ..	99
Figure 5-21. Solar powered data acquisition system and monthly data collection.....	100
Figure 5-22. Photos of placing the instrumentation and the data loggers at the job site.....	101
Figure 5-23. Schematic of instrumentation plan.....	102
Figure 5-24. Total deformation and iso-thermal concrete deformation measured by A1 VWSG at 5-minute intervals (A1 sensor located at top surface of the pavement at the wheel path parallel to traffic).....	104
Figure 5-25. Deformation analyzer software interface.....	105
Figure 5-26. Warping mechanism by temperature gradient (Huang 2004).....	107
Figure 5-27. Curling caused by moisture gradient (Huang 2004).....	107
Figure 5-28. Iso-thermal strain of different mixtures at A1 location (top surface at wheel path parallel to traffic).....	108
Figure 5-29. Iso-thermal strain of different mixtures at A2 location (mid-height at wheel path parallel to traffic).....	110
Figure 5-30. Iso-thermal strain measured at A3 for different mixtures (mid-height at wheel path perpendicular to traffic).....	111
Figure 5-31. Iso-thermal strain at A4 for different mixtures (bottom part of pavement at wheel path parallel to traffic).....	112
Figure 5-32. Iso-thermal strain at B1 for different mixtures (top surface of pavement at wheel path parallel to traffic).....	112
Figure 5-33. Iso-thermal strain at B2 for different mixtures (bottom pavement at wheel path parallel to traffic).....	113

Figure 5-34. Iso-thermal strain at C1 for different mixtures (top surface of pavement at center line parallel to traffic)	114
Figure 5-35. Iso-thermal strain at C2 for different mixtures (bottom part of pavement at center line parallel to traffic)	114
Figure 5-36. Iso-thermal strain measured by the VWSG at different depths at location A for the Reference mixture	115
Figure 5-37. Iso-thermal strain measured by the VWSG at different depths at location A for the 30% RCA mixture	116
Figure 5-38. Iso-thermal strain measured by the VWSG at different depths at location A for the 30% RCA-TSMA mixture	116
Figure 5-39. Iso-thermal strain measured by the VWSG at different depths at location A for the 40% RCA mixture	117
Figure 5-40. Iso-thermal strain measured by the VWSG at B1 and B2 locations for the Reference mixture	118
Figure 5-41. Iso-thermal strain measured by the VWSG at C1 and C2 locations for the Reference mixture	118
Figure 5-42. Iso-thermal strain measured by the VWSG at C1 and C2 locations for the 30% RCA mixture	119
Figure 5-43. 40 Iso-thermal strain measured by the VWSG at B1 and B2 locations for the 30% RCA-TSMA mixture	119
Figure 5-44. Iso-thermal strain measured by the VWSG at C1 and C2 locations for the 30% RCA-TSMA mixture	120
Figure 5-45. Iso-thermal strain measured by the VWSG at B1 and B2 locations for the 40% RCA mixture	120
Figure 5-46. Iso-thermal strain measured by the VWSG at C1 and C2 locations for the 40% mixture	121
Figure 5-47. Iso-thermal strain of the Reference mixture near the top of the pavement (A1, B1, and C1)	122
Figure 5-48. Iso-thermal strain of the 30% RCA mixture near the top of the pavement (A1 and C1)	122
Figure 5-49. Iso-thermal strain of the 30% RCA-TSMA mixture near the top of the pavement (A1, B1, and C1)	123
Figure 5-50. Iso-thermal strain of the 40% RCA mixture measured near the top of the pavement (A1, B1, and C1 sensors)	123
Figure 5-51. Iso-thermal strain measured at bottom part of pavement (A4, B2, and C2) for the Reference mixture	124
Figure 5-52. Iso-thermal strain measured at bottom part of pavement (A4 and C2) for the 30% RCA mixture	124
Figure 5-53. Iso-thermal strain measured at bottom part of pavement (A4, B2, and C2) for the 30% RCA-TSMA mixture	125

Figure 5-54. Iso-thermal strain near the bottom of the pavement (A4, B2, and C2) for the 40% RCA mixture.....	125
Figure 6-1. Photos of the location of the sensors.....	130
Figure 6-2. Deep metal scanner used for detecting sensor baskets (left) and simultaneous monitoring deformation to ensure exact location of sensors (right).....	131
Figure 6-3. Time history deformation obtained during the first truck loading test campaign....	132
Figure 6-4. Data logger used for the second truck loading test (Campbell Scientific Co. 2014)	133
Figure 6-5. Schematic of truck load configuration, dimensions in in.....	134
Figure 6-6. Sample deformations registered at top and bottom of the pavement due to slow moving truck.....	135
Figure 6-7. Variations in stress direction during the truck movement – bottom part of pavement.....	136
Figure 6-8. Comparisons of measured deformation to strain values estimated using Equation 6-1.....	139
Figure 6-9. Total deformation registered at the bottom part of the reference concrete at wheel path.....	140
Figure 6-10. Maximum strain recorded during static loading.....	140
Figure 6-11. Maximum strain recorded during the low speed loading.....	141
Figure 6-12. Average tensile strains recorded during the loading with different speeds.....	141

List of Tables

Table 2-1. Typical physical properties of RCA (FHWA 2008).....	11
Table 2-2. RCA acceptance criteria in different countries (McNeil and Kang, 2013)	12
Table 2-3. Influence of RCA on properties of concrete (NCHRP 2013).....	13
Table 3-1. Physical properties and chemical compositions of cement	22
Table 3-2. Chemical compositions of fly ash (Wolfe 2011).....	23
Table 3-3. Physical properties of the aggregates	25
Table 3-4. Test matrix used for the first step of the laboratory investigations	36
Table 3-5. Mixture proportions of concrete mixtures used in the study.....	37
Table 3-6. Test methods and standard used in the study	38
Table 4-1. Fresh properties of mixtures used for initial stage of characterizing.....	39
Table 4-2. Compressive strength results at different ages (psi).....	40
Table 4-3. Splitting tensile strength results at different ages (psi)	42
Table 4-4. Volume of permeable void at different ages (%)	48
Table 4-5. Slump, air content, and unit weight of concrete mixtures	49
Table 4-6. Compressive strength results (psi).....	50
Table 4-7. Splitting tensile strength results (psi).....	51
Table 4-8. Flexural strength results (psi).....	53
Table 4-9. Modulus of elasticity results (ksi).....	55
Table 4-10. Slump, air content, unit weight, and bleeding of fresh concrete	57
Table 4-11. Correlation between the surface resistivity and chloride ion permeability	59
Table 4-12. Surface electrical resistivity measurements (k Ω cm).....	60
Table 4-13. Bulk electrical resistivity (k Ω cm)	62
Table 4-14. Permeable void volume (%)	63
Table 4-15. Variations in durability factor of specimens after 300 cycles	65
Table 4-16. De-icing salt scaling rating of investigated mixtures	67
Table 5-1. Mixture proportions of concrete used in field study	74
Table 5-2. Fresh properties of concrete mixtures at the batching plant	75
Table 5-3. Fresh properties of mixtures sampled at the job site	78
Table 5-4. Sampling and testing program performed on the job site.....	80
Table 5-5. Compressive strength results (psi), 4 \times 8 cylinders, MoDOT lab.....	81
Table 5-6. Splitting tensile strength results, 6 \times 12 cylinders, MoDOT lab	83
Table 5-7. Flexural strength results (psi)	85
Table 5-8. MOE results, 4 \times 8 in. cylinders.....	87
Table 5-9. MOE and Poison’s ratio results, 6 \times 12 in. cylinders	88
Table 5-10. Rapid chloride-ion permeability results	90
Table 5-11. Density, absorption, and permeable void volume results at 91 days.....	91
Table 5-12. Durability factors after finishing the freeze/thaw testing (%) -ASTM C666.....	94
Table 5-13. Coefficient of thermal expansion results- MoDOT lab.....	95

Table 5-14. Properties of the core samples	96
Table 5-15. Comparing back-calculated CTE with laboratory measurements	105
Table 6-1. Axle weights and pressure at tire-pavement contact area (driver side).....	134
Table 6-2. Peak deformation registered through Static loading ($\mu\text{m/m}$)	137
Table 6-3. Peak deformation registered for slow moving load ($\mu\text{m/m}$)	137
Table 6-4. Peak deformation registered for high speed moving load ($\mu\text{m/m}$).....	138
Table 6-5. Three-way ANOVA results at 0.05 significance level	143
Table 6-6. Contrast results at 0.05 significance level	144
Table 6-7. Second set of three-way ANOVA results at 0.05 significance level.....	145
Table 6-8. Grouping the means of speed levels	145

Executive summary

The aim of research presented in this report was to evaluate the fresh and hardened properties, durability, and in-situ performance of concrete containing recycled concrete aggregate (RCA) that was used in experimental pavement construction carried out in 2013 by the Missouri department of Transportation (MoDOT).

The project involved the field evaluation of special concrete made using RCA in pavement construction as a part of the Stan Musial Veterans Memorial Bridge, Inaugurated in Feb, 2014. Variety of samples were taken to investigate the mechanical properties and durability of concrete employed at the job site. Instrumentation was embedded in pavement sections to monitor the long-term deformation of different concrete mixtures incorporated in the filed study. Truck load testing was conducted to evaluate deformation characteristics of RCA concrete compared to that of the Reference concrete mixture made without any RCA. Core samples were extracted to evaluate the in-situ properties of concrete.

In addition, laboratory research was conducted to investigate the performance of concrete mixtures made with different amounts of fine RCA varying from 0 to 20%, different fly ash contents ranging from 25% to 40%, and different water-to-cementitious materials ratio of 0.37 to 0.42.

Based on the data presented in the report the following conclusions were warranted:

- Using up to 40% coarse RCA in pavement application will not lead to significant decrease in performance of the mixtures. It can be stated that the RCA mixtures develop comparable performance to the Reference concrete made with the virgin aggregate in terms of mechanical properties, drying shrinkage, abrasion resistance, and durability. All the mixtures

met the minimum compressive strength requirement of 4000 psi at 28 days. No significant difference was observed in the case of the splitting tensile strength and flexural strength of concrete made with up to 40% RCA compared to the Reference concrete made without any RCA. An average of 8% and 12% decrease in modulus of elasticity was observed in the case of 30% RCA and 40% RCA mixtures, respectively.

- No significant difference in 91-day rapid chloride-ion permeability was observed. A slight increase of 240 and 330 Coulomb was registered for the 30% and 40% RCA mixtures, respectively. All mixtures exhibited good frost durability with durability factors in range of $90 \pm 3\%$ for both the ASTM C666, A and B procedures. 5% increase in coefficient of thermal expansion was observed in 11-month old 40% RCA concrete specimens.
- Core samples were taken to evaluate the in-situ properties of concrete mixtures. All mixtures had acceptable mechanical properties, in line with laboratory results. Abrasion resistance of concrete mixtures was evaluated using the core samples. All mixtures had similar performance, with no spread due to the use of RCA.
- Scanning electron microscope analysis was conducted to investigate the micro-structural properties of RCA concrete. Higher concentration of micro-cracks was observed in the case of RCA mixtures, which may be attributed to the crushing process during RCA production.
- All mixtures exhibited low iso-thermal deformation values varying from 50 to $-150 \mu\epsilon$ after more than one year. It was observed that pavement deformation pattern is changing through the year and is sensitive to variation in environmental conditions. Slightly higher seasonal effects are observed in the case of the RCA mixtures. Sensors located at the top part of the pavement sections are shown to be more sensitive to environmental effects.

- Increase in deformation due to traffic loading was observed in the case of the RCA mixtures. Magnitude of such deformation, however, was much lower than those caused by the shrinkage and environmental effects.
- Decrease in deformation was observed as a result of an increase in truck loading speed. Tandem axle was also shown to produce higher deformation compared to the single axle of the truck. Maximum deformation values were observed in the case of the static loading.

Acknowledgement

The work in this report was supported by the National university Transportation center (NUTC) at Missouri University of Science and Technology, project number R332 and in-kind contribution provided by the Missouri Department of Transportation (MoDOT). The authors also take this opportunity to express a deep sense of gratitude to Mr. William Stone, Mrs. Jennifer Harper, and Mr. Brett Trautman from MoDOT for their cordial support, and constant encouragement and monitoring throughout this project. The authors would like to thank to Mr. Hyatt Bangert from Millestone Bangert Co. for assistance in the field implementation. Support provided by the research team at Center for Infrastructure Engineering Studies (CIES) at Missouri University of Science and Technology (Missouri S&T) is highly appreciated. Special thanks to Dr. Soo-duck Hwang for contribution and technical support. The authors are also grateful to Dr. Nicolas Libre for his assistance in analyzing the filed data. Valuable technical support provided by the technical staff at CIES and Civil and Environmental Engineering Department at Missouri S&T, Mr. Jason Cox, Mr. John Bullock, Mr. Brian Smith, and Mr. Gary Abbott is highly appreciated. The cooperation and support from Abigayle Sherman, Gayle Spitzmiller, and Cheryl Geisler staff members of CIES is greatly acknowledged.

1. Introduction

1.1. Background

Sustainable solutions for the concrete industry should couple the durability of the material, the environmental impact on the structure, and the cost of the project (Kim 2013). Due to the increasing rate of demolition, it is essential to effectively reuse demolition waste to conserve the nonrenewable natural resources. Decrease in natural resources, increasing problems in waste management, ecological hazards, landfill limitations, and increase in distance between natural resources and consumption markets, support the idea of using recycled wastes for new concrete production (Padmini et al., 2009). Besides, the reduction in the carbon footprint of the most commonly used construction material, concrete, is a key factor to decrease the total greenhouse gas emissions produced by the construction industry (McIntyre 2009).

The use of recycled concrete aggregate (RCA) to preserve natural resources and decrease the amount of disposals in landfills has been growing in the recent years. Given the variable characteristics of recycled concrete aggregates while compared to the virgin aggregate sources, there still exists a conservative approach that limits the use of RCA in field implementations (Surya 2013). Therefore, RCA is mostly being used in granular bases, embankments, sound barriers, fills, etc. (Kim 2013, Gabr 2012).

Due to the economic and environmental merits of recycled materials, research has been undertaken to investigate the effect of RCA on the properties of concrete designated for pavement applications at Missouri University of Science and Technology in collaboration with the National University Transportation Center (NUTC) and the Missouri Department of Transportation (MoDOT). The project involves mix design, field implementation, structural health monitoring of pavement

performance, and in-situ loading of the instrumented pavement sections. The output of the project can endorse the development of guidelines for design of RCA concrete for future implementation of this technology in rigid pavement applications.

1.2. Objective

The main objective of this research is to evaluate the feasibility of using RCA for concrete production in rigid pavement applications. The experimental program was undertaken to investigate the performance of different concrete made with different amounts of RCA, water-to-cementitious materials ratios (w/cm), and Class C fly ash contents to develop sustainable concrete designated for rigid pavement.

The scope of work was implemented to achieve the objective of the research study is presented below:

Task #1: The purpose of this task is to conduct a literature review of past experience and previous research on RCA. RCA properties as well as the behavior of concrete containing RCA, including the fresh and hardened properties (e.g., workability, compressive strength, flexural strength, shrinkage), and durability (e.g., freeze-thaw resistance, permeability, scaling).

Specifically, the literature review focuses on studies that investigated performance of rigid pavement made with partial or full replacement of RCA.

Task #2: The purpose of this task is to optimize concrete mixtures incorporating various levels of RCA. Various amounts of coarse and fine RCA were used as replacements of virgin aggregate. Alternative mixing procedures are used to develop concrete with RCA.

Task #3: The performance of the optimized concrete mixtures is evaluated in terms of: fresh properties: slump, air content, and bleeding; mechanical properties: compressive strength, splitting tensile strength, flexural strength, modulus of elasticity, and shrinkage; as well as durability: permeable void volume, absorption, surface electrical resistivity, bulk electrical resistivity, freeze/thaw durability, and de-icing salt scaling.

Task #4: The proven RCA-made concrete mixtures are then employed into the construction of pavement sections of the approach towards the Stan Musial Veterans Memorial Bridge in St. Louis, Missouri. Fresh properties of the concrete mixtures are investigated at the job site. In addition, samples are taken to further evaluation of mechanical properties and durability of the employed mixtures. Field instrumentation is carried out to monitor the long-term deformation characteristics of the pavement sections. Detailed information about the field implementation is presented in Chapter 5 of this report. Pavement structure is described in detail in Chapter 6.

Task #5: Truck load testing is carried out to evaluate the in-situ performance of the pavement sections. Various loading scenarios are considered to monitor the deformation characteristics of the instrumented sections under controlled traffic loading.

1.3. Outline of report

This report includes seven chapters. This section outlines the information that are presented in more detail throughout this report.

Chapter 1 provides an introduction to the report and offers a brief background of recycled aggregate and experiences on performance of concrete made with RCA. It also discusses the research objective, scope of work, and research plan.

Chapter 2 presents a brief summary of existing literature on RCA, properties of RCA-made concrete, and its application as rigid pavement material.

Chapter 3 details the experimental program and introduces the properties of the constituent materials and the concrete mix design methods used in this research.

Chapter 4 presents the performance of investigated concrete evaluated and different analyses on the fresh properties, mechanical performance, and durability of the laboratory produced specimens.

Chapter 5 presents detailed information obtained from the field implementation of the RCA concrete at Stan Musial Veterans Memorial Bridge in St. Louis, Missouri. Data obtained from the evaluation of concrete sampled on the job site are presented as well as the results of in-situ evaluation.

Chapter 6 presents the results of dynamic loading test undertaken on the instrumented pavement sections.

Chapter 7 provides a summary and conclusion from this study.

2. Literature review on recycled concrete aggregate

2.1. General

Based on the definition provided by the United Nations, sustainable development is development that meets the needs of the present without compromising the ability of future generations to meet their own needs (United Nations General Assembly 1987). The pavement industry is one of the fields where hard work is devoted to develop a focused meaning of sustainability in terms of design, materials, construction, and maintenance (Garber et al. 2011). Interest for environmentally friendly concrete in pavement has grown in recent years. Candidate technologies to improve the sustainability of pavement concrete include the use of supplementary cementitious materials (SCMs) to partially replace Portland cement, the incorporation of recycled materials in concrete production, and in particular recycled concrete aggregate (RCA), as well as the design of materials with greater durability to increase service life. Considering the fact that fine and coarse aggregate occupy about 30% and 40% of the total concrete volume in rigid pavement, respectively, the partial replacement of recycled aggregate can be employed to reduce the need to use natural resources. This sustainable practice assists in saving large areas of landfill space and provides potential savings to suppliers and contractors. This supports the idea of using recycled aggregates sources including concrete with RCA.

With the introduction of waste legislation in the form of regulations and directives in many places, a significant movement towards the sustainable management of construction and demolition (C&D) waste is becoming a legal requirement. In response, different sectors of the construction industry are undertaking various initiatives to minimize waste generation and

improve the management of C&D waste to maximize economic and environmental benefits, generally by placing emphasis on increasing recycling for reuse (Limbachiya et al., 2007).

The building industry in particular is a major consumer of materials and at the same time a major producer of waste (Padmini et al., 2009). According to Abbas et al. (2009), concrete accounts for up to 67% of construction and demolition waste, by mass. The amount of demolition waste dumped at landfill sites in the United Kingdom is said to be in excess of 20 million tons per year. The bulk of this material is concrete (50% to 55%) and masonry (30% to 40%) with only small percentages of other materials, such as metals, glass, and timber (Tam et al., 2007). In the Netherlands, about 14 million tons of building and demolishing waste per year are produced, in which about 8 million tons are recycled, mainly for unbound road base courses (Tam et al., 2007). It is also estimated that approximately 200 million tons of waste concrete are currently produced annually in the mainland of China (Xiao et al., 2012). Due to the increasing rate of demolition, it is essential to effectively reuse demolition waste and conserve nonrenewable natural resources.

This chapter presents a brief review of concrete properties made with RCA used in rigid pavement applications. A summary of existing experiences on the performance of rigid pavement made with RCA is also presented.

2.2. Use of recycled concrete aggregate in concrete production

2.2.1. Background

RCA can be obtained by crushing Portland cement concrete from various sources, including pavements and buildings. However, the Federal Highway Administration (FHWA 2004), limits the definition of RCA to processed concrete by-products obtained from old Portland cement

concrete pavements, bridge structures/decks, sidewalks, curbs, and gutters in which steel is removed from the old concrete. Based on the definition provided by the FHWA, (2004), RCA is a granular material manufactured by removing, crushing, and processing hydraulic-cement concrete pavement for reuse with a hydraulic cementing medium to produce fresh paving concrete. The aggregate retained on the #4 sieve is called coarse aggregate and the material passing the #4 sieve is called fine aggregate.

The main idea supporting such definition is to provide RCA from high quality state approved old concrete (NCHRP 2013). The state projects historically use high-quality aggregate sources with consistent quality accepted by the state agencies. RCA produced from processing state approved high-quality and durable old concrete may be useful in producing concrete for other state applications. On the other hand, the RCA obtained from construction and demolition waste may be useful in base and/or fill applications as it might be more prone to contaminations including bricks, wood, ceramics, and glass, etc.

The Construction Material Recycling Association (2009) indicates that RCA can be used to:

- Provide high-quality material in some highway applications
- Provide aggregate acceptable by ASTM and AASHTO standards
- Produce concrete and asphalt products
- Provide improved base and subbase materials
- Reduce haul and material costs
- Reduce landfill waste streams
- Minimize environmental impacts.

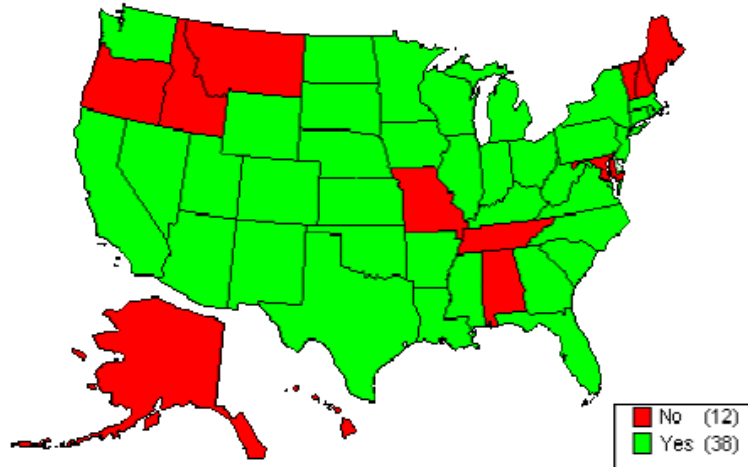


Figure 2-2. States recycling concrete as aggregate base (FHWA 2004)

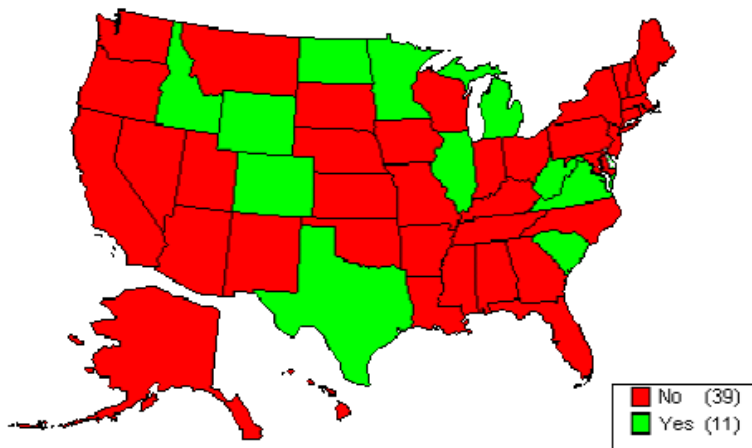


Figure 2-3. States recycling concrete as aggregate for new concrete production (FHWA 2004)

2.2.2. Engineering properties of RCA

RCA is typically regarded as a double phase material which consists of the original virgin aggregate and the adhered residual mortar. The RCA-made concrete will have more constituents: the new mortar and the new virgin coarse aggregates. Thus, there are two types of interfacial transition zones (ITZs) in RCA-made concrete mixtures: one, the old ITZ between the original virgin coarse aggregate and the adhered mortar and the one between the new mortar and the RCA. (Figure 2-4)

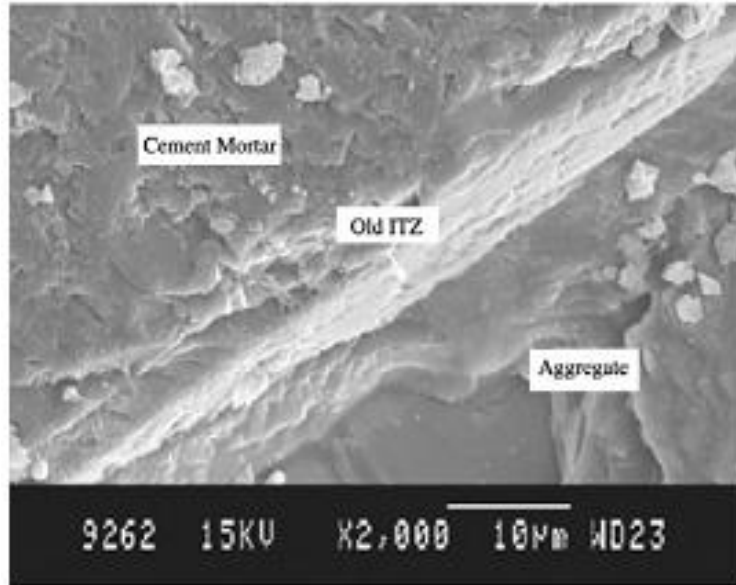


Figure 2-4. Scanning electron microscope (SEM) of old ITZ in RCA particle (Xiao et al., 2012)

As a result of high amounts of adhered mortar content in recycled aggregates, RCA can have higher water absorption, lower specific gravity, and higher porosity compared to natural aggregate (Kou et al. 2012). Both fine and coarse RCA particles are believed to have rough surface texture compared to virgin aggregate due to the crushing process. Some technical problems, including weak ITZ between cement paste and aggregate, porosity and traverse cracks within demolition concrete, high level of sulphate and chloride contents, impurity, and high variations in quality, render the use of RCA more challenging. Table 2-1 provides a breakdown of the typical properties of RCA provided by FHWA (2008).

It is usually believed that adhered mortar is the main cause of the lower properties of RCA compared to virgin aggregates. For a clear understanding of the recycled aggregate and to predict its possible effects on concrete, the constituents of these composite particles must be identified separately (Nagataki et al., 2000).

Table 2-1. Typical physical properties of RCA (FHWA 2008)

Property	Fine RCA	Coarse RCA
Specific gravity	2.0 to 2.3	2.2 to 2.5
Absorption	4% to 8%	2% to 6%
Loss Angeles abrasion loss		20 to 45
California bearing ratio (CBR)	94% to 148%	

It has also been suggested that the quality of RCA increases with a decrease in residual mortar content attached to the virgin aggregate particles. Adjustments to crushing methods used for RCA production can help minimizing the mortar content. However, too much crushing might compromise the integrity of the original aggregate and may not be cost effective (Garber et al., 2011).

Unit weight and water absorption are usually used as criteria for selecting RCA for different applications. A summary of acceptance criteria for RCA used in different countries is presented in Table 2-2 provided by (McNeil and Kang, 2013)

2.3. Properties of concrete made with RCA

In general, the quality of RCA-made concrete is tied to the properties of the original waste concrete, the new composition, the mixing approach, and the deterioration conditions of the recycled aggregates. Initial investigations on the use of recycled aggregate usually focused on incorporating recycled aggregate and its influence on mechanical and durability properties of the RAC. It was an adopted concept that although the use of recycled aggregate may be viable, a decrease in the performance of the RAC should be regarded as a normal outcome which can be

mitigated through various approaches such as increasing cement content in mixture etc. (Bagragi et al., 1990).

Table 2-2. RCA acceptance criteria in different countries (McNeil and Kang, 2013)

Country or standard	Recycled aggregate type	Oven-dry density criterion (kg/m ³)	Absorption criterion (%)
Australia (AS1141.6.2) (AS1996)	Class 1A	≥ 2100	≤ 6
	Class 1B	≥ 1800	≤ 8
Germany (DIN 4226-100) (DIN 2006)	Type 1	≥ 2000	≤ 10
	Type 2	≥ 2000	≤ 15
	Type 3	≥ 1800	≤ 20
	Type 4	≥ 1500	No limit
Hong Kong (Works Bureau of Hong Kong 2002)	-	≥ 2000	≤ 10
Japan (JIS A 5021, 5022, and 5023) (JIS 2011, 2012a, b)	Coarse- Class H	≥ 2500	≤ 3
	Fine- Class H	≥ 2500	≤ 3.5
	Coarse- Class M	≥ 2300	≤ 5
	Fine- Class M	≥ 2200	≤ 7
	Coarse- Class L	No limit	≤ 7
	Fine- Class L	No limit	≤ 13
Korea (KS F 2573) (KS 2002)	Coarse	≥ 2500	≤ 3
	Fine	≥ 2200	≤ 5
RILEM (1994)	Type 1	≥ 1500	≤ 20
	Type 2	≥ 2000	≤ 10
	Type 3	≥ 2500	≤ 3
Spain (EHE 2000)	-	≥ 2000	≤ 5

Table 2-3 provides a summary of the influence of RCA on some key properties of Portland cement concrete obtained from a survey by the National Cooperative Highway Research Program (NCHRP 2013).

Table 2-3. Influence of RCA on properties of concrete (NCHRP 2013)

Property	Expected changes in properties	
	Coarse RCA only	Coarse and fine RCA
Specific gravity	0 to 10% lower	5% to 15% lower
Compressive strength	0 to 24% lower	15% to 40% lower
Tensile strength	0 to 10% lower	10% to 20% lower
Strength variability	Slightly greater	Slightly greater
Modulus of elasticity	10% to 33% lower	25% to 40% lower
Creep	30% to 60% higher	30% to 60% higher
Drying shrinkage	20% to 50% higher	70% to 100% higher
Permeability	0 to 500% higher	0 to 500% higher
Coefficient of thermal expansion	0 to 30% higher	0 to 30% higher
Corrosion rate	May be faster	May be faster
Freeze/thaw durability	Dependent on air void system	Dependent on air void system
Sulfate resistance	Dependent on mixture	Dependent on mixture

2.3.1. Fresh properties

Unit weight. As a result of high amounts of adhered mortar existing in RCA particles, the density of RCA is usually lower than that of virgin aggregates which in turn decreases the unit weight of concrete containing RCA (Xiao et al., 2012).

Workability. Surface texture of the RCA particles may have positive or negative effect on workability. Domingo et al., (2009) reported that a greater presence of recycled aggregates decreases the workability of the concrete, which may be related to the shape, texture, and absorption characteristics of the recycled aggregate. This necessitates the use of saturated recycled aggregate or a greater amount of superplasticizers to maintain workability. On the other hand, Sagoe et al. (2001) reported that plant processing of recycled aggregate could result in relatively smoother spherical particles, which leads to improved concrete workability in comparison with some natural aggregate concrete with equivalent grading and ratio of fine to coarse aggregate content.

2.3.2. Mechanical properties

Compressive strength. The use of RCA can lead in significant effect on compressive strength of concrete. This is mainly due to the inferior properties of the residual mortar phase of the RCA particles. However, this effect can be negligible for replacement levels up to 30% (Xiao et al., 2012). Nixon (1978) found that the compressive strength of concrete made with RCA replacement is somewhat lower compared to that of control mixtures without any RCA. Hansen (1986) concluded that the compressive strength of RCA-made concrete is largely controlled by a combination of the w/cm of the original concrete from which the RCA is produced and that of the RAC when other factors are essentially identical. Volz et al., (2014) observed no significant difference in compressive strength of the specimens made with up to 100% replacement of

coarse recycled aggregate with reference concrete. The RCA was produced from crushing concrete made with $w/c=0.4$, and the studied RCA-made concrete was proportioned with $w/cm=0.45$.

Splitting tensile strength. As in the case of compressive strength, RCA replacement mostly results in a decrease in splitting tensile strength of concrete. Ravindrarajah et al., (1985) reported that the splitting tensile strength of concrete made was consistently 10% lower than that of conventional concrete without RCA. Tabsh and Abdelfatah (2009) reported that about 25% to 30% drop in the tensile strength was observed in concrete made RCA. Kou et al. (2012) observed that regardless of the type of the recycled aggregate used, the splitting tensile strength of the specimens decreased with an increase in RCA replacement ratio before the age of 28 days. However, for some types of the RCAs used, an increase in the splitting tensile strength at the age of 90 days is observed. Sagoe et al., (2001), reported that there is no significant difference between the splitting tensile strength of the reference and the recycled aggregate concrete specimens. Limbachiya (2012) and Yong and Teo (2009) reported that while replacing up to 50% of coarse aggregate with RCA, there was no difference in splitting tensile and flexural strengths between the RAC and the reference, but at complete replacement results were improved for RCA due to better interlocking.

Flexural strength. The RCA replacement does not have significant negative effects on flexural strength of concrete. Xiao and Li (2005), Hu (2007), and Cheng (2005) have reported that up to 100% RCA replacement at concrete mixtures of w/cm varying from 0.43 to 0.57 only has marginal effects on flexural strength of concrete. Ravindrarajah and Tam (1985) have also reported that increasing the RCA content does not have a significant effect on flexural strength.

Topçu and Sengel (2004) have reported that the flexural strength is decreasing due to the increase in RCA replacement level.

Modulus of elasticity. Given the lower modulus of elasticity of the residual mortar attached to the RCA particles, the modulus of elasticity is expected to decrease with the increase in RCA replacement ratio (Xiao et al., 2012). Similar results were also reported by Hoffmann et al., (2012) and Cabo et al., (2009) who concluded that the modulus of elasticity decreases with the increase in RCA replacement.

Shrinkage. Kou et al., (2007), Kou and Poon (2012), Hansen and Boegh (1985), Fathifazl et al., (2011), Nassar and Soroushian (2012), and Gomez (2002) studied the shrinkage behavior of the RCA-made concrete and reported that the drying shrinkage increases with the increase in RCA content. However, this increase is negligible up to 20% replacement ratio (Kou et al., 2007). This increase in shrinkage is attributed to the lower restraining capacity of the RCA particles due to an increase in the total mortar content and a decrease in the volume of total stiff virgin aggregate in the mixture (Xiao et al., 2012).

Domingo-Cabo et al., (2009) found that the RAC with a RCA replacement level of 20% exhibited a similar shrinkage to the conventional concrete at early age. For a period of 6 months, the shrinkage in RAC was only 4% higher. In the case of a RCA replacement level of 50%, the shrinkage was 12% greater than that of the conventional concrete after 6 months. Moreover, Sagoe et al., (2001) reported that drying shrinkage of RAC was about 25% higher than that of conventional concrete. Kou et al., (2012) reported that drying shrinkage of RAC increases as the RCA replacement ratio increases. They also observed that recycled aggregates with lower water absorption capacities result in lower shrinkage rates. Kim and Bentz (2008) investigated the drying shrinkage in concrete mixtures made with RCA. They reported that the RCA can provide

internal curing in concrete, which is useful in reducing drying shrinkage. Similar results were reported by Hu et al., (2013) who reported that incorporating fine RCA is useful in decreasing the drying shrinkage through internal curing.

2.3.3. Durability

Chloride ion permeability. The chloride-ion permeability of concrete made with RCA is higher than conventional concrete. However, in the case of high quality RCA there is only slight difference between the chloride-ion penetration of RAC and that of conventional concrete.

Sim and Park (2011) observed that in the case of concrete made with coarse RCA and partial replacement of fine recycled aggregates, there is no significant difference between the total charges passing through the specimens (electrical conductivity) up to 100% fine recycled aggregate replacement. However, as the curing time increases, the incorporation of greater volume of fine recycled aggregate can lead to a decrease in conductivity. The increasing curing period and incorporating proper types and contents of supplementary cementitious materials (SCMs), the chloride-ion permeability could be controlled (Sim and Park, 2011). Kou et al., (2012) reported that the chloride-ion permeability increases with the increase in the coarse RCA replacement. However, the negative effect is more significant in the case of low grade RCA. Similar results were reported by Otsuki et al., (2001) and Shayan and Xu (2003).

Freeze/thaw resistance. Concrete made with RCA was shown to be more susceptible to damage due to the freeze/thaw cycles (Xiao et al., 2012). Medina (2013), Richardson (2011), Ajdukiewicz (2002), and Limbachyia (2000) have investigated the frost durability of the RCA-made concrete mixtures and reported that given the similar strength grade, there is no significant difference in freeze/thaw resistance of the RCA-made and conventional concrete.

De-icing salt scaling. Speare and Ben-Othman have reported that there is no difference between the studied the de-icing salt scaling performance of RCA made concrete and that of the virgin aggregate mixtures. Movassaghi (2006) has also studied the de-icing salt scaling resistance of concrete made with RCA and reported that the scaling resistance is increasing with an increase in the age of the RCA source.

Carbonation depth. Carbonation depth is proven to increase with the increase in the RCA content in concrete (Abbas et al., 2009). The mortar phase attached to the virgin aggregate available in RCA particles provide permeable paths through the RCA-made concrete. This increases the depth to which carbon dioxide can reach.

Absorption. Absorption of RCA concrete is usually reported to be higher than that of virgin aggregate concrete. This is mainly due to the attached porous mortar content of the RCA particles that can provide more water reservoirs, thus maintaining higher relative humidity inside the pore solution (Volz et al., 2014).

2.4. Use of RCA in rigid pavement construction

Most of the application of RCA in the U.S. involves the use of RCA as aggregate in base and subbase layers (FHWA 2004). Other applications include cement-treated base, backfill, embankment, stabilization, erosion control (riprap), and landscaping (ACPA 2009). According to a survey conducted by Garber et al., (2011), the use of RCA in new concrete production is rather advanced in European and East Asian countries. For example, in Finland, 10% of all RCA applications are bound applications implying new concrete mixtures or cement-treated bases (Englesen et al., 2005). In Austria, RCA is used for producing the bottom layer in two-lift

concrete pavement applications. In Australia, RCA is allowed for use in new concrete production for curbs and sidewalks.

Several states in the U.S. have used RCA to construct experimental pavement sections in 1980's to 1990's. Cuttall et al., (1997) have collected data related to the long term performance of the pavement sections. Three of the most common rigid pavement types including jointed plain concrete pavement (JPCP), jointed reinforced concrete pavement (JRCP), and continuously reinforced concrete pavement (CRCP) were used in Connecticut, Kansas, Minnesota, Wisconsin, and Wyoming. The visual inspections and data obtained from the core samples taken from these experimental sections proved that:

The RCA-made pavement sections exhibited good overall performance over the time. The data presented by Cuttall et al., (1997) indicated that the cores taken from the RCA-made sections had higher average compressive strength values compared to the reference sections which is said to be due to probably lower w/cm at the RCA-made sections or due to the use of fine RCA for concrete production. No significant difference between the splitting tensile strength of the control and the RCA concrete was detected. The modulus of elasticity results were proved to be up to 18% lower than that of the control concrete. All the measured coefficients of thermal expansion values were higher in the case of the RCA-made sections.

Salas et al., (2010) used up to 100% RCA for producing concrete for rigid pavement applications as a part of O'Hare Airports modernization project using the two stage mixing approach developed by Tam et al., (2005). This method is described in section 3.3.2. Similar or higher compressive strength compared to the virgin aggregate mixtures, similar shrinkage to the virgin

aggregate mixtures at early ages, reduced bleeding and segregation, and similar concrete workability was reported as a result of using RCA in concrete production.

Choi and Won (2009) studied the performance of a CRCP highway section made totally with fine and coarse RCA located in Houston, TX. Based on the results by testing core samples, it was observed that the average compressive strength decreased due to use of RCA. The modulus of elasticity of the RCA concrete was lower than that of the virgin aggregate mixture. It is interesting to note that the coefficient of thermal expansion of the RCA concrete was similar to the virgin aggregate mixtures. Higher chloride ion concentrations were observed in the case of the RCA mixtures. However, the rapid chloride-ion permeability results of the RCA concrete were surprisingly lower than that of the virgin aggregate concrete and rated as “Very low” based on the ASTM C1202. The sulfate content of the RCA-made and the virgin aggregate mixtures were found to be similar. It was also reported that the RCA sections had overall good performance after more than 10 years of service life with no structural distress taking place. The transverse crack distributions were also found to be similar to that of the virgin limestone mixtures Choi and Won (2009).

2.5. Concluding remarks

Due to the variable properties of RCA particles compared to the virgin aggregate sources, the mechanical properties and durability of concrete made with RCA may be lower than conventional concrete without any RCA. However, depending on the fresh concrete composition and source of RCA, this decrease may be negligible.

This project evaluates the performance of environmentally friendly RCA-made concrete mixtures for rigid pavement application. The study focuses on performance of concrete mixtures

proportioned with various amounts of fine and coarse RCA, different w/cm and fly ash contents. Field implementation is also conducted to investigate the in-situ performance of RCA-made mixtures. Long-term deformation of the pavement sections made with RCA is also monitored. Truck loading is also conducted to evaluate deformation caused by controlled traffic loading.

3. Experimental program

3.1. Material properties

All the mixtures investigated in this study were proportioned with a binary blend of Type I/II Portland cement and Class C fly ash. Physical properties and chemical compositions of the cement are presented in Table 3-1. Table 3-2 includes the typical chemical analysis of the Class C fly ash used in the study.

Table 3-1. Physical properties and chemical compositions of cement

Physical properties	
Property	Type I/II Cement
Blaine fineness, m ² /kg	380
Specific gravity	3.15
Chemical compositions	
Component	% of mass
SiO ₂	19.8
Al ₂ O ₃	4.5
Fe ₂ O ₃	3.2
CaO	64.2
MgO	2.7
SO ₃	3.4
Na ₂ O	0.52 equivalent
LOI	2.6
C ₃ A	61
C ₂ S	8
C ₃ S	6
C ₄ AF	9

Two types of fine aggregates and two types of coarse aggregates were used in the study. Well graded Class A Missouri River sand was used as the virgin fine aggregate. Fine RCA obtained while crushing concrete for RCA production was used as the other source of fine aggregate. Crushed limestone with maximum nominal size of 1.0 in. was used for the virgin coarse

aggregate. Besides, the same sized coarse RCA procured from a commercial recycling center was used as the second source of coarse aggregate.

The RCA (both fine and coarse) were produced by recycling old concrete available in the Lambert Airport area in St. Louis, Missouri. Dry-rodded unit weight, absorption, specific gravity, and Loss Angeles abrasion resistance of the materials are determined according to ASTM standards for both the virgin and recycled aggregates.

Table 3-2. Chemical compositions of fly ash (Wolfe 2011)

Component	Range (%)
SiO ₂	30.5 - 36.4
Al ₂ O ₃	16.4 - 20.8
Fe ₂ O ₃	6.8 - 7.7
CaO	24.3 - 26.1
MgO	4.8 - 5.5
SO ₃	2.2 - 2.4
Na ₂ O	1.5 - 2.0
K ₂ O	0.4 - 0.6
TiO ₂	1.4 - 1.6
P ₂ O ₅	1.0 - 1.9
MnO	0.03 - 0.04
SrO	0.4 - 0.5
BaO	0.7 - 0.9
LOI	0.24 - 1.15

The residual mortar content of the RCA was determined based on the method proposed by Abbas et al., (2009). In this method, RCA particles are submerged in a saturated solution of sodium sulphate being subjected to cycles of freezing and thawing. Due to the combined effect of the chemical solution and thermal stresses, the mortar phase of the RCA particles is separated from the old virgin aggregate. Two series of samples were used for measuring the residual mortar

content of the RCA. Each of these samples contained four individual groups of aggregates retained on 3/4 in., 1/2 in., 3/8 in., and #4 sieves. The residual mortar content of each sample was calculated based on the weight of the separated mortar and grain size distribution of the RCA, as suggested by Abbas et al., (2009). The residual mortar content is then computed as a percentage of the mass of the RCA particles. Figure 3-1 shows one of the RCA samples before the cycles and after the separation of the residual mortar.



Figure 3-1. RCA particles before separating the mortar (left) and after separating the residual mortar (right)

Table 3-3 presents physical properties of the fine and coarse aggregates. The gradation curve of the aggregates is compared to the ASTM C33 standard in Figure 3-2 and Figure 3-3. Figure 3-4 plots the amount of coarse aggregates retained on each sieve. The ideal shape of this gradation curve is a symmetric bell shaped one. Both the coarse aggregates (virgin and RCA) exhibited adequate gradation as presented in Figure 3-4.

Table 3-3. Physical properties of the aggregates

Aggregate	Specific gravity	Dry rodded unit weight (pcf)	Absorption (%)	LA abrasion (%)	Residual mortar (% of wt.)
Missouri River sand	2.63	-	0.34	-	-
Fine RCA	2.41	-	6.8	-	-
Limestone	2.64	100.3	0.5	24	-
Coarse RCA	2.38	91.0	4.2	33	36

It should be noted that the Los Angeles abrasion results are the average values calculated for two series of samples obtained from the coarse aggregate piles.

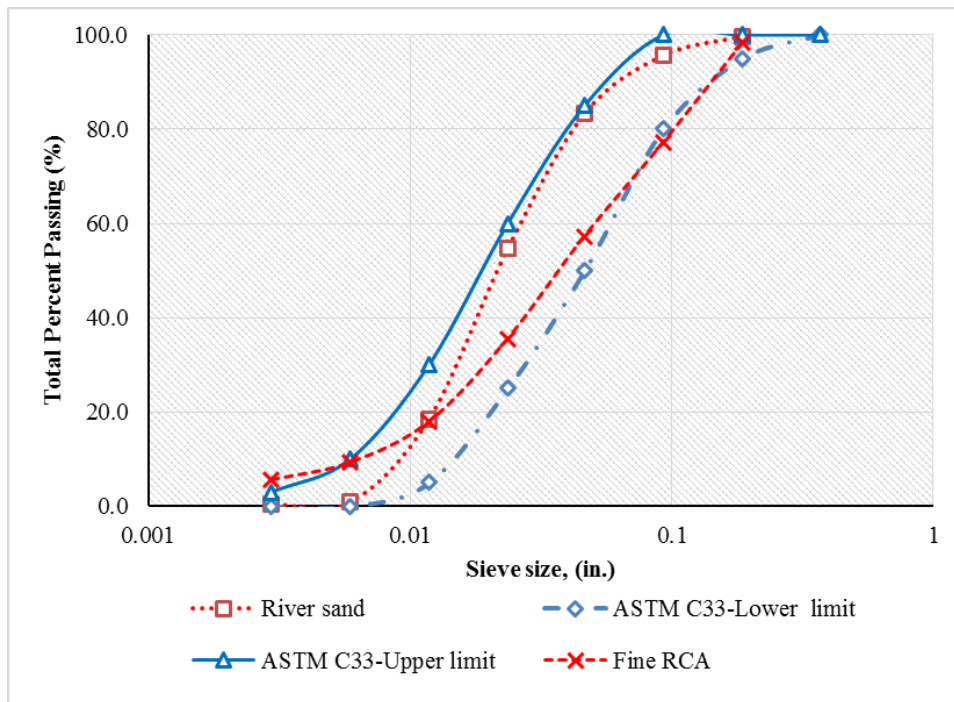


Figure 3-2. Particle size distribution of the fine aggregate

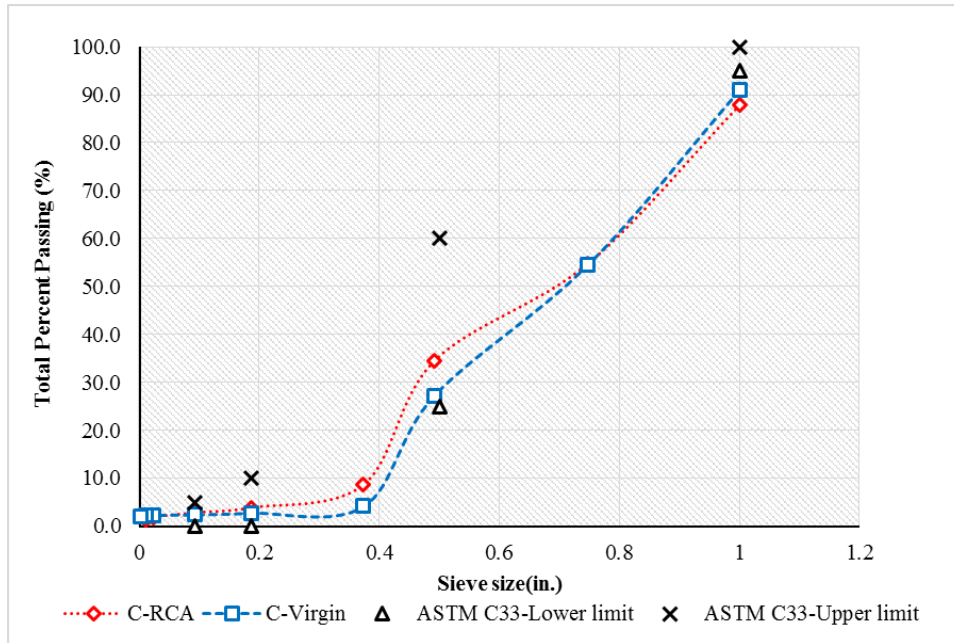


Figure 3-3. Particle size distribution of the coarse aggregate

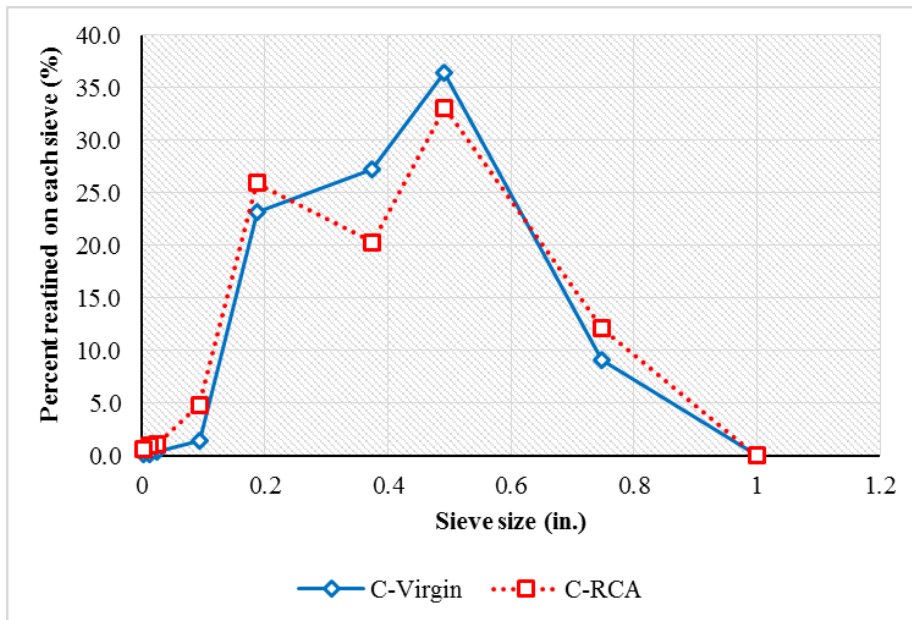


Figure 3-4. Individual percentages retained on each sieve

3.2. Mixture proportions

3.2.1. Conventionally proportioned mixtures

All mixtures were proportioned with sand-to-aggregate ratio of 40% and total cementitious material content of 545 lb/yd³, except for the mixture proportioned based on the equivalent

mortar volume (EMV) method. This method is detailed in section 3.2.3. Class C fly ash was incorporated at a replacement rate of 25% to 40%, by mass of cementitious materials. The w/cm varied from 0.37 to 0.42.

3.2.2. Two stage mixing approach

The Two Stage Mixing Approach (TSMA) was used to vary the batching sequence for some of the mixtures. The main idea of the TSMA is to encapsulate the RCA particles with a low w/cm of high quality cement paste to enhance the surface properties of the RCA as well as the interfacial transition zone (ITZ) formed between the RCA particle and the fresh surrounding hydrated cement paste (Otsouki et al., 2003, Ryu 2002, Tam et al., 2005, 2007, 2008, and 2009, Elhakam et al., 2012, Li et al., 2012). In order to produce the concrete with TSMA, the coarse RCA was loaded in the mixer along with a quarter of the mixing water and the air-entraining admixture. After one minute of mixing, the cementitious materials were added during one minute of mixing, and then, the half of the remaining water was introduced and allowed to mix for one minute to coat the RCA particles with a rich cement paste. The rest of the materials were then loaded followed by two minutes of mixing.

3.2.3. Equivalent mortar volume mixture proportioning method

Fathifazl et al. (2009) have introduced a mixture proportioning method for making concrete with coarse RCA as a replacement for virgin coarse aggregate. Considering the residual mortar content of RCA as part of the total mortar content of the RCA-made concrete is the basis of this method of mixture proportioning. In the proposed method, the RCA-made concrete mixture is proportioned to have the same total mortar volume as a companion concrete mixture made entirely with fresh virgin (here also referred as natural) aggregates, with the companion mixture made with the same type of coarse aggregate as that in RCA. Mixture proportioning based on the

proposed method essentially involves proper determination of the amounts of RCA and fresh mortar in RCA- made concrete. The method proceeds as follows (Fathifazl et al. 2009):

A companion concrete should be proportioned based on the conventional concrete mixture proportioning methods, only with natural aggregate being used in composition. It is assumed that the natural aggregate (NA) used in this mixture has the same gradation and maximum size as the RCA. This mixture is referred to as the natural aggregate concrete (NAC). A second mixture containing both natural aggregate and RCA is produced and referred to as the RCA-concrete.

The volume of NA in the RCA-concrete mixture is: $V_{NA}^{RCA-concrete}$.

The relative content of the natural aggregate, R, is:

$$R = \frac{V_{NA}^{RCA-concrete}}{V_{NA}^{NAC}} \quad (3-1)$$

where $V_{NA}^{RCA-concrete}$ = volume of natural aggregate in RCA-concrete and V_{NA}^{NAC} = volume of natural aggregate in NAC.

R = 0 refers to a concrete mixture with no NA (i.e. 100% RCA) in composition, and R = 1 corresponds to a mixture with 100% NA (i.e. with no RCA). For the RCA-concrete and its NAC to have the same properties, the proposed method requires that the two following conditions are satisfied:

1. The total mortar content in the NAC should be equal to the total mortar content of the RCA-concrete mixture. The total mortar content of the RCA-concrete mixture can be determined by the summation of residual mortar content attached to the RCA particles available in RCA-concrete mixture and the fresh mortar content of the same mixture.

2. The total NA content in the NAC to be equal to the total NA content of the RCA-concrete mixture. The total NA content of the RCA-concrete mixture can be determined by the summation of the original virgin aggregate available in the RCA particles and the NA content of the RCA-concrete mixture.

These two conditions are summarized in the following Equations:

$$V_{TM}^{RCA-concrete} = V_M^{NAC} \quad (3-2)$$

$$V_{TNA}^{RCA-concrete} = V_{NA}^{NAC} \quad (3-3)$$

where $V_{TM}^{RCA-concrete}$ = total mortar (TM) volume in RCA-concrete, V_M^{NAC} = mortar volume in the companion concrete made entirely with natural aggregate, and $V_{TNA}^{RCA-concrete}$ = total natural aggregate (TNA) volume in RCA-concrete.

Therefore, Equations (3-2) and (3-3) can be reformed as:

$$V_{TM}^{RCA-concrete} = V_{RM}^{RCA-concrete} + V_{NM}^{RCA-concrete} \quad (3-4)$$

$$V_{TNA}^{RCA-concrete} = V_{OVA}^{RCA-concrete} + V_{NA}^{RCA-concrete} \quad (3-5)$$

where $V_{RM}^{RCA-concrete}$ = residual mortar (RM) volume in RCA-concrete, $V_{NM}^{RCA-concrete}$ = volume of the fresh or new mortar (NM) in RCA-concrete; and $V_{OVA}^{RCA-concrete}$ = original virgin aggregate volume in RCA concrete.

It is assumed that the difference between strength and density of the residual mortar and fresh mortar and the difference between the original virgin aggregate (OVA) and fresh NA type and/or shape may have negligible effect on the overall properties of RCA-concrete compared to the companion NAC. It is also assumed that the severely damaged mortar will not survive the crushing process during RCA production. This ensures the quality of the residual mortar attached to the RCA particles.

In order to ensure the conditions stated in Equation (3-5), amount of original virgin aggregate in RCA-concrete should be quantified:

$$V_{OVA}^{RCA-concrete} = V_{RCA}^{RCA-concrete} \times (1 - RMC) \times \frac{SG_b^{RCA}}{SG_b^{OVA}} \quad (3-6)$$

where $V_{RCA}^{RCA-concrete}$ = volume of RCA in RCA-concrete and SG_b^{RCA} and SG_b^{OVA} = bulk specific gravities of RCA and original virgin aggregate (OVA) available in the RCA particles, respectively. Again it should be noted that the RMC is the residual mortar content of the RCA.

The required volumes of RCA and fresh natural aggregate in the RCA-concrete can be determined using the Equations (3-1), (3-2), (3-5), and (3-6):

$$V_{RCA}^{RCA-concrete} = \frac{V_{NA}^{NAC} \times (1 - R)}{(1 - RMC) \times \frac{SG_b^{RCA}}{SG_b^{OVA}}} \quad (3-7)$$

$$V_{RCA}^{RCA-concrete} = V_{NA}^{NAC} \times R \quad (3-8)$$

$$W_{OD-RCA}^{RCA-concrete} = V_{RCA}^{RCA-concrete} \times SG_b^{RCA} \times 1000 \quad (3-9)$$

$$W_{OD-NA}^{RCA-concrete} = V_{NA}^{RCA-concrete} \times SG_b^{NA} \times 1000 \quad (3-10)$$

where $W_{OD-RCA}^{RCA-concrete}$ = required oven-dry weight of RCA in RCA-concrete, $W_{OD-NA}^{RCA-concrete}$ = required oven-dry weight of natural aggregate in RCA-concrete, and SG_b^{NA} = bulk specific gravity of natural aggregate.

The next step is to determine the amount of required water, cement, and fine aggregate proportions in RCA-concrete Mixture. The residual mortar content available in RCA-concrete should be quantified to satisfy the condition expressed in Equation (3-2).

$$V_{RM}^{RCA-concrete} = V_{RCA}^{RCA-concrete} \times [1 - (1 - RMC) \times \frac{SG_b^{RCA}}{SG_b^{OVA}}] \quad (3-11)$$

The amount of fresh mortar in RCA-concrete can be determined using Equations (3-2), (3-4), and (3-11):

$$V_{NM}^{RCA-concrete} = V_M^{NAC} - V_{RM}^{RCA-concrete} \quad (3-12)$$

where $V_{NM}^{RCA-concrete}$ is the new (fresh) mortar content in RCA-concrete, V_M^{NAC} is the total mortar content of natural aggregate concrete, and $V_{RM}^{RCA-concrete}$ is the volume of residual mortar in RCA-concrete.

The corresponding quantities of water, cement, and fine aggregate in RCA-concrete can be determined as follows:

$$W_w^{RCA-concrete} = W_w^{NAC} \times \frac{V_{NM}^{RCA-concrete}}{V_M^{NAC}} \quad (3-13)$$

$$W_c^{RCA-concrete} = W_c^{NAC} \times \frac{V_{NM}^{RCA-concrete}}{V_M^{NAC}} \quad (3-14)$$

$$W_{OD-FA}^{RCA-concrete} = W_{OD-FA}^{NAC} \times \frac{V_{NM}^{RCA-concrete}}{V_M^{NAC}} \quad (3-15)$$

where $W_w^{RCA-concrete}$ and W_w^{NAC} are the weights of water in RCA-concrete and natural aggregate concrete, $W_c^{RCA-concrete}$ and W_c^{NAC} are the weights of cement in RCA-concrete and natural aggregate concrete, and $W_{OD-FA}^{RCA-concrete}$ and W_{OD-FA}^{NAC} are the oven dried weights of fine aggregate in RCA-concrete and NAC respectively.

An upper limit exists for the RCA content in the EMV method. This limit is a function of the residual mortar content of the RCA. The theoretical lower and upper limits of residual mortar

content, 0 and 100%, respectively, should be examined to determine the effect of residual mortar content on RCA-concrete mixture proportioning. Given the fact that the maximum amount of any coarse aggregate, including RCA, which can be placed in a unit volume of concrete, is equal to the dry-rodded unit volume of that aggregate. Therefore, the upper limit of RCA content in RCA concrete is the dry-rodded volume of RCA ($V_{DR-RCA}^{RCA-concrete}$). Hence, the maximum volume of RCA that can be added to a unit volume of RCA-concrete can be calculated as:

$$V_{maxRCA}^{RCA-concrete} = \frac{SG_{DR}^{RCA}}{SG_b^{RCA}} \quad (3-16)$$

where $V_{maxRCA}^{RCA-concrete}$ = maximum volume of RCA that can be added to a unit volume of RCA-concrete, SG_{DR}^{RCA} = dry-rodded specific gravity of RCA, and SG_b^{RCA} = bulk specific gravity of RCA.

The absolute volume of natural aggregate in natural aggregate concrete, in Equation (3-7) can be related to its dry-rodded volume as:

$$V_{NA}^{NAC} = V_{DR-NA}^{NAC} \times \frac{SG_{DR}^{NA}}{SG_b^{NA}} \quad (3-17)$$

where V_{NA}^{NAC} = volume of natural aggregate in NAC, SG_{DR}^{NA} = dry-rodded specific gravity of natural aggregate, and SG_b^{NA} = bulk specific gravity of natural aggregate.

By substituting Equations (3-16) and (3-17) in Equation (3-7), the minimum replacement ratio (R_{min}) can be calculated as:

$$R_{min} = 1 - \frac{(1 - RMC)}{V_{DR-NA}^{NAC}} \times \frac{SG_{DR}^{RCA}}{SG_{DR}^{OVA}} \times \frac{SG_b^{NA}}{SG_b^{OVA}} \geq 0 \quad (3-18)$$

where RMC = residual mortar content of the RCA, V_{DR-NA}^{NAC} = dry-rodded volume of natural aggregate in natural aggregate concrete, SG_{DR}^{RCA} = dry-rodded specific gravity of RCA, SG_{DR}^{OVA} = dry-rodded specific gravity of original virgin aggregate available in RCA particles, SG_b^{NA} = bulk specific gravity of natural aggregate, and SG_b^{OVA} = bulk specific gravity of original virgin aggregate.

By assuming identical shape and size gradation for RCA and NA, it can be written that:

$$\frac{SG_{DR}^{RCA}}{SG_{DR}^{NA}} = \frac{SG_b^{RCA}}{SG_b^{NA}} \quad (3-19)$$

Assuming the fresh natural aggregate that is used as replacement of RCA to be similar to the original virgin aggregate in RCA, the ratio $\frac{SG_b^{NA}}{SG_b^{OVA}}$ in Equation (3-18) would become one.

Therefore, by substituting Equation (3-19) into Equation (3-18), one obtains:

$$R_{min} = 1 - \frac{(1 - RMC)}{V_{DR-NA}^{NAC}} \times \frac{SG_b^{RCA}}{SG_b^{NA}} \geq 0 \quad (3-20)$$

It should be noted that the negative value for R_{min} implies that one can make a concrete mixture with 100% RCA, without the need for any fresh natural aggregate.

As the residual mortar content increases and approaches 100%, the required volume of RCA in RCA-concrete in Equation (3-7) increases hyperbolically and approaches infinity ($V_{RCA}^{RCA-concrete} / V_{NA}^{NAC} \rightarrow \infty$). However, if the $(1-R)$ in the numerator of Equation (3-7) is set equal to the denominator, $((1 - RMC) \times \frac{SG_b^{RCA}}{SG_b^{OVA}})$, the resulting equation would be valid for any residual mortar content. The physical interpretation of the latter action is replacement of residual mortar

volume in RCA with the fresh natural aggregate ($V_{NA}^{RCA-concrete} = V_{RM}^{RCA-concrete}$) to compensate for the deficiency of the total natural aggregate in RCA-concrete compared to the companion natural aggregate concrete. Therefore:

$$R = \frac{V_{RM}^{RCA-concrete}}{V_{RCA}^{RCA-concrete}} \quad (3-21)$$

where $V_{RM}^{RCA-concrete}$ = volume of residual mortar in RCA-concrete, and $V_{RCA}^{RCA-concrete}$ = volume of RCA in RCA-concrete.

By substituting Equations (3-21) and (3-11) into Equation (3-7), the required RCA and natural aggregate volumes can be found as:

$$V_{RCA}^{RCA-concrete} = V_{NA}^{NAC} \quad (3-22)$$

$$V_{NA}^{RCA-concrete} = V_{NA}^{NAC} \times [1 - (1 - RMC) \times \frac{SG_b^{RCA}}{SG_b^{OVA}}] \quad (3-23)$$

where $V_{NA}^{RCA-concrete}$ = required volume of natural aggregate in RCA-concrete.

3.3. Experimental program

An experimental program was undertaken to investigate the performance of RCA concrete mixtures for pavement applications. MoDOT's Class PCCP concrete mixture was used as a reference concrete. The mixture was prepared with 545 lb/yd³ of cementitious materials, 25% Class C fly ash, w/cm of 0.40, and S/A of 0.4. A mid-range water reducing admixture (MRWRA) and an air-entraining admixture (AEA) were incorporated to secure a slump value of 2 ± 0.5 in. and an air content of 6±1%, respectively.

The majority of the scientific literature recommends limiting the content of RCA to 30%. Early experience of MoDOT seems to support these findings (Volz et al. 2014). Therefore, all the mixtures were proportioned with 30% of coarse RCA replacement except for the reference mixture which had no RCA.

Table 3-4 summarizes the studied mixtures. The first stage of the mixture optimization involved the variation of w/cm, fly ash, and fine RCA content. This was carried out to enhance the engineering properties and durability of the concrete containing fine RCA and to investigate the feasibility of producing a more sustainable material using fly ash and fine RCA. The influence of incorporating a limited amount of fine RCA and the increase in fly ash content on the performance of concrete is evaluated.

A coding system was developed for labeling different mixtures. Codes are composed of three numbers indicating the fly ash content, fine RCA content, and w/cm respectively. As an example, code “35-0-40” refers to a mixture made with 35% of fly ash, no fine RCA, and w/cm of 0.40. Code “25-10-40” refers to a mixture made with 25% of fly ash, 10% of fine RCA, and w/cm of 0.40. All the mixtures were proportioned with 30% of coarse RCA, except for the Reference mixture that was made without any RCA.

A total of 20 mixtures were investigated in the first stage of optimization. The mixtures number 35-10-40, 25-10-40, and 25-0-40 were repeated using the TSMA. Mechanical properties, shrinkage, and permeable void volume were determined for all of the investigated mixtures. Durability was evaluated for selected mixtures. The equivalent mortar volume method was employed to produce an additional mixture. The mixture compositions of the concrete mixtures are presented in Table 3-5.

Table 3-4. Test matrix used for the first step of the laboratory investigations

Fly ash		25%				35%				40%			
Fine RCA (%)		0	10	15	20	0	10	15	20	0	10	15	20
	0.42						*						
w/cm	0.40	Ref.**	*	*		*	*	*	*				
	0.37		*	*				*	*		*	*	*

**The reference mixture had no RCA. Remaining mixtures were proportioned with 30% of coarse RCA replacement.

Table 3-5. Mixture proportions of concrete mixtures used in the study

Mixture ID	Ref.	35-0-40	35-10-40	35-15-40	35-20-40	35-15-37	35-20-37	40-10-37	40-15-37	40-20-37	35-10-42	25-10-40	25-15-40	25-15-37	25-10-37	25-0-40	EMV
Cement Type I (lb/yd ³)	409	354	354	354	354	354	354	327	327	327	354	409	409	409	409	409	357
Class C fly ash, by mass (%)	25	35	35	35	35	35	35	40	40	40	35	25	25	25	25	25	25
Fly ash (lb/yd ³)	136	191	191	191	191	191	191	218	218	218	191	136	136	136	136	136	119
Cementitious materials (lb/yd ³)	545	545	545	545	545	545	545	545	545	545	545	545	545	545	545	545	476
w/cm	0.4	0.4	0.4	0.4	0.4	0.37	0.37	0.37	0.37	0.37	0.42	0.4	0.4	0.37	0.37	0.4	0.4
Water (lb/yd ³)	218	218	218	218	218	202	202	202	202	202	229	218	218	202	202	218	191
Sand/aggregate, by volume (%)	40	40	40	40	40	40	40	40	40	40	40	40	40	40	40	40	36 (by mass)
Fine RCA, by volume (%)	-	-	10	15	20	15	20	10	15	20	10	10	15	15	10	-	-
Fine RCA (lb/yd ³)	-	-	115	172	230	172	230	115	172	230	115	115	172	172	115	-	-
Sand (lb/yd ³)	1256	1256	1130	1067	1005	1067	1005	1130	1067	1005	1130	1130	1067	1067	1130	1256	1166
RCA, by volume (%)	-	30	30	30	30	30	30	30	30	30	30	30	30	30	30	30	30 (by mass)
Coarse virgin aggregate content (lb/yd ³)	1890	1323	1323	1323	1323	1323	1323	1323	1323	1323	1323	1323	1323	1323	1323	1323	1417
Coarse RCA content (lb/yd ³)	-	510	510	510	510	510	510	510	510	510	510	510	510	510	510	510	625

3.4. Sampling and testing

The sampling and test methods to investigate fresh properties, mechanical properties, and durability are summarized in Table 3-6. A vibrating table was used to facilitate the consolidation of the fresh concrete.

Table 3-6. Test methods and standard used in the study

PROPERTY	TEST METHOD	DESCRIPTION
Unit Weight	ASTM C 138	Standard Test Method for Density (Unit Weight).
Air Content	ASTM C 231	Standard Test Method for Air Content of Freshly Mixed Concrete by the Pressure Method.
Bleeding	ASTM C 232	Standard Test Methods for Bleeding of Concrete.
Compressive Strength, 4×8 in. cylinders, (1, 7, 28, 56, and 91 d)	ASTM C 39	Standard Test Method for Compressive Strength of Cylindrical Concrete Specimens.
Splitting Tensile Strength, 4×8 in. cylinders, (7, 28, and 56 d)	ASTM C 496	Standard Test Method for Splitting Tensile Strength of Cylindrical Concrete Specimens.
Flexural Strength, 6×6×20 in. beams (28, 56 d)	ASTM C 78	Standard Test Method for Flexural Strength of Concrete.
Modulus of Elasticity, 4×8 in. cylinders, (28, 56 d)	ASTM C 469	Standard Test Method for Static Modulus of Elasticity.
Shrinkage, 3×3×11.25 in. prisms	ASTM C 157	Standard Test Method for Length Change of Hardened Hydraulic-Cement Mortar and Concrete
Permeable void ratio, 4×8 in. cylinders, (28, 56, and 91 d)	ASTM C 642	Standard Test Method for Density, Absorption, and Voids in Hardened Concrete
Elect. Resistivity, 4×8 in. cylinders, (28, 56, and 91d)	ASTMC 1760	Standard Test Method for Bulk Electrical Conductivity of Hardened Concrete
Surface Resistivity, 4×8 in. cylinders, (28, 56, and 91d)	AASHTO TP 95	Surface Resistivity Indication of Concrete's Ability to Resist Chloride Ion Penetration
Freeze Thaw Resistance, procedure A, 3×4×16 in. prisms	ASTM C 666	Standard Test Method for Resistance of Concrete to Rapid Freezing and Thawing.
Deicing-salt Scaling Resistance, 3×10×11 in. panels	ASTM C 672	Standard Test Method for Scaling Resistance of Concrete Surfaces Exposed to Deicing Chemicals.

Molded samples were kept under wet burlap and covered by plastic sheets for 24 hours before demolding. They were then placed in lime-saturated water at 70±5 °F until the age of testing.

4. Results and discussion

4.1. Step one, initial investigations

4.1.1. General

A batch of 3.0 ft³ concrete was prepared to evaluate the properties of each mixture. The targeted slump and air content were 2.0 ± 0.5 in. and $6.0 \pm 1.0\%$, respectively. Fresh properties of the investigated mixtures are presented in Table 4-1.

Table 4-1. Fresh properties of mixtures used for initial stage of characterizing

Mixture	Slump (in.)	Air content (%)	Unit weight (pcf)
Ref.	2.0	5.4	150.1
35-0-40	1.5	5.0	148.5
35-10-40	2.5	5.4	148.5
35-10-40-TSMA	2.5	5.3	147.2
35-15-40	3.5	7.5	142.3
35-20-40	3.0	6.3	145.4
35-15-37	2.0	5.5	146.0
35-20-37	2.0	5.5	144.4
40-10-37	3.5	5.0	146.0
40-15-37	2.0	5.4	146.1
40-20-37	3.0	5.2	145.5
35-10-42	5.0	5.3	144.9
25-10-40	3.0	5.8	146.6
25-10-40- TSMA	2.0	5.7	146.0
25-15-40	2.5	5.2	146.5
25-15-37	2.5	5.4	145.3
25-10-37	2.5	5.8	145.5
25-0-40	4.5	6.6	142.9
25-0-40- TSMA	3.5	6.8	145.4
EMV	1.5	5.8	149.5

4.1.2. Compressive strength

The compressive strength results up to 91 days are summarized in Table 4-2. For each age, three 4×8 in. cylindrical specimens were tested for the compressive strength. A sulfur-based capping compound was used to prepare the specimen surfaces.

Table 4-2. Compressive strength results at different ages (psi)

Mixture	1 day	7 days	28 days	56 days	91 days
Ref.	3125 (3.9*)	4950 (4.2)	6575 (2.1)	7320 (0.6)	7515 (3.1)
35-0-40	2185 (2.7)	5340 (0.5)	6010 (3.9)	7005 (2.3)	7665 (4.3)
35-10-40	2875 (5.5)	4385 (3.9)	6460 (5.2)	7305 (10.9)	7910 (6.8)
35-10-40-TSMA	2145 (17.6)	4870 (6.1)	6220 (3.6)	6950 (1.1)	7215 (3.5)
35-15-40	1785 (4.7)	4600 (5.9)	5460 (5.0)	5530 (8.2)	6155 (13.3)
35-20-40	1850 (16.6)	4710 (12.7)	6350 (5.9)	6700 (9.9)	7150 (7.4)
35-15-37	2365 (7.1)	4730 (4.2)	6205 (1.3)	6955 (5.4)	7810 (9.6)
35-20-37	1970 (11.9)	5965 (3.3)	6880 (1.7)	7445 (4.5)	7530 (3.3)
40-10-37	2040 (1.3)	4650 (9.2)	5680 (6.6)	6190 (2.7)	6890 (6.1)
40-15-37	2165 (3.1)	4895 (8.3)	6420 (1.5)	6745 (10.1)	7205 (9.2)
40-20-37	2675 (4.6)	5710 (2.3)	6530 (4.9)	7425 (4.7)	7990 (3.6)
35-10-42	2515 (7.4)	4265 (1.0)	5975 (2.1)	6545 (3.0)	7210 (12.2)
25-10-40	2115 (0.8)	4672 (7.3)	5050 (1.9)	6325 (12.8)	7475 (5.3)
25-10-40- TSMA	2630 (5.0)	3950 (15.2)	5465 (7.2)	6780 (3.0)	7060 (2.7)
25-15-40	2740 (5.0)	5465 (3.4)	6160 (4.9)	7350 (4.3)	7765 (7.2)
25-15-37	2695 (3.7)	5290 (11.1)	6615 (1.5)	6815 (9.4)	7360 (14.2)
25-10-37	2785 (5.5)	4810 (4.3)	6280 (2.6)	7110 (7.6)	7205 (8.4)
25-0-40	2830 (5.4)	3890 (21.8)	4310 (13.1)	6635 (8.5)	7280 (2.4)
25-0-40- TSMA	2050 (5.9)	4085 (8.8)	5330 (8.1)	6800 (2.0)	7345 (3.5)
EMV	3275 (2.3)	5115 (4.6)	6105 (7.3)	6720 (3.4)	7225 (5.8)

* C.O.V. (%).

As expected, an increase in w/cm led to a decrease in compressive strength. Only 3% reduction in compressive strength (from 7515 psi to 7280 psi) was observed with the use of 30% coarse RCA compared to the reference mixture. A 20% of fine RCA replacement did not lead to significant effect on compressive strength. The increase in fly ash replacement level from 25% to 40% led to average of 24% decrease in the compressive strength at early age (one day strengths). However, this was not the case for later ages and average reduction in strength was limited to 3% at 91 days. The TSMA method did not contribute in any improvement in compressive strength. The EMV mixture exhibited higher early-age strength but had similar strength values at 91 days compared to the reference and the 25-0-40 mixtures, respectively.

4.1.3. Splitting tensile strength

The splitting tensile strength results of the mixtures are presented in Table 4-3. For each age, three 4×8 in. cylindrical specimens were used to determine the splitting tensile strength.

As in the case of the compressive strength, an increase in the w/cm resulted in a decrease in the splitting tensile strength. The increase in the coarse RCA content from 0 to 30% did not have any significant effect on the splitting tensile strength (Reference vs. 25-0-40 mixture). Increasing the fine RCA content to 20% did not lead to any influence in splitting tensile strength. Similarly, an increase in fly ash content from 25% to 40% did not have any significant effect on splitting tensile strength. No significant difference in the splitting tensile strength was found, regardless of the production method. It is important to note that given the greater aggregate interlock, the EMV mixtures, developed higher 28-day tensile strength than similar mixtures.

Table 4-3. Splitting tensile strength results at different ages (psi)

Mixture	7 days	28 days	56 days
Ref.	375 (3.2*)	470 (7.5)	525 (8.6)
35-0-40	430 (11.7)	465(1.4)	670 (7.2)
35-10-40	455 (8.7)	495 (5.0)	545 (3.2)
35-10-40-TSMA	435 (3.9)	490 (2.8)	500 (2.7)
35-15-40	480 (5.7)	475 (1.1)	455 (7.6)
35-20-40	440 (6.1)	495 (6.6)	480 (6.6)
35-15-37	455(13.1)	475 (4.2)	525 (8.7)
35-20-37	460 (9.2)	595 (8.8)	550 (2.9)
40-10-37	480 (10.9)	485 (11.3)	510 (8.5)
40-15-37	405 (8.4)	440 (15.0)	525 (10.7)
40-20-37	525 (17.6)	465 (23.5)	560 (10.1)
35-10-42	395 (9.9)	430 (7.0)	495 (6.1)
25-10-40	415 (24.3)	530 (20.8)	530 (4.0)
25-10-40- TSMA	435 (16.4)	455 (9.8)	530 (6.6)
25-15-40	390 (8.1)	505 (14.9)	510 (18.1)
25-15-37	485 (10.5)	470 (15.6)	405 (5.5)
25-10-37	420 (6.2)	510 (24.3)	545 (0.6)
25-0-40	350 (13.9)	445 (2.8)	520 (15.6)
25-0-40- TSMA	420 (3.5)	465 (7.2)	565 (4.7)
EMV	515 (4.8)	530 (9.6)	565 (7.8)

*C.O.V. (%)

4.1.4. Drying shrinkage

Three 3.0×3.0×11.25 in. prisms were used to monitor drying shrinkage. The specimens were demolded 24 hours after casting and placed in lime-saturated water at 70±5 °F (21±3°C) for seven days. The samples were then kept in an environmental chamber at 70±5 °F (21±3°C) and relative humidity of 50 ± 5%. Shrinkage was monitored until the age of 180 days when the deformation was stable. A digital length comparator was used to monitor the length of the specimens as shown

in Figure 4-1. The initial length of the specimens corresponds to that determined immediately after removing the specimens from the curing tank was registered and used as the reference for determining the shrinkage deformation. The same device was used for measuring the length of specimens at different time intervals.



Figure 4-1. Photo of length measurement for drying shrinkage

Drying shrinkage results of the specimens made with w/cm of 0.37 are presented in Figure 4-2. The shrinkage values with respect to time for mixtures made with 0.40 and 0.42 w/cm are presented in Figure 4-3. Shrinkage deformation of the EMV and TSMA mixtures and the corresponding conventionally mixed concrete mixtures are compared in Figure 4-4.

In general, a reduction in w/cm led to a significant decrease in shrinkage. An example of such behavior was observed comparing the shrinkage of the mixture 35-10-42 and 35-10-40. The increase in fly ash replacement resulted in a slight decrease in shrinkage. An example of such behavior was observed comparing the shrinkage of the mixture 25-15-37 and 35-15-37. Despite a slight improvement in drying shrinkage with using fine RCA in some cases, such as increasing

fine RCA content from 0 to 20% in case of the mixtures 35-0-40 and 35-20-40, the effect of the fine RCA on shrinkage might be negligible given the low variations in fine RCA content. On the other hand, the incorporation of 30% coarse RCA led to 14% increase in the drying shrinkage at 180 days. This is attributed to the lower restraining capacity of the RCA particles compared to the virgin coarse aggregates (Anderson et al., 2009).

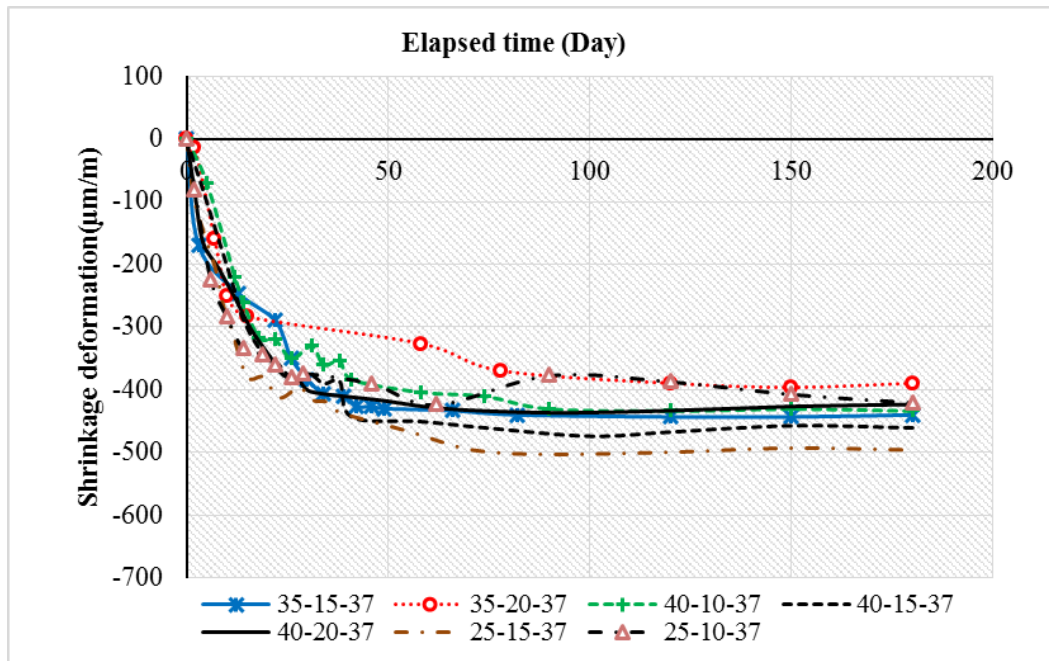


Figure 4-2. Variation of drying shrinkage with respect to time for mixtures made with w/cm of 0.37

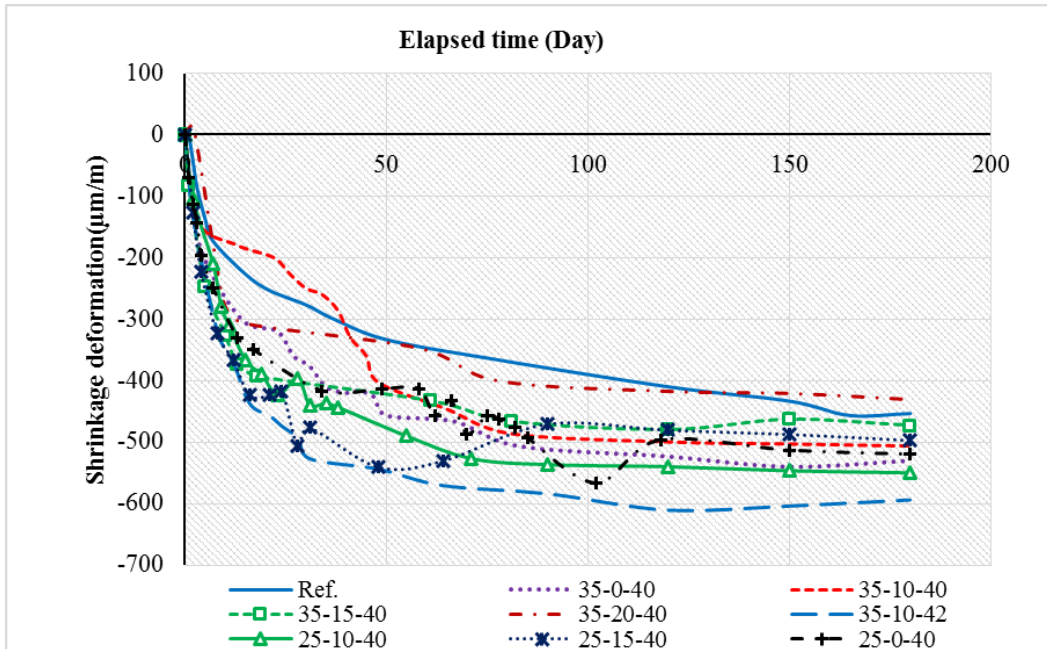


Figure 4-3. Variation of drying shrinkage with respect to time for mixtures made with w/cm of 0.40 and 0.42

The use of the TSMA did not lead to any clear or consistent effect on drying shrinkage. The performance of concrete proportioned using the TSMA varied with the mixture composition. It is interesting to note that drying shrinkage of the EMV specimens was significantly lower than that of mixture 25-0-40 proportioned with 0.4 w/cm and 25% fly ash. Both mixtures were made without fine RCA. This is due to the lower fresh paste content and higher aggregate amount available in the EMV specimens.

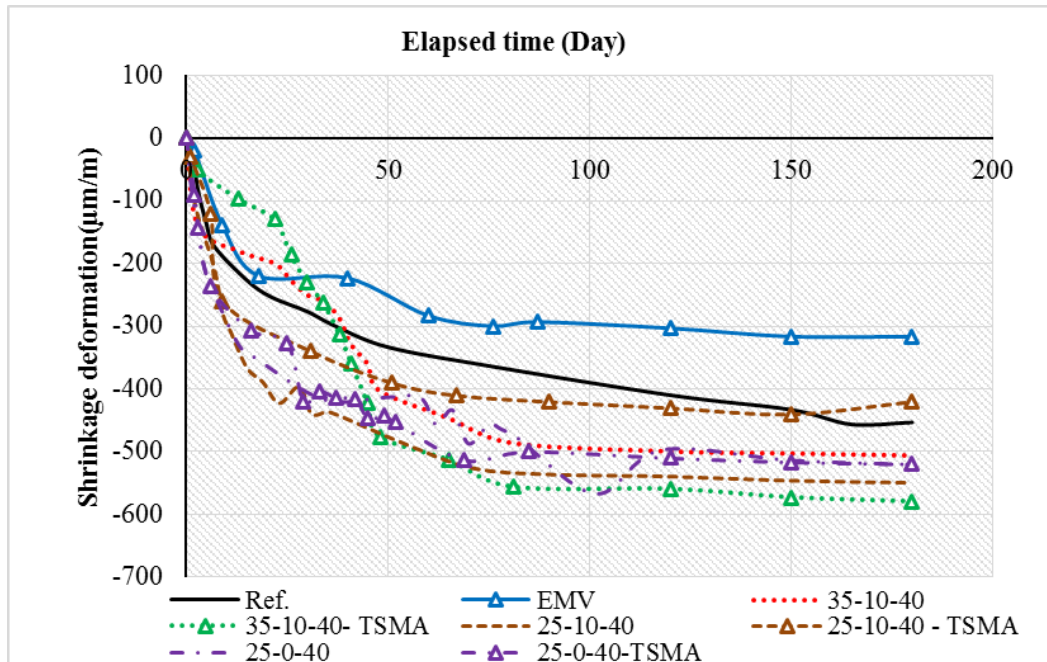


Figure 4-4. Variation of drying shrinkage with respect to time for mixtures made with the two-stage mixing approach and the equivalent mortar volume methods

4.1.5. Permeable void volume

The ASTM C642 method measures the volume of permeable voids of a concrete sample as a percentage of the volume. This method determines the water absorption after immersion in water at room temperature and after immersion in boiling water for five hours. The high temperature applied during the boiling affects both the viscosity and the mobility of the water molecules which enable the greater displacement of water within the pore system of the hardened concrete (CCAA 2009). For each concrete, two samples were used. A concrete cylinder was cut into half to have two cylindrical samples measuring 4 in. in diameter and 4 in. in height. The cut samples were oven dried at a temperature of 220 ± 10 °F (105 ± 5 °C) until reaching constant mass. The oven-dried concrete mass (A) was measured after cooling down to room temperature. The specimens were then immersed in water at room temperature until complete saturation. Then, the saturated surface dried (SSD) mass of the specimen was determined. After registering this weight (B), the specimens were immersed in boiling water for five hours, followed by a 14 hours period of rest to

cool down to room temperature. The SSD weight after boiling was measured (C). Finally, the submerged weight of specimens was determined (D). The following equations were used for measuring the absorption, density, and permeable void volume of the specimens:

$$\text{Bulk dry density } (g_1) = [A/(C-D)] \times \rho \times 100 \quad (4-2)$$

$$\text{Apparent density } (g_2) = [A/(A-D)] \times \rho \times 100 \quad (4-3)$$

$$\text{Permeable void volume } (\%) = (g_2 - g_1) / g_2 \times 100 \quad (4-4)$$

where ρ is the density of water equal to 1 g/cm^3

The values of the permeable void volume are summarized in Table 4-4. In general, the increase in the coarse RCA content from zero to 30% resulted in an increase in the permeable void volume from 10.7% to 11.1% at 91 days (Reference vs. 25-0-40). No significant spread in the permeable void was found, regardless of fly ash content, variations in fine RCA content, and the TSMA. As expected, mixture 35-10-42 made with w/cm of 0.42 had slightly higher void volume compared to the other mixtures prepared with lower w/cm. It should be noted that given the lower volume of fresh mortar, the EMV specimens had the lowest void volume at 56 and 91 days among the RCA mixtures.

4.2. Mechanical properties and durability of selected mixtures

4.2.1. General

Mixtures 35-10-40, 35-15-37, 40-20-37, 35-10-42, 25-15-40, and 25-10-37 were selected for further investigation. Mixture 25-10-40 was repeated using the TSMA to evaluate the effect of the two stage mixing approach on concrete performance (25-10-40-TSMA). The EMV method was also used to produce a concrete made with 30% replacement of coarse RCA by mass and with no RCA fine aggregate. The mixtures were made in two successive batches. The first batch

of 4 ft³ was used to sample for mechanical properties. The second batch of 3 ft³ was used to determine bleeding and sample specimens to evaluate durability.

Table 4-4. Volume of permeable void at different ages (%)

Mixture	56 days	91 days
Ref.	10.8	10.7
35-0-40	12.0	12.1
35-10-40	11.8	11.6
35-10-40-TSMA	12.0	11.8
35-15-40	12.1	11.5
35-20-40	11.7	11.4
35-15-37	11.9	11.7
35-20-37	11.6	11.2
40-10-37	12.4	11.5
40-15-37	12.3	12.0
40-20-37	11.9	11.6
35-10-42	12.5	12.1
25-10-40	11.3	11.2
25-10-40- TSMA	11.8	11.6
25-15-40	11.6	11.2
25-15-37	11.9	11.2
25-10-37	11.7	11.3
25-0-40	11.2	11.1
25-0-40- TSMA	11.3	11.2
EMV	10.9	10.6

It should be noted that the EMV mixture was initially prepared with the RCA replacement levels recommended by Fathifazl et al., (2009). However, the mixture was harsh due to low content of fresh mortar. Therefore, several mixtures with different RCA replacement levels were made to determine the maximum practical replacement that can be produced with adequate workability.

Based on the trial mixtures, the R value of 0.78 was selected for the use for the EMV mixture proportioning. This yields approximately 30% replacement ratio of RCA by mass of the total coarse aggregate. The total amount of fresh mortar that is available in the EMV mixture is 12.4% lower than that of the reference mixture. Therefore, 12.4% lower content of cementitious materials can be used compared to the reference concrete. The sand content and water amount of the EMV mixture was then decreased by 12.4%. The EMV mixture was proportioned with 0.4 w/cm and 25% Class C fly ash replacement. The total amount of coarse aggregate of the EMV mixture was 2042 lb/yd³ which is 13% more than the reference (MoDOT's PCCP) mixture.

4.2.2. Fresh properties

As presented in Table 4-5, the air contents of the investigated mixtures were within the targeted range of 6.0%±1.0 %, except for the 25-10-40-TSMA mixture where the air content was slightly higher. Slump values were also within the targeted range of 2.0±0.5 in. The mixture 35-10-40 and the 25-10-40-TSMA mixture had slump values of 3.5 and 4.0 in., respectively.

Table 4-5. Slump, air content, and unit weight of concrete mixtures

Mixture ID	Ref	35-10-40	35-15-37	40-20-37	35-10-42	25-15-40	25-10-37	25-0-40	25-10-40-TSMA	EMV
Air content (%)	5.5	5.2	5.5	5.3	5.3	5.2	6.0	5.9	8.5	5.5
Slump (in.)	2.5	3.5	2.0	2.0	2.5	2.0	1.5	1.5	4.0	1.0
Unit weight (pcf)	149.3	147.2	146.5	145.7	146.9	145.9	145.3	145.7	141.1	149.3

4.2.3. Mechanical properties

Compressive strength. The compressive strength results are summarized in Table 4-6.

Figure 4-5 compares the compressive strength results up to 91 days.

Table 4-6. Compressive strength results (psi)

Mixture ID	Ref.	35-10-40	35-15-37	40-20-37	35-10-42	25-15-40	25-10-37	25-0-40	25-10-40-TSMA	EMV
1 day	2875 (1.2*)	2935 (0.6)	2710 (0.4)	2510 (2.3)	2870 (1.8)	3225 (2.7)	3090 (2.0)	2710 (3.1)	3130 (1.8)	3540 (1.5)
7 days	5135 (5.8)	5170 (3.0)	5145 (1.0)	5500 (5.5)	4800 (1.9)	5455 (19.3)	4935 (1.3)	4950 (2.5)	4640 (5.4)	5240 (0.6)
28 days	6315 (7.3)	7560 (2.2)	7780 (1.0)	7030 (5.7)	6200 (23.4)	7185 (1.7)	7075 (2.5)	6105 (4.7)	5425 (2.9)	6050 (5.8)
56 days	6980 (4.4)	7710 (10.1)	7950 (1.5)	8075 (3.0)	7175 (8.2)	7600 (4.4)	7255 (2.3)	6765 (3.5)	5800 (4.1)	6475 (2.8)
91 days	7510 (2.3)	8220 (1.0)	7710 (5.9)	7875 (9.7)	7380 (7.2)	7300 (2.2)	7575 (0.6)	6955 (1.2)	5950 (1.3)	7065 (11.1)

*C.O.V. (%)

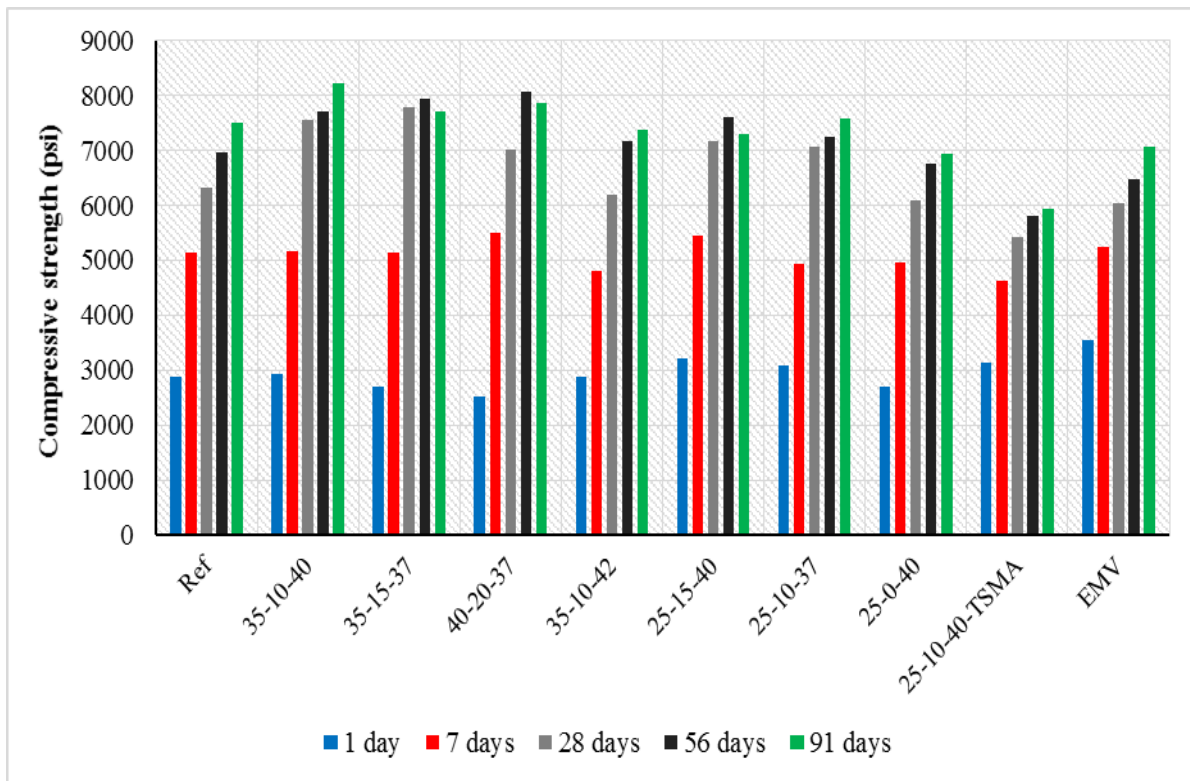


Figure 4-5. Compressive strength results

In general, results are in good agreement with data obtained in previous step, as presented in Table 4-2. A decrease of 7% in 91-day compressive strength was observed due to increase in the

coarse RCA content from zero to 30% (Reference vs. 25-0-40). It was observed that all the mixtures had 28-day compressive strength of higher than the target value of 4000 psi. The lowest values were observed in the case of the 25-10-40-TSMA mixture with 5425 psi at 28 days. This might be traced in the 8.5% air content of this mixture. A slight decrease in compressive strength was observed at 91 days in the case of mixtures 35-15-37, 40-20-37, and 25-15-40. This might be due to experimental error during the test. The highest results were observed in the case of mixtures 35-10-40, and 40-20-37 made with 35% and 40% of fly ash respectively. The EMV specimens had the highest initial strength values at the first day of testing.

Splitting tensile strength. The splitting tensile strength results are given in Table 4-7 .

Table 4-7. Splitting tensile strength results (psi)

Mixture ID	Ref.	35-10-40	35-15-37	40-20-37	35-10-42	25-15-40	25-10-37	25-0-40	25-10-40-TSMA	EMV
7 days	385 (4.3*)	405 (2.1)	390 (8.3)	400 (9.8)	405 (5.6)	365 (7.9)	460 (7.9)	395 (5.4)	405 (5.6)	535 (1.6)
28 days	505 (5.7)	480 (3.4)	520 (10.0)	505 (5.0)	540 (9.9)	520 (5.5)	500 (12.1)	470 (8.3)	445 (8.3)	550 (2.3)
56 days	560 (7.2)	555 (9.5)	490 (6.6)	585 (7.4)	480 (13.5)	510 (7.9)	505 (13.2)	525 (0.9)	470 (12.0)	585 (1.9)

*C.O.V. (%)

A slight decrease of 6% in 56-day splitting tensile strength was observed with the increase in coarse RCA from 0 to 30%. However, incorporation of up to 20% of fine RCA did not yield any significant effect on tensile strength. Figure 4-6 presents the splitting tensile strength results obtained for the mixtures up to 56 days of age. Mixture 40-20-37 and the EMV mixture had the best performance compared to the other mixtures (585 psi at 56 days). The 25-10-40-TSMA mixture had the lowest performance (470 psi at 56 days) compared to the rest of the mixtures, which could be due to the high air content of 8.5%.

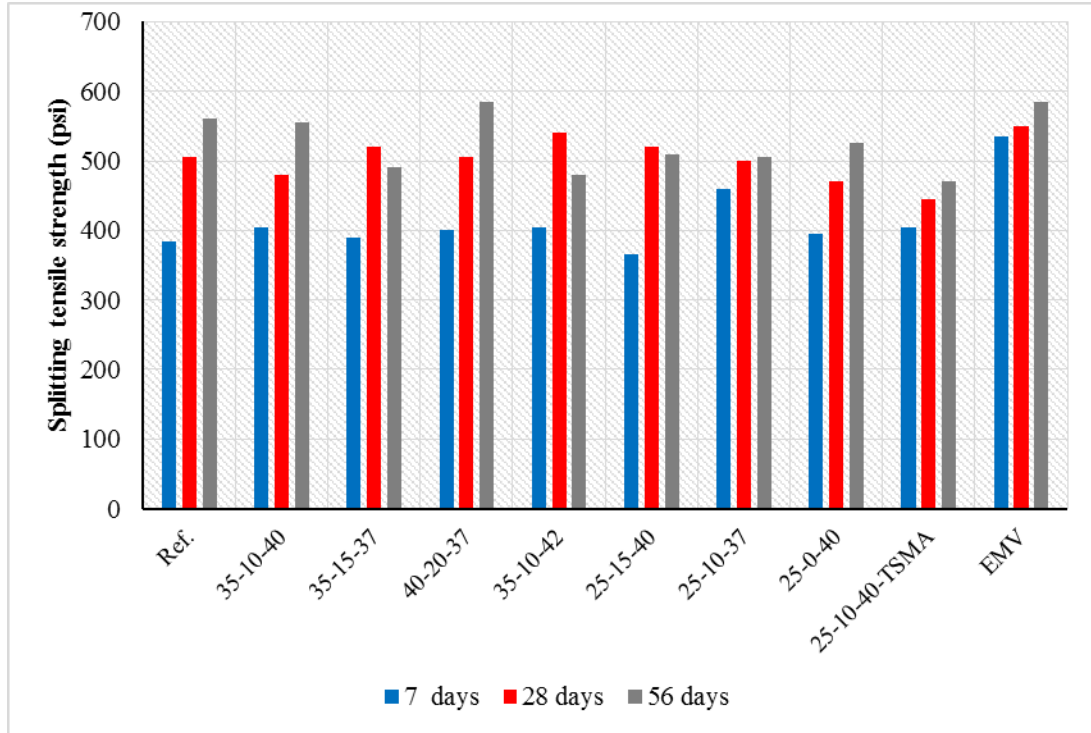


Figure 4-6. Splitting tensile strength results

Flexural strength. The flexural strength, was measured on 6×6×21 in. beams in accordance with ASTM C78. Two specimens were tested for each mixture. A four-point bending setup was used for testing the flexural strength. A schematic of the test setup is presented in Figure 4-7. Two rigid supports were located approximately 1.5 in. away from each side of the specimen. The load is applied on the concrete beam, and the failure load (P) is recorded. The flexural strength is then calculated using the following equation:

$$R = \frac{Pl}{bh^2} \quad (4-5)$$

where R = modulus of rupture (psi), P = the ultimate load (lb), l = span length equal to 18 in., b = average beam width at fracture (in.), and h = average beam height at fracture (in.).

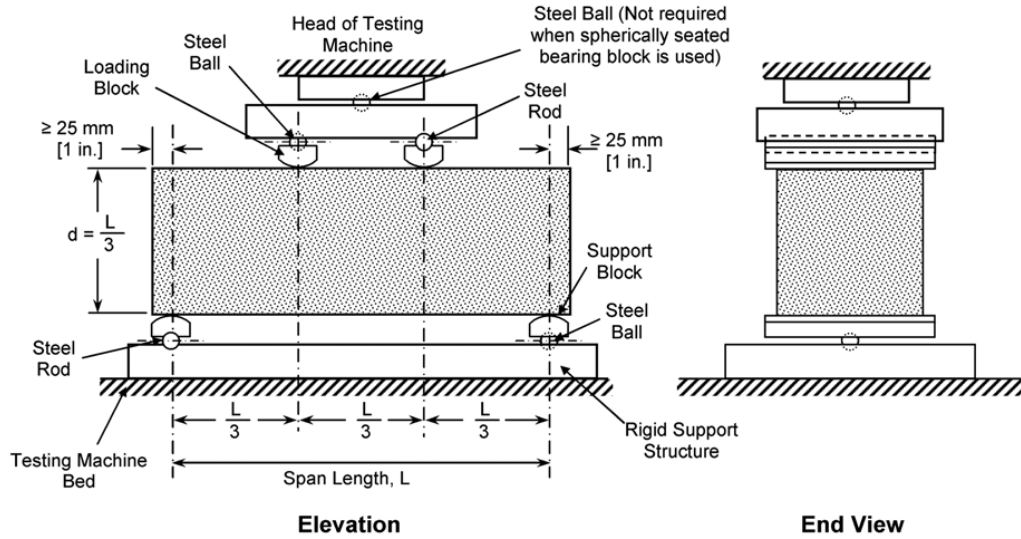


Figure 4-7. Simply supported beam for determining the flexural strength (ASTM C78)

Table 4-8 includes the flexural strengths.

Table 4-8. Flexural strength results (psi)

Mixture ID	Ref.	35-10-40	35-15-37	40-20-37	35-10-42	25-15-40	25-10-37	25-0-40	25-10-40-TSMA	EMV
28 days	655	605	805	665	605	685	855	640	735	770
56 days	795	675	805	725	640	700	845	755	700	880

A 5% decrease in flexural strength was observed as a result of increasing the coarse RCA content from zero (Reference) to 30% in the case of the mixture 25-0-40. All the mixtures had flexural strengths of higher than 600 psi at 28 days, as presented in Figure 4-8. The highest 56 day results were observed in the case of the EMV mixture. This might be due to the high amount of coarse aggregate and good aggregate interlock effect in this mixture. Mixtures 35-15-37, 40-20-37, and 25-10-37 made with w/cm of 0.37 had good flexural strength. The minimum results were observed in the case of the mixture 35-10-42 with 0.42 w/cm. A slight decrease in flexural

strength of the TSMA specimens was observed at 56 days. The flexural strength of the TSMA specimens is not really affected by the high air content of the fresh mixture.

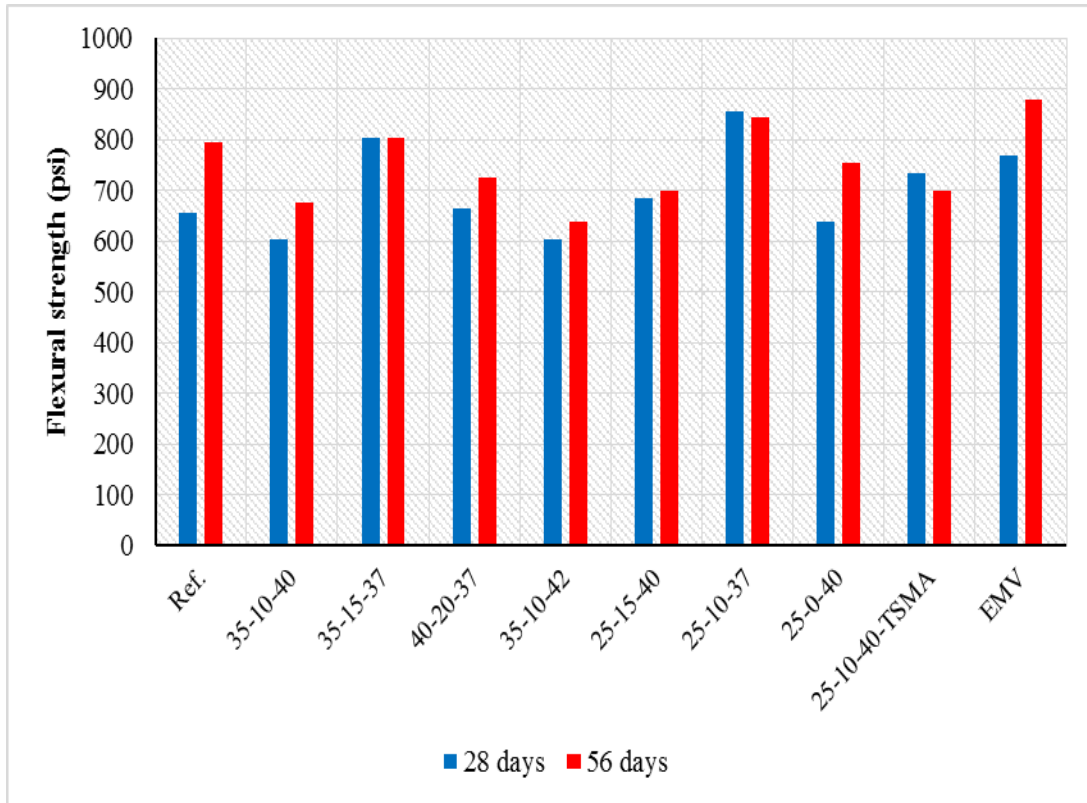


Figure 4-8. Flexural strength results

Modulus of elasticity. Table 4-9 includes a summary of the static modulus of elasticity (Young’s modulus) results. For each testing age, three 4×8 in. cylindrical specimens were used for determining the modulus of elasticity, according to ASTM C469. Specimen end surfaces were grinded to ensure uniform load distribution over the specimen surfaces. Figure 4-9 shows the test setup used for measuring the modulus of elasticity.



Figure 4-9. Modulus of elasticity test setup

The loading cycles were repeated three times for each sample. The vertical strain of the specimen corresponding to each stress level was measured using a LVDT system. The results were then used for determining the modulus of elasticity based on the following equation:

$$E = \frac{S_2 - S_1}{\varepsilon_2 - 0.000050} \quad (4-6)$$

where E = chord modulus of elasticity (psi), S_2 = stress corresponding to 40% of the ultimate load capacity, S_1 = stress corresponding to a longitudinal strain of 0.000050, and ε_2 = longitudinal strain caused by the stress S_2 .

Table 4-9. Modulus of elasticity results (ksi)

Mixture ID	Ref.	35-10-40	35-15-37	40-20-37	35-10-42	25-15-40	25-10-37	25-0-40	25-10-40-TSMA	EMV
28 days	5115 (3.4*)	5315 (3.0)	5300 (1.6)	5250 (1.0)	4950 (4.3)	5170 (3.0)	5200 (3.5)	4990 (2.7)	4835 (3.3)	5385 (5.9)
56 days	5880 (2.8)	5775 (1.8)	5450 (1.8)	5885 (1.3)	5385 (1.9)	5225 (3.4)	5050 (1.4)	5455 (1.6)	5285 (3.6)	5585 (5.4)

*C.O.V. (%)

Figure 4-10 compares the modulus of elasticity results obtained for different specimens at 28 and 56 days of age.

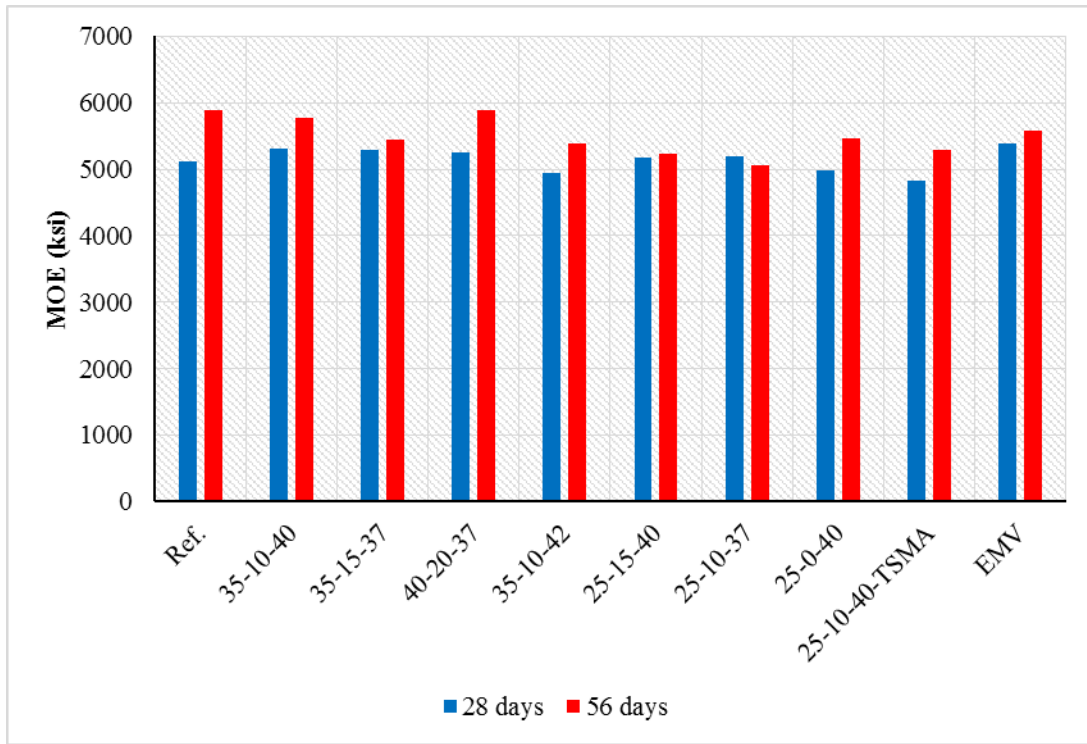


Figure 4-10. Modulus of elasticity results

All mixtures had modulus of elasticity results higher than 4500 ksi at 28 days, as presented in Figure 4-10. The reference concrete and the mixtures 40-20-37 and 35-10-40 had the highest modulus of elasticity results followed by the EMV mixture. The modulus of elasticity of concrete with 30% coarse RCA replacement (mixture 25-0-40) was 7% lower than the Reference concrete. The replacement of up to 15% sand by fine RCA did not lead to considerable drop in elastic modulus (4% decrease at 91 days). Similar results were observed in the case of mixture 40-20-37 made with 0.37 w/cm and 20% of fine RCA replacement.

4.2.4. DURABILITY

Table 4-10 summarizes the fresh properties of the mixtures prepared to sample specimens to evaluate durability.

Table 4-10. Slump, air content, unit weight, and bleeding of fresh concrete

Mixture ID	Ref.	35-10-40	35-15-37	40-20-37	35-10-42	25-15-40	25-10-37	25-0-40	25-10-40-TSMA	EMV
Air content (%)	5.3	5.1	5.3	5.0	5.2	5.3	5.9	5.6	7.0	6.0
Slump (in.)	2.0	3.0	2.5	1.5	3.0	2.5	1.5	2.5	3.0	1.5
Unit weight (pcf)	150.1	146.4	146.2	145.0	145.2	147.6	146.8	148.7	144.7	146.7
Accumulated bleeding water (g)	2.9	1.2	0.8	0	2.5	1.1	0	3.2	2.7	0.0
Accumulated bleeding water (g/in. ²)	0.03	0.01	0.01	0	0.03	0.01	0	0.03	0.03	0.0

The air content and slump results were within the targeted values of 6.0%±1.0 % and 2.0±0.5 in., respectively, except for the mixtures 35-10-42 and 25-10-40-TSMA with slump values 0.5 in. higher than the desired range. The amount of bleed water was monitored up to two hours. All mixtures had negligible bleed water, as reported in Table 4-10.

Surface electrical resistivity. Resistivity is a material property that quantifies the degree to which an object prevents the passage of an electrical current. While solid materials in concrete have a relatively high resistivity, capillary pores are partially to fully saturated with a concentrated alkaline solution that has a relatively low resistivity. Thus, electrical current flows primarily through the pore solution, thus providing an indirect measure of the quality of the microstructure. The Resipod resistivity meter with a uniform electrode spacing of 1.5 in. was used to measure the surface resistivity of 4×8 in. cylindrical concrete specimens. The Resipod is a resistivity meter operating on the principle of the Wenner probe. The Wenner probe consists of four equally spaced, co-linear electrodes placed in contact with a concrete specimen. An alternating current is applied to the outermost electrodes, and the voltage between the middle two electrodes is used to determine the resistance, as illustrated in Figure 4-11.

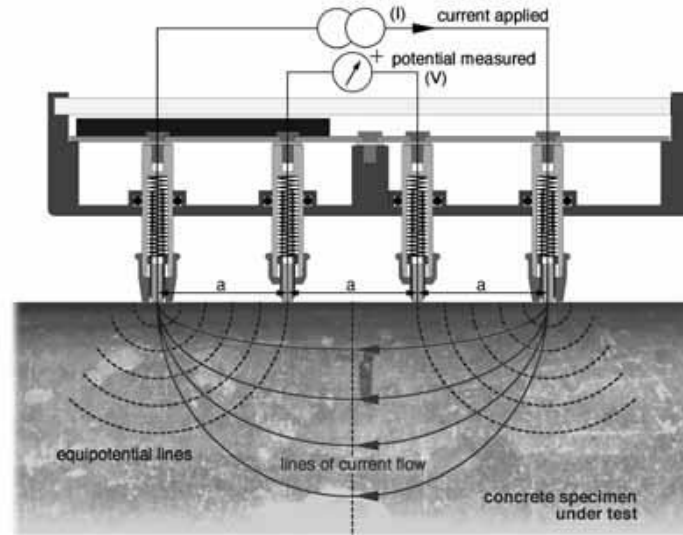


Figure 4-11. Schematic view of the surface resistivity measurement principles (Proseq SA 2013)

The sample resistivity is calculated from the resistance, the distance between the electrodes and the dimensions of the cylinder using the following equation:

$$\rho = 2\pi aV/I \quad (4-7)$$

where:

ρ = surface resistivity (k Ω cm), a = electrode spacing (1.5 in.), V = potential difference (V), and I = applied electric current

A correction factor of 1.1 was applied to the measurements for compensating the effect of lime-saturated water curing, according to AASHTO TP-95. Three 4×8 in. cylindrical specimens were used for determining the surface resistivity. The same specimens were tested at different ages to monitor the variations in electrical resistivity with time. The specimens were stored in lime-saturated water up to the test time. Before starting the test, specimens were rinsed to ensure proper measurements on a clean and wet surface.

Figure 4-12 shows the surface resistivity measurement. For each specimen, four separate readings were taken around the circumference of the cylinder at 90-degree increments (0°, 90°, 180°, and

270°). Measurements were repeated several times at each angle for the most reliable reading.

Table 4-12 summarizes the results of the surface resistivity measurements. Figure 4-13 shows the surface resistivity data obtained for the specimens up to 91 days of age.



Figure 4-12. Surface resistivity measurement

Chini et al. (2003) conducted a comprehensive study in collaboration with the Florida Department of Transportation (FDOT) to correlate the surface resistivity to other electrical resistivity test methods such as the rapid chloride ion permeability test (RCPT) as presented in Table 4-11.

Several types of concrete mixtures made with different types and contents of SCMs were studied.

Table 4-11. Correlation between the surface resistivity and chloride ion permeability

Chloride ion permeability	RCPT test	Surface resistivity (kΩcm)	
	Charge passed (Coulomb)	28 days	91 days
High	>4000	<12	<11
Moderate	2000-4000	12-21	11-19
Low	1000-2000	21-37	19-37
Very low	100-1000	37-254	37-295
Negligible	<100	>254	>295

Table 4-12. Surface electrical resistivity measurements (kΩcm)

Mixture ID	Ref.	35-10-40	35-15-37	40-20-37	35-10-42	25-15-40	25-10-37	25-0-40	25-10-40-TSMA	EMV
28 days	12.9	11.9	12.1	12.1	11.4	10.1	11.0	11.9	7.6	8.1
56 days	15.3	14.3	14.6	14.7	13.0	12.5	13.2	15.1	8.7	11.4
91 days	22.5	19.9	22.0	21.1	18.4	17.2	18.7	21.3	9.0	13.9

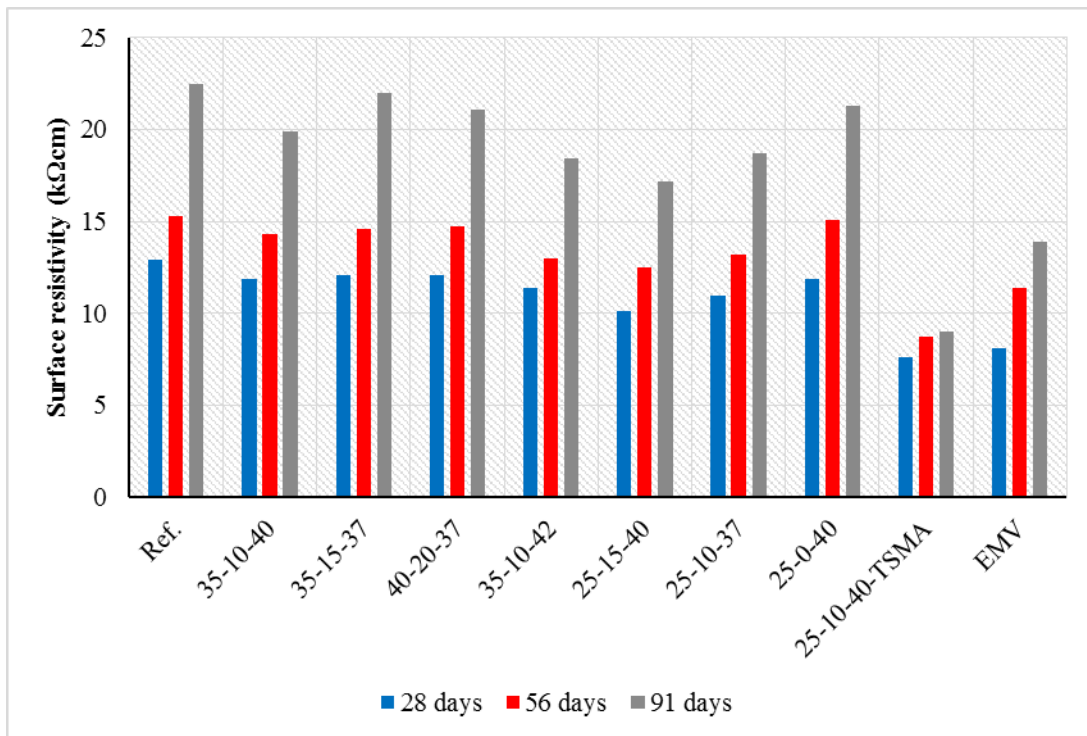


Figure 4-13. Surface resistivity results

The Reference concrete made without any RCA had 5% higher surface resistivity compared to the mixture 25-0-40 made with 30% RCA. A 24% decrease in 91-day surface resistivity was observed as a result of 15% fine RCA replacement in mixture 12 while compared to the Reference concrete.

Based on the criteria presented in Table 4-11, all the mixtures exhibited high chloride permeability at 28 days. Except for the mixtures 35-15-37 and 40-20-37 with resistivity values slightly higher than 12 kΩcm that can be classified as the Moderate permeability.

At the age of 91 days, mixtures 35-10-40, 35-15-37, and 40-20-37 had resistivity values higher than 19 kΩcm, which correspond to Low chloride ion permeability based on the criteria introduced in Table 4-11. Rest of the mixtures had Moderate chloride permeability, except for the 25-10-40-TSMA which can be classified as High chloride permeability.

Bulk electrical resistivity. Besides the surface resistivity, the bulk electrical conductivity of the specimens was measured. The same samples used for surface resistivity testing were used for measuring the bulk conductivity, according to ASTM C1760. In order to conduct this test, it is necessary to place pieces of wet foam on the top and bottom of the specimen, between the concrete surface and the metal plates of the test setup. The foam ensures proper electrical contact with the concrete. However, depending on the moisture condition, these foam pieces may have some electrical resistivity that should be taken into account to determine the true value of the sample's bulk resistivity. Figure 4-14 presents the three steps required for bulk resistivity measurements.

First, the resistivity of the upper foam should be determined (R_{upper} , kΩcm). The bottom foam is then placed between the plates, with the specimen on the top plate to simulate the effect of the weight of the specimen on foam thickness and porosity. The resistivity of the bottom foam is recorded (R_{lower} , kΩcm). Finally, the bulk resistivity of the sample with foam at top and bottom is measured ($R_{measured}$, kΩcm). The net bulk resistivity of the sample can be calculated as follows:

$$R_{cylinder} = R_{measured} - R_{upper} - R_{lower} \quad (4-8)$$

The bulk resistivity results are presented in Table 4-13. Results are in good agreement with the surface resistivity values. The reference mixture had higher bulk resistivity values compared to the other mixtures. A 6% decrease in bulk resistivity was observed as a result of 30% increase in coarse RCA content in mixture 25-0-40. Again, the 25-10-40-TSMA had the lowest resistivity compared to the other mixtures. The bulk resistivity of the EMV mixture was 20% and 15% lower than the reference specimens and mixture 25-0-40, respectively.



Figure 4-14. Measuring bulk electrical resistivity

Table 4-13. Bulk electrical resistivity (kΩcm)

Mixture ID	Ref.	35-10-40	35-15-37	40-20-37	35-10-42	25-15-40	25-10-37	25-0-40	25-10-40-TSMA	EMV
28 days	12.6	11.4	10.8	12.0	11.2	9.5	10.4	12.1	7.7	9.3
56 days	17.4	13.6	13.6	14.8	13.3	10.9	12.0	16.3	9.3	12.7
91 days	23.2	21.8	22.5	24.2	20.3	17.9	19.6	21.7	11.6	18.5

Permeable void volume. The permeable void results are summarized in **Table 4-14**. The void volume of each mixture is the mean of the two samples. Results are in agreement with the data obtained during the first step of laboratory investigation, as presented in **Table 4-4**. The 91-day void volume increased from 10.8% to 11.1% due to the increase in coarse RCA content from 0 to 30%. The 91-day void volume also increased from 11.1% to 11.6% due to increase in the fine RCA content from 0 to 15%. For all concrete mixtures, decrease in void volume was observed as a function of increase in age.

Table 4-14. Permeable void volume (%)

Mixture ID	Ref.	35-10-40	35-15-37	40-20-37	35-10-42	25-15-40	25-10-37	25-0-40	25-10-40-TSMA	EMV
28 days	11.5	11.7	11.2	11.9	12.1	12.0	10.7	11.4	11.2	10.1
56 days	11.1	11.6	11.6	11.5	12.3	11.7	11.0	11.4	10.9	10.8
91 days	10.8	11.4	11.5	11.5	11.8	11.6	10.9	11.1	11.2	10.7

Freeze and thaw resistance. Prismatic samples measuring 3×4×16 in. were used to determine the frost durability of concrete according to ASTM C666, Procedure A. The prisms were cured in lime-saturated water for four weeks before the start of the freezing and thawing cycles. It is important to note that the period of water curing of the standard test is 14 days; however, given the use of a minimum 25% fly ash replacement, the initial duration of water curing was increased to 28 days. The prisms were subjected to 300 freezing and thawing cycles. After every 36 cycles, the specimens were removed, and the dynamic modulus of elasticity of the concrete was determined using the ultrasonic pulse velocity test, as is illustrated in Figure 4-15.



Figure 4-15. Freezing and thawing cabinet (left); measurement of pulse velocity (right)

A drop in durability factor reflects the presence of internal cracking of the concrete due to damage from repetitive frost cycles. Durability factor values greater than 80% after 300 cycles of freezing and thawing reflect adequate frost durability. The variations of the dynamic modulus of elasticity with respect to the freeze/thaw cycles are presented in Table 4-15 and Figure 4-16.

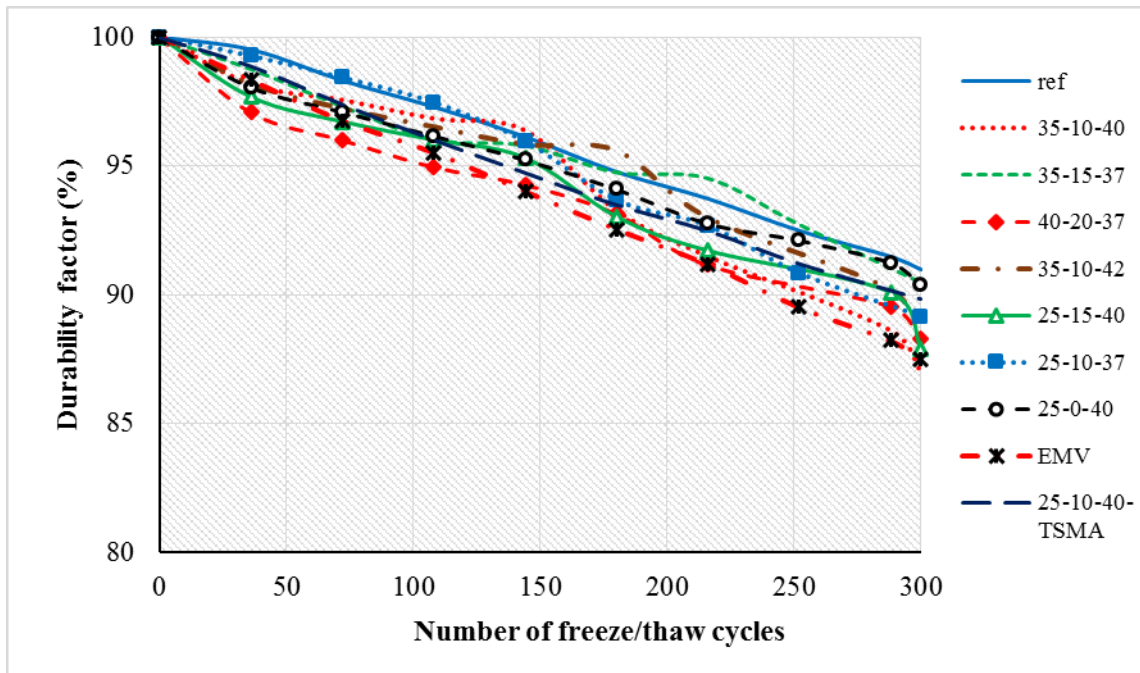


Figure 4-16. Variation of durability factor as a function of freeze/thaw cycles

Table 4-15. Variations in durability factor of specimens after 300 cycles

Mixture ID	Ref.	35-10-40	35-15-37	40-20-37	35-10-42	25-15-40	25-10-37	25-0-40	25-10-40-TSMA	EMV
DF (%)	91	87	90	88	88	88	89	90	90	87

All the mixtures exhibited good frost resistance with durability factors higher than 88% by the end of test cycles. No difference was observed as a result of 30% coarse RCA replacement in mixture 25-0-40 compared to the Reference. Durability factor of 88% in the case of mixture 40-20-37 indicates that using up to 20% fine RCA does not have a significant effect on frost durability. Similar performance was observed in the case of mixtures 35-10-40 and 35-10-42 with w/cm of 0.4 and 0.42 and durability factors of 87% and 88%, respectively. Both the EMV and 25-10-40-TSMA mixtures had acceptable frost resistance with durability factors of 87% and 90% respectively.

De-icing salt scaling. De-icing salt scaling can result in mortar flaking and surface spalling of non-air-entrained concrete during frost conditions. The de-icing salt scaling was determined in accordance with ASTM C672. Slabs with minimum surface area of 72 in.² and minimum thickness of 3.0 in. are recommended for this test. A dike is placed on the finished surface of the specimen. This dike is used for ponding the surface of the specimen with a solution of calcium chloride with a concentration of 4.0%. The specimens were subjected to 50 cycles of freezing and thawing. The top surface of the slab was washed, and the damage was assessed after each five cycles. The level of deterioration was rated in a qualitative manner from zero to four according to the criteria presented in Figure 4-17. Examples of surface appearance corresponding to each rating are given in Figure 4-17.

Mixtures made with various amounts of fly ash replacement (25% to 40%) and fine RCA contents varying from 0 to 20% were investigated. The TSMA and the EMV specimens were also investigated. For each concrete, three slabs measuring 3×10×11 in. were cast. The specimens were cured in lime-saturated water for 28 days. It should be noted that ASTM C672 recommends moist curing period of two weeks, followed by air drying for two weeks before testing. However, the moist curing period was extended to four weeks followed by two weeks of air drying at 70±5 °F (21±3 °C) and 50%±5% relative humidity to ensure greater hydration of fly ash used in the concrete mixtures. The specimens were then carefully transported to the MoDOT material laboratory in Jefferson City, Missouri, to carry out testing.

The results of de-icing salt scaling are presented in Table 4-16. Sample photos taken after 50 cycles of de-icing salt scaling are presented in Figure 4-18. Concrete mixtures 35-10-42 and 35-10-40 made with 35% fly ash and w/cm of 0.42 and 0.4 respectively, had de-icing salt scaling rate of 5 (severe scaling). Mixtures 25-15-40 and 25-10-37 made with 25% fly ash and w/cm of 0.4 and 0.37 respectively, had de-icing salt scaling rating of 4 (moderate to severe scaling). Mixtures 35-15-37 and 40-20-37 with 0.37 w/cm and fly ash content of 35% and 40% respectively, had de-icing salt scaling rating of 5 (severe scaling). The TSMA specimens made with 25% fly ash and 10% fine RCA had the best performance (rating 1, no scaling) followed by the EMV specimens with rating 2 (very slight scaling).

Table 4-16. De-icing salt scaling rating of investigated mixtures

Mixture ID	35-10-40	35-15-37	40-20-37	35-10-42	25-15-40	25-10-37	25-10-40-TSMA	EMV
5 cycles	1	1	1	2	1	1	1	1
10 cycles	3	3	4	4	1	2	0	1
15 cycles	3	3	4	5	3	3	1	1
20 cycles	4	4	5	5	3	3	1	2
25 cycles	4	4	5	5	3	3	1	2
30 cycles	4	4	5	5	3	4	1	2
35 cycles	4	4	5	5	3	4	1	2
40 cycles	4	5	5	5	4	4	1	2
45 cycles	4	5	5	5	4	4	1	2
50 cycles	5	5	5	5	4	4	1	2







Rating	0	1
Condition of Surface	No scaling	Very slight scaling
Typical surface appearance		
Rating	2	3
Condition of Surface	Slight to moderate scaling	Moderate scaling
Typical surface appearance		
Rating	4	5
Condition of Surface	Moderate to severe scaling	Severe scaling
Typical surface appearance		

Figure 4-17. Rating scale for scaling resistance

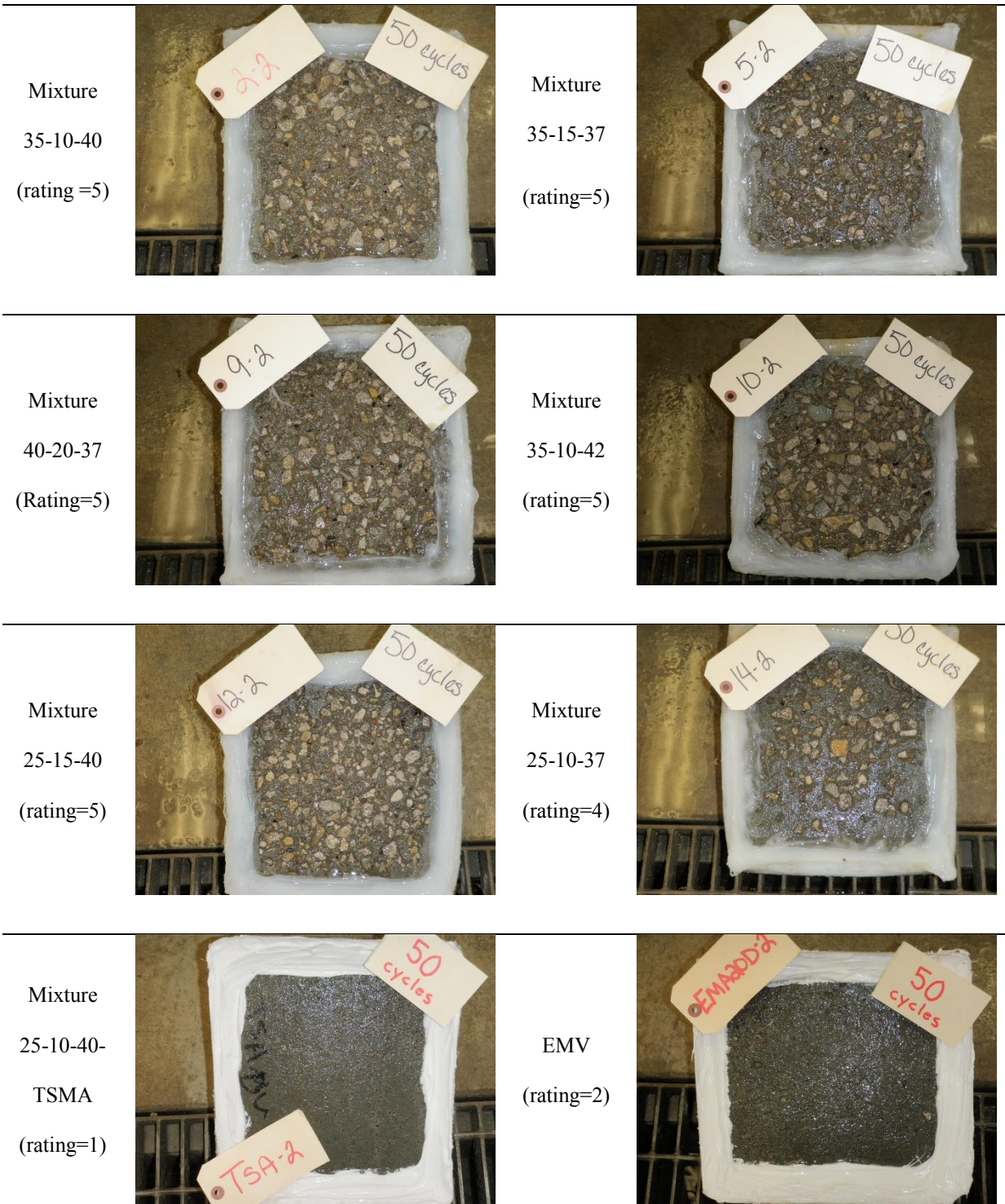


Figure 4-18. Appearance of the top surfaces after 50 cycles of deicing salt seiling test

4.3. Summary and conclusion

Based on the data obtained through the laboratory investigations, the following conclusions are made:

- Increasing the fine RCA content from zero up to 20% had no significant effect on compressive strength. The increase in fly ash replacement level from 25% to 40% led to average of 24% decrease in the compressive strength at early age (one day strengths). However, this was not the case for later ages and average reduction in strength was limited to 3% at 91 days. Concrete made with the EMV method exhibited compressive strength higher than the targeted value of 4000 psi at 28 days.
- No significant difference in splitting tensile strength was noticed as a result of incorporating fine RCA. Increasing the fly ash from 25 % to 40% did not have a significant effect on tensile strength. The EMV specimen had the highest splitting tensile strength value. Similar trend was observed in the case of the flexural strength results.
- All mixtures exhibited modulus of elasticity values of greater than 4500 ksi at 28 days. The replacement of up to 15% sand by fine RCA did not lead to considerable drop in elastic modulus (4% decrease at 91 days). Similar results were observed in the case of mixture 40-20-37 made with 0.37 w/cm and 20% of fine RCA replacement.
- Results were consistent in the case of the surface and bulk electrical resistivity measurements. The minimum values were observed in the case of the TSMA and the EMV specimens. Rest of the mixtures proved to have Low and/or Moderate permeability index at 91 days.

- All mixtures had good resistance to freeze/thaw cycles with durability factors higher than 88%. No difference was observed as a result of 30% coarse RCA replacement. Durability factor of 88% in the case of mixture 40-20-37 indicates that using up to 20% fine RCA does not have a significant effect on frost durability. Both the EMV and 25-10-40-TSMA mixtures had acceptable frost resistance with durability factors of 87% and 90% respectively.
- Specimens made with the EMV method and the 25-10-40-TSMA, proportioned with 0.4 w/cm and 25% fly ash had the best resistance to deicing salt scaling. The remaining mixtures had damage due to deicing salt scaling test. Incorporating fine RCA and higher volume of fly ash may be the reason for this observations.

5. Field implementation

5.1. Project overview and objectives

This chapter includes a summary of performance of four concrete mixtures used for the casting of the approach pavement to the Stan Musial Veterans Memorial Bridge in St. Louis that was undertaken on April 29, 2013 by the Missouri Department of transportation (MoDOT). The field demonstration involved the construction of a 22.5-ft wide ramp approach (outside lane and shoulder) from the Cass Ave. stub out to the EB Parkway Bridge over I-70 in St. Louis. The first part of the section was used to cast the control, or reference, concrete pavement using conventional MoDOT pavement concrete. The experimental sections made with RCA were cast afterward till to the end of the length of the lane and shoulder in three different sections. Approximately 600 cubic yards of experimental and reference concrete mixtures were used in this field evaluation. Figure 5-1 shows a general view of the ramp approach with the reference concrete section already in place.

An extensive campaign of sampling and testing was carried out by MoDOT and Missouri S&T to evaluate fresh and mechanical properties of the concrete as well as shrinkage and key durability characteristics. Short-term and long-term performance of the concrete is evaluated using embedded sensors to monitor variations in temperature and deformation in the pavement over time. The sensors were also used to evaluate the response of pavement sections to controlled traffic loading.



Figure 5-1. General view of the ramp approach with the reference section already in place

5.2. Concrete mixture and material properties

Concrete was produced at the Millstone Bangert batching plant shown in Figure 5-2. The batching plant was located at Lambert Airport area in St. Louis, 30 minutes from the job site. The batching plant was a 12 yd³ portable central mix. Concrete was mixed for one minute in the drum with maximum speed of 15 rpm. Concrete batches were produced and hauled in 8 yd³ deliveries.

Table 5-1 summarizes the properties of the reference and the three mixtures made with RCA. The w/cm was kept constant at 0.40, and the sand-to-aggregate ratio was fixed at 0.42, by volume. Three of the mixtures were produced according to the normal (automatic controlled) mixing sequence used at the Millstone Bangert batching plant. On the other hand, one of the mixtures made with 30% RCA replacement was produced using the two stage mixing approach (TSMA). In order to produce the concrete with TSMA, the batching plant had to operate in a manual mode. In this case, the RCA was first loaded to the mixing drum along with the

cementitious materials. After one minute of mixing, half of the mixing water was introduced and allowed to mix for one minute to coat the RCA particles with a rich cement paste. The rest of the materials were then loaded followed by two minutes of mixing.

Table 5-1. Mixture proportions of concrete used in field study

Mixture type	Reference	30% RCA	30% RCA-TSMA	40% RCA
Cement Type I (lb/yd ³)	409	409	409	409
Class C fly ash, by mass (%)	25	25	25	25
Fly ash (lb/yd ³)	136	136	136	136
Cementitious materials (lb/yd ³)	545	545	545	545
Water (lb/yd ³)	218	218	218	218
w/cm	0.40	0.40	0.40	0.40
Sand (lb/yd ³)	1338	1338	1338	1338
Sand/Aggregate, by volume (%)	42.5	42.5	42.5	42.5
Coarse virgin aggregate (lb/yd ³)	1811	1268	1268	1268
Coarse RCA (lb/yd ³)	-	509	509	679
RCA, by mass (%)	-	30	30	40

5.3. Experimental program of the field evaluation

5.3.1. Fresh properties

Two groups worked simultaneously at the job site and at the batching plant to sample and test the fresh concrete properties of the four concrete mixtures.

Batching plant sampling. In order to monitor the variations in fresh concrete properties with time, a group of Missouri S&T students and staff was present at the batching plant prior to concrete delivery and casting. Slump value and air content of the produced mixtures were

determined initially after the batching process (Figure 5-2). Concrete samples were tested at 15 and 30 minutes to evaluate fresh properties. Table 5-2 presents fresh properties of mixtures produced at the batching plant. Variations in fresh properties of the concrete with respect to time are presented in Figure 5-3 and Figure 5-4.

Table 5-2. Fresh properties of concrete mixtures at the batching plant

Test	Time	Reference	30% RCA	30% RCA-TSMA	40% RCA
Slump (in.)	initial	2.75	3.0	4.0	2.5
Air (%)		8.5	8.3	9.5	8.0
Slump (in.)	After 15 minutes	1.5	2.0	2.5	1.5
Air (%)		8.0	6.0	9.0	7.5
Slump (in.)	After 30 minutes	0.75	1.0	2.25	1.0
Air (%)		6.5	6.5	8.5	6.5



Figure 5-2. Photos of fresh property tests at the batching plant

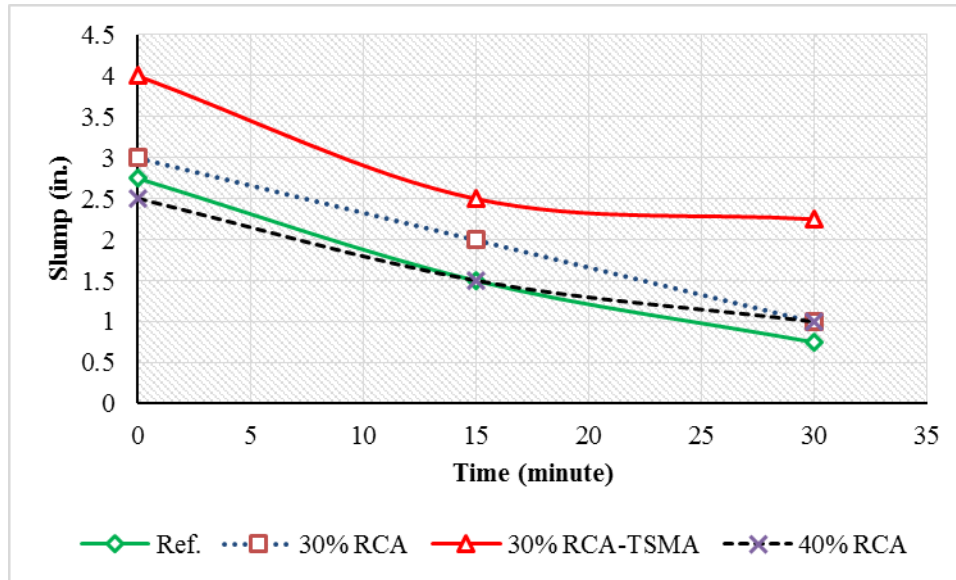


Figure 5-3. Variation in slump during the simulated transport period at the concrete batching plant

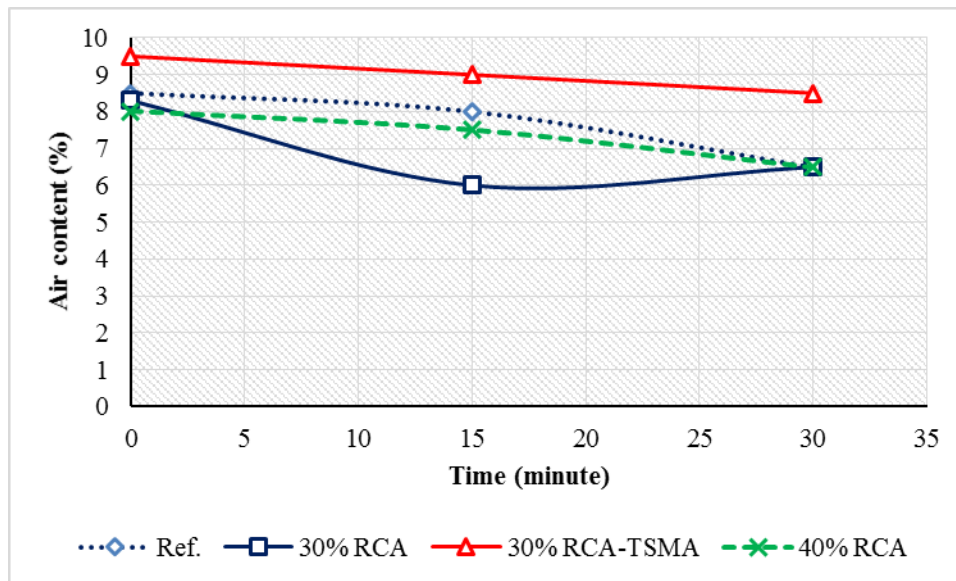


Figure 5-4. Variation in air content during the simulated transport period at the concrete batching plant

All mixtures had initial slump values slightly higher than the desired maximum of 2.5 in., except for the 40% RCA mixture. The slump after 30 minutes was within the targeted range of 2.0 ± 0.5 in. for the 30% RCA-TSMA mixture, while the rest of the mixtures exhibited slump

values about 0.5 in. less than the desired value. All mixtures exhibited similar rate of slump loss, except for the 30% RCA-TSMA mixture.

The initial air content varied from 8.0% to 9.5%. However, the air contents decreased to about 6.5% for the reference, 30% RCA, and 40% RCA mixtures at 30 minutes. The air content at 30 minutes of the 30% RCA-TSMA mixture was 8.5%.

Work at the job site. Samples were taken from the concrete during casting to monitor the fresh properties of the both the reference and the experimental mixtures as shown in Figure 5-5. Slump, unit weight, and air content were determined and are reported in Table 5-3.

Samples were also taken for determining the bleeding potential of the concrete. No bleeding was observed in any of the tested mixtures.

Table 5-3. Fresh properties of mixtures sampled at the job site

Test	Reference	30% RCA	30% RCA-TSMA	40% RCA
Slump (in.)	1.5	1.3	2.0	1.3
Air content (%)	5.5	6.5	8.0	6.5
Unit weight (lb/yd ³)	149	145	140	143

All the slump values were within the desired range of 2.0±0.5 in. The measured air content of the 30% RCA-TSMA was higher than the targeted range. Rest of the mixtures had air contents within the desired range.



Figure 5-5. Photos of fresh property testing at job site

5.3.2. Sampling for laboratory investigation

Several samples were taken by Missouri S&T and MoDOT staff to determine the mechanical properties, shrinkage, and durability characteristics (Figure 5-6). MoDOT samples were rodded, while those sampled by Missouri S&T were consolidated using a vibrating table. Table 5-4 summarizes the sampling and testing program.

Table 5-4. Sampling and testing program performed on the job site

PROPERTY	TEST METHOD	MISSOURI S&T	MoDOT
Compressive strength, 4×8 in. cylinders, (1, 7, 28, 56, and 91 d)	ASTM C 39		✓
Splitting tensile strength, 4×8 in. and 6×12 cylinders, (7, 28, and 56 d)	ASTM C 496	✓	✓
Flexural strength, 3.5×4.5×16 in. beams (28 and 56 d)	ASTM C 78		✓
Modulus of elasticity, 4×8 in. and 6×12 cylinders, (28, 56 d)	ASTM C 469	✓	✓
Drying shrinkage, 3×3×11.25 in. prisms	ASTM C 157	✓	
Abrasion resistance, 6 in. diameter core samples (170 d)	ASTM C799, C	✓	
Permeable void ratio, 4×8 in. cylinders	ASTM C 642	✓	
Rapid chloride ion permeability, 4×8 in. cylinders, (28, 56, and 91 d)	ASTMC 1202, AASHTO T277		✓
Freeze thaw resistance, procedure A: 3×4×16 in. prisms, Procedure B: 3.5×4.5×16 in. prisms	ASTM C 666, A and B	✓	✓
Coefficient of thermal expansion, 4×8 in. cylinders (2 and 11 months)	AASHTO T336		✓

Specimens were stored at the job site under wet burlap and plastic cover for 24 hours before transport to the Advanced Construction Materials Laboratory (ACML) of the Center of Infrastructures Engineering Studies (CIES) at Missouri S&T. The specimens were then demolded and the cured with temperature of 70±5 °F (21±3°C) up to the age of testing. The same was done for samples taken by MoDOT where specimens were transported to MoDOT’s State Materials Laboratory for curing and testing.



Figure 5-6. Sampling at the job site

Compressive strength. Compressive strength results of 4×8 in. cylindrical specimens tested up to 91 days are summarized in Table 5-5. Figure 5-7 presents the variations in the compressive strength with respect to time.

Table 5-5. Compressive strength results (psi), 4×8 cylinders, MoDOT lab

Mix.	Reference			30% RCA			30% RCA-TSMA			40% RCA		
	Avg.	σ^*	C.O.V. (%)	Avg.	σ	C.O.V. (%)	Avg.	σ	C.O.V. (%)	Avg.	σ	C.O.V. (%)
1 day	2640	128	4.8	2360	162	7.0	1910	229	12.0	2030	105	5.0
7 days	4610	168	3.6	4050	241	6.0	3370	268	8.0	4100	115	3.0
29 days	5450	64	1.2	4740	191	4.0	4150	119	2.9	4830	229	5.0
56 days	5660	208	3.7	5260	535	10.0	4600	114	2.48	5380	361	7.0
91 days	6180	139	2.2	5770	230	4.0	4910	100	2.03	5440	167	3.0

* Standard deviation

The compressive strength of the reference concrete was 7% and 13% higher than that of mixtures made with 30% and 40% RCA replacements at 91 days, respectively. In the case of specimens made with 30% RCA replacement prepared using the TSMA, the compressive strength was 25% lower than the reference at 91 days. Such a behavior was not observed in the case of the laboratory investigated TSMA mixtures.

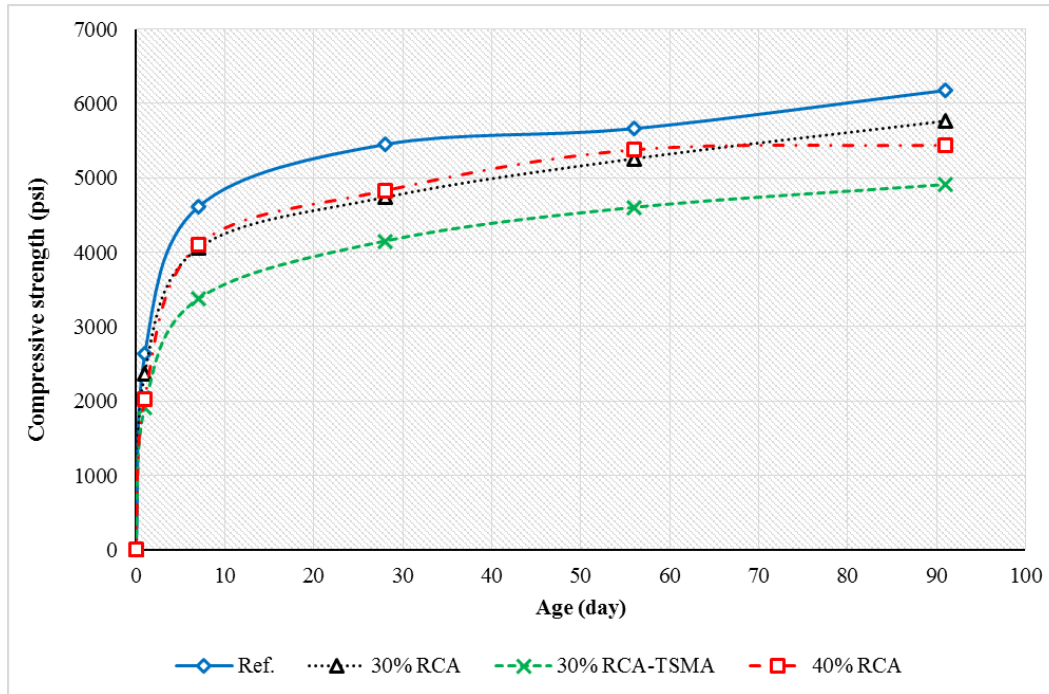


Figure 5-7. Variation of compressive strength with respect to time

The lower strength of the TSMA specimens is contradictory to investigation carried out by Ryu (2002) where an increase in compressive strength of 17% was observed by using the two stage mixing method. Outsuki et al., (2003) also reported up to 13% increase in compressive strength as a result of double mixing method. Tam et al., (2005, 2007-9) reported beneficial effects of TSMA for improving the compressive strength of RCA-made concrete mixtures as well. The low w/c paste, which is formed during the initial stage of the mixing process, can enhance the quality of the ITZ, and thus improving hardened properties. However, with an extended transportation time in truck, it seems that the positive effects observed in the laboratory investigations may dissipate. This may be through the continuous water movement between the initially formed low w/c paste and the rest of the mixture which affects the "dense ITZ" that is supposed to be formed with the two stage mixing approach. It also should be noted that the air content of the 30%RCA-TSMA mixture measured at the job site was 8.0% compared to the 5.5% value determined for

the reference concrete. The spread in air content of 2.5% is considerable and can, at least in part, be the reason for the inferior properties of the 30% RCA-TSMA compared with the reference concrete. The 91-day compressive strength of the 30%RCA-TSMA concrete was 15% lower than that of the mixture made also with 30% RCA replacement prepared using the normal batching and mixing approach. The air content of the 30% RCA was measured 6.5%, i.e. 1.5% lower than the 30%RCA-TSMA mixture. Concrete made with 30% and 40% RCA replacements exhibited the same strength up to 56 days (both mixtures had 6.5% fresh air volume). However, at 91 days, the compressive strength of the concrete with 30% RCA was slightly (6%) higher than that of 40% RCA specimens. This may be due to the potential micro-cracks available in residual mortar attached to the RCA particles.

Splitting tensile strength. Table 5-6 and Figure 5-8 summarize the splitting tensile strength results. At 28 days, the splitting tensile strengths of the reference specimens were slightly (4%) higher than the 30% and 40% RCA mixtures. Concrete made with 30% RCA-TSMA had the lowest results at 28 and 56 days of 415 and 385 psi, respectively, which might be due to the higher air content in the mixture of 8%.

Table 5-6. Splitting tensile strength results, 6×12 cylinders, MoDOT lab

Mixture	Reference		30% RCA		30% RCA-TSMA		40% RCA	
Age (day)	Avg. (Psi)	F _t /F' _c (%)	Avg. (Psi)	F _t /F' _c (%)	Avg. (Psi)	F _t /F' _c (%)	Avg. (Psi)	F _t /F' _c (%)
7	425	9.3	375	9.3	340	10.13	435	10.6
28	460	8.4	440	9.3	415	9.97	440	9.2
56	480	8.5	500	9.5	385	8.36	490	9.2

At 56 days, the splitting tensile strength of the specimens made with 30% and 40% of RCA replacements were slightly (up to 4.0%) higher than the reference concrete. For all the mixtures, the ratio of the splitting tensile strength to the corresponding compressive strength was varying from 8% to 10% at all ages.

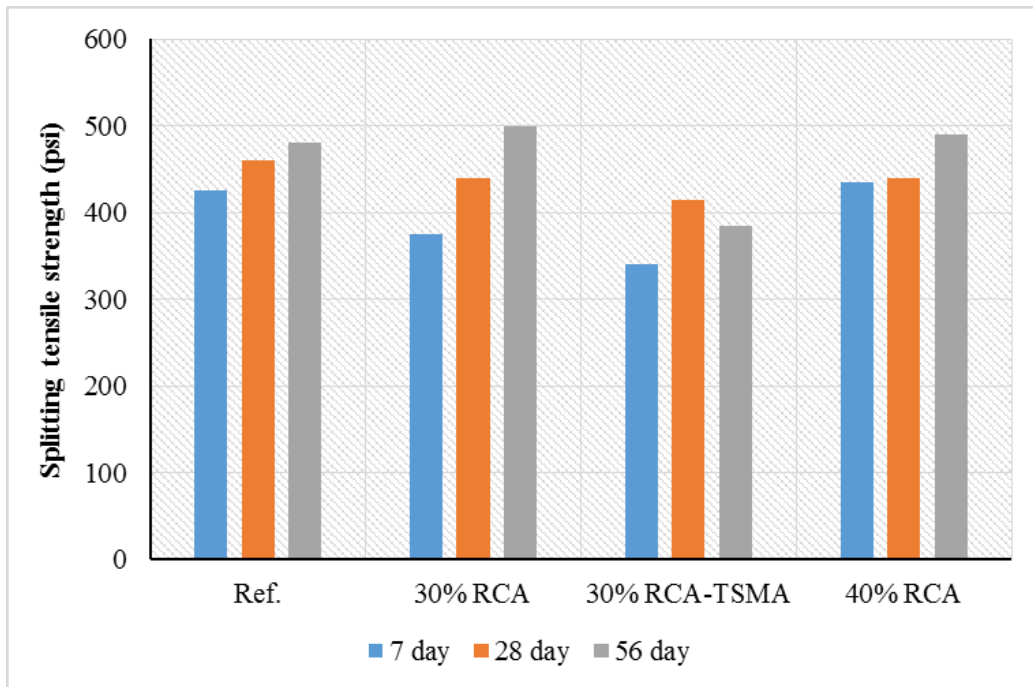


Figure 5-8. Splitting tensile strength results

Flexural strength. Table 5-7 summarizes the flexural strength results at 35 and 56 days. Dimensions of the samples were the same as those used for testing the freeze/thaw resistance since the residual flexural strength was determined after the completion of the freeze/thaw testing (ASTM C666-B).

The flexural strength results are in line with those of the splitting tensile strength; with the highest strength observed for the 30% RCA replacement at 56 days, followed by the reference concrete and the 40% RCA concrete. Again, specimens made with 30% RCA-

TSMA had the lowest flexural strength; which was 22% lower than that of the reference concrete.

Table 5-7. Flexural strength results (psi)

Mixture	Reference			30% RCA			30% RCA-TSMA			40% RCA		
	Avg.	σ	C.O.V. (%)	Avg.	σ	C.O.V. (%)	Avg.	σ	C.O.V. (%)	Avg.	σ	C.O.V. (%)
35	805	52	6.5	755	67	8.8	650	7	1.1	780	32	4.1
56	840	56	6.7	850	5	0.6	660	26	3.9	825	20	2.4
After F/T testing	640	50	7.8	645	70	10.9	545	17	3.1	550	42	7.6

Concrete specimens subjected to 300 cycles of freeze and thaw (ASTM C666-B) significantly lower flexural strength than those not subjected to frost action after 56 days of age. This was especially the case for the mixture made with 40% RCA. In the case of the Reference concrete and the mixture made with 30% RCA, 25% reduction in flexural strength was observed after freeze/thaw testing compared to the 56 day results. The decrease in flexural strength by the freeze/thaw cycles was to 35% in the case of mixture with 40% RCA replacement. Xiao et al., (2013), and Dai et al., (2007) observed that the loss of strength due to freeze/thaw damage is more significant in mixtures containing RCA.

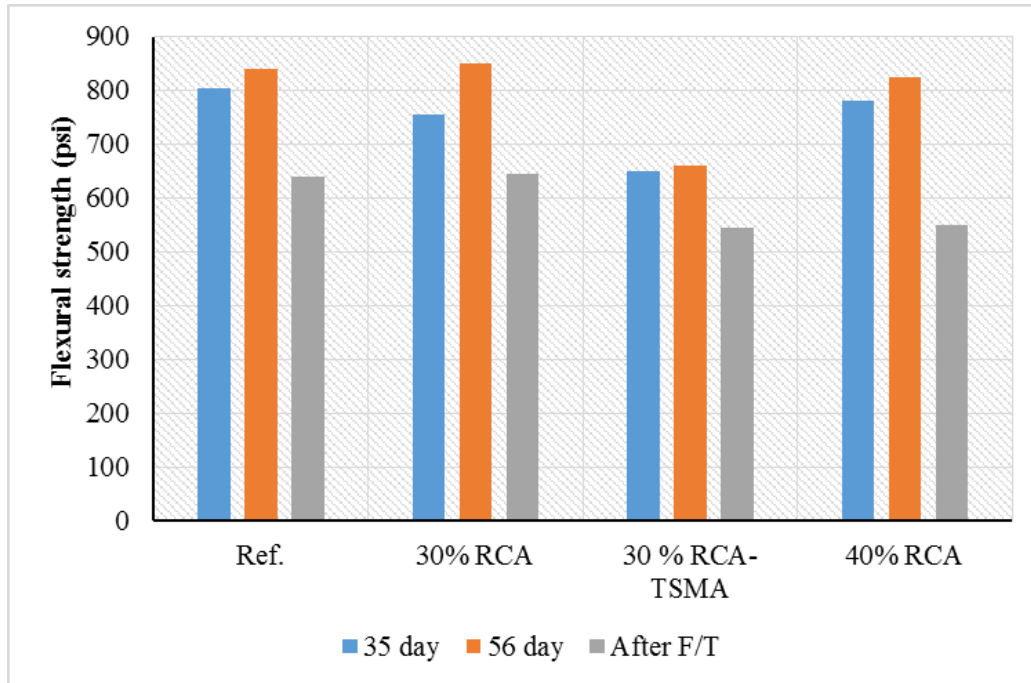


Figure 5-9. Flexural strength results

Drying shrinkage. Three prismatic specimens were sampled to monitor drying shrinkage according to ASTM C157. The samples were demolded one day after casting and placed in lime-saturated water of 70 ± 5 °F (21 ± 3 °C) for seven days. They were then kept in an environmental chamber at 70 ± 5 °F (21 ± 3 °C) and a relative humidity of $50\% \pm 5\%$. Length variations in the specimens due to the shrinkage are presented in Figure 5-10.

All mixtures have acceptable shrinkage performance with 120 day values less than $600\mu\epsilon$. However, drying shrinkage is shown to increase with the increase in RCA content. The increase in shrinkage is most probably due to the lower restraining capacity of the RCA particles due to increase in the total mortar content and decrease in the total stiff virgin aggregate in the mixture (Xiao et al. 2012). Concrete made with 40% RCA replacement had the highest shrinkage followed by concrete made with 30% RCA-TSMA and 30% RCA. The maximum spread in shrinkage value of $100\mu\epsilon$ was observed in the case of the reference and 40% RCA mixture at

120 days. Negligible difference between shrinkage of the reference concrete and that of the 30% RCA mixture was found.

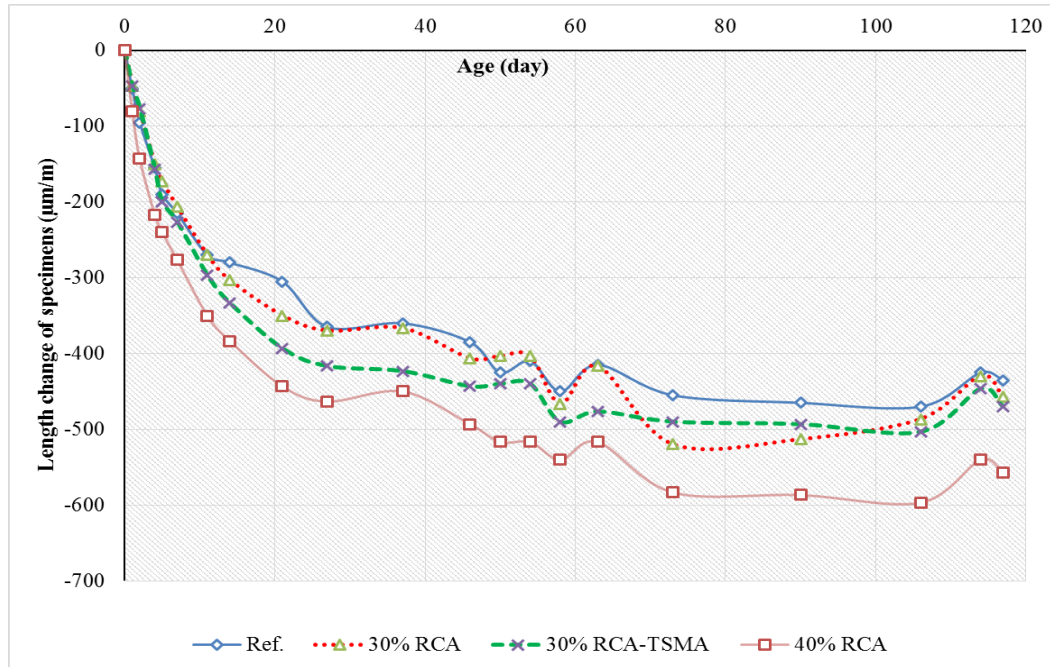


Figure 5-10. Variation of drying shrinkage with time

Modulus of elasticity. Two types of specimens were used to determine the modulus of elasticity (MOE) according to ASTM C469. At each age, three 4×8 in. cylinders were tested at Missouri S&T, and two 6×12 in. cylinders were tested by MoDOT. Table 5-8 and Table 5-9 summarize the results. Figure 5-11 and Figure 5-12 plot the variations in results.

Table 5-8. MOE results, 4×8 in. cylinders

Mix.	Age	Ref			30% RCA			30% RCA-TSMA			40% RCA		
		Avg	σ	C.O.V (%)	Avg	σ	C.O.V (%)	Avg	σ	C.O.V (%)	Avg	σ	C.O.V (%)
M.O.E (ksi)	28 days	4880	110	2	4550	130	3	3590	50	1.3	4000	490	12
	56 days	5625	-	-	4417	388	9	3590	180	4.5	4825	-	-

Table 5-9. MOE and Poison's ratio results, 6×12 in. cylinders

Mixture	Age	Reference	30% RCA	30% RCA-TSMA	40% RCA
MOE (ksi)	28 days	4860	4890	4160	4500
Poison's Ratio	28 days	0.22	0.24	0.23	0.23
MOE (ksi)	56 days	4984	5063	4250	4564
Poison's Ratio	56 days	0.22	0.16	0.24	0.17

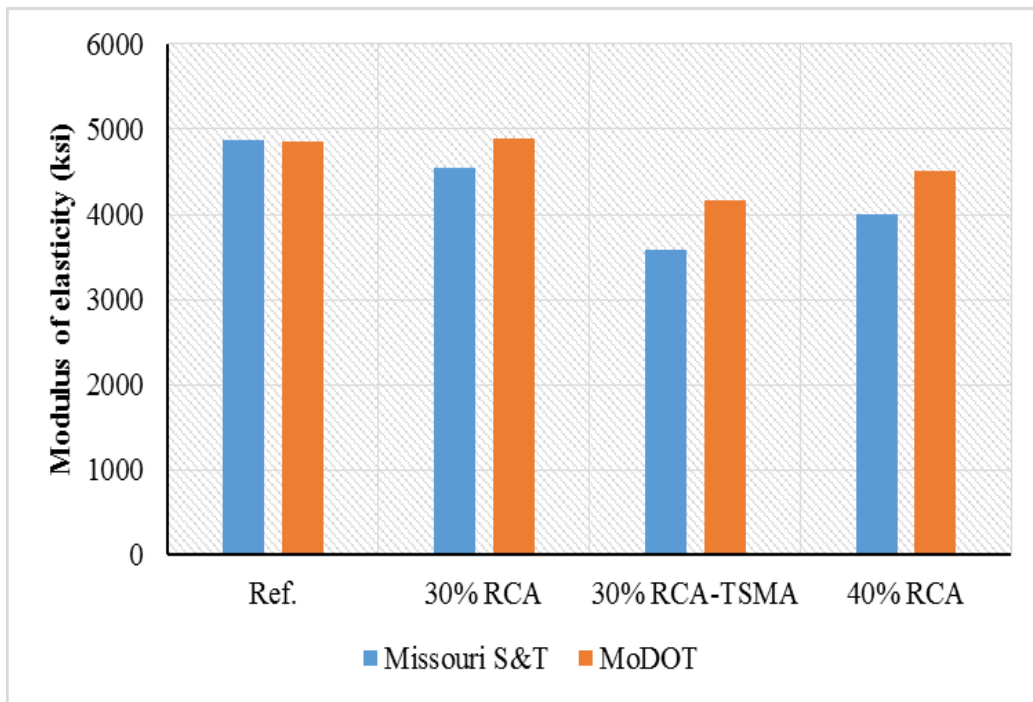


Figure 5-11. Comparison of the MOE results at 28 days

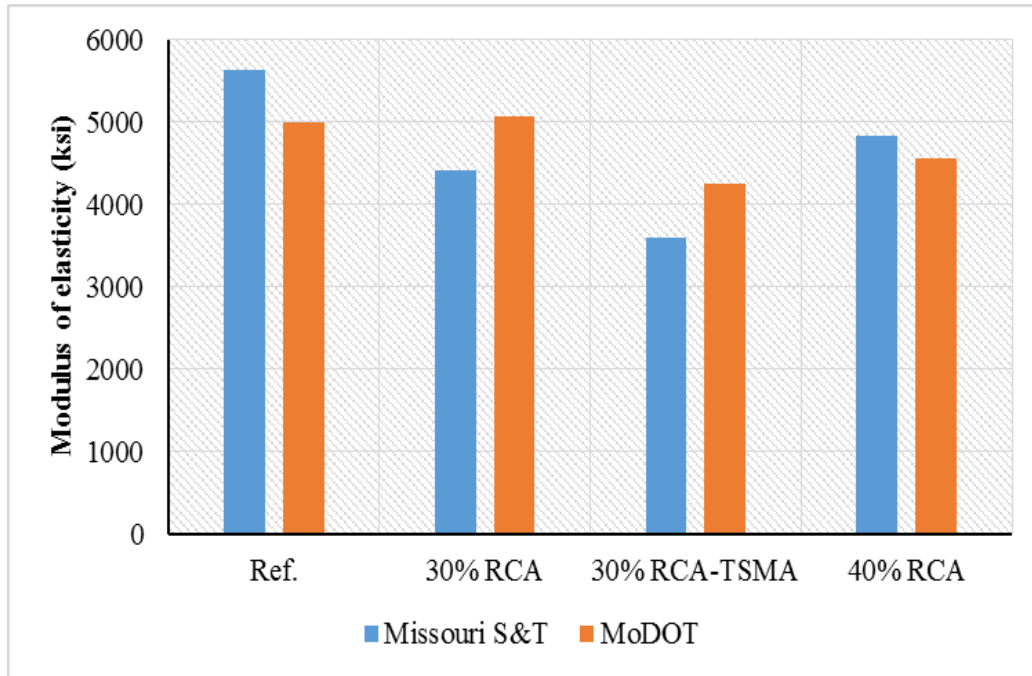


Figure 5-12. Comparison of the MOE results at 56 days

Maximum MOE values were observed for the reference specimens and those made with 30% RCA. Results were consistent for both the 4×8 in. and 6×12 in. specimens. In average, 8% and 12 % decrease in MOE was observed as a result of increasing the RCA replacement ratio to 30% and 40% respectively. In the case of concrete made with 30%RCA-TSMA, 23% and 18% decrease in MOE was observed compared to the Reference and 30% RCA mixtures. For both the 28 and 56 day results, MOE results are in agreement with the compressive strength results where maximum and minimum values are associated with the reference and the 30%RCA-TSMA specimens, respectively.

In general MOE decreases with an increase in the RCA replacement ratio. This is due to the comparatively lower MOE of the residual mortar attached to the RCA particles, which decreases the stiffness of aggregate skeleton in RCA-made concrete (Xiao et al., 2012, Hoffman et al., 2012, and Domingo et al., 2009).

Chloride-ion permeability. The rapid chloride-ion permeability test was performed in accordance with ASTM C1202 at 30, 56, and 91 days of age. The results of permeability test are presented in Table 5-10 and Figure 5-13.

Table 5-10. Rapid chloride-ion permeability results

Mixture	Age (day)	Reference	30% RCA	30% RCA-TSMA	40% RCA
Permeability (Coulomb)	30	2,040	2,020	2,000	2260
	56	1,395	1,425	1,510	1,515
	91	990	1230	1300	1320

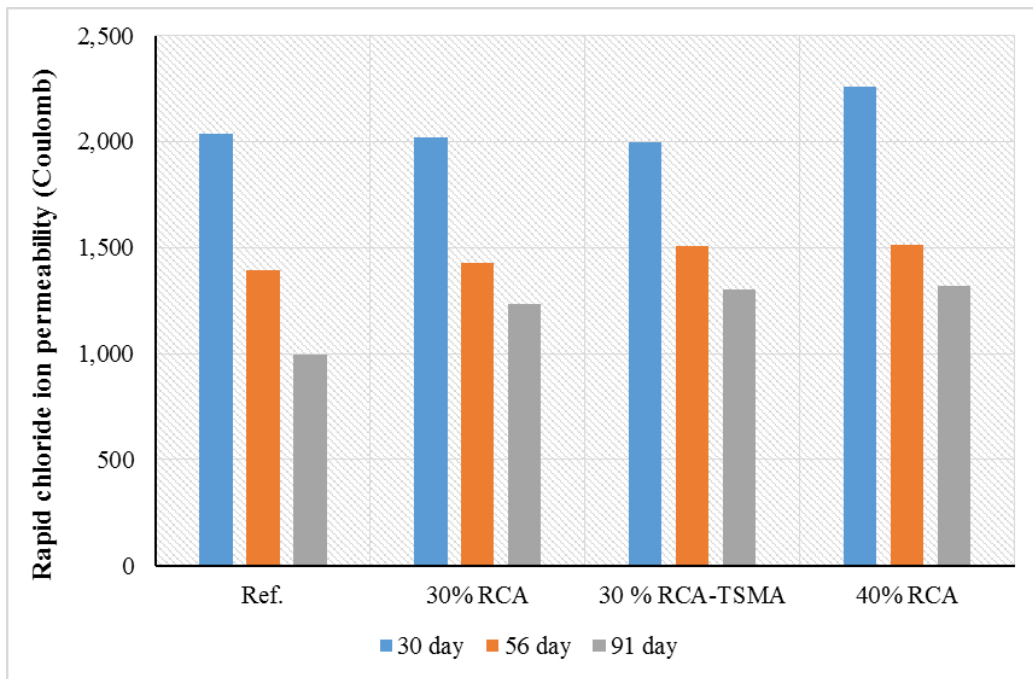


Figure 5-13. Rapid chloride-ion permeability results (Coulomb)

The 91-day rapid chloride-ion permeability increased by 240 and 330 Coulomb with the increase in RCA content to 30% and 40% respectively. In general, for a given age, the difference in rapid chloride-ion permeability was not significant. At 56 days, all concrete mixtures had approximate rapid chloride-ion permeability values of 1500 Coulomb, which is considered to be low. At 91

days, the Reference concrete had the lowest rapid chloride-ion permeability value of 900 Coulomb, which is considered to be very low. The RCA mixtures exhibited permeability values about 1300 Coulomb at 91 days, which is categorized as low permeability.

The permeability values increased very slightly with an increase in RCA replacement ratio and the minimum permeability values are observed in the case of conventional concrete. Similar trends were also observed by Hu et al., (2009), Otsuki et al., (2003), Shayan and Xu (2003), and Sim and Park (2011).

Permeable void volume. The 91-day permeable void results are presented in Table 5-11. Minimum void volume results were observed in the case of Reference concrete. 17% and 22% increase in results was observed due to 30% and 40% RCA replacement respectively. The concrete made with 30% RCA-TSMA had similar performance to the 30% RCA mixture. Minimum absorption values were observed in the case of the Reference concrete. Increase in absorption was observed after boiling the specimens. Increase in absorption after boiling was limited to 0.1% for the Reference concrete. An average increase of 0.4% was observed for the RCA mixtures, which is indicative of micro cracking in RCA-mixtures.

Table 5-11. Density, absorption, and permeable void volume results at 91 days

Mixture	Reference	30% RCA	30% RCA-TSMA	40% RCA
Absorption after immersion (%)	4.4	5.1	5.4	5.3
Absorption after boiling (%)	4.5	5.5	5.8	5.8
Permeable void (%)	10.8	12.6	12.8	13.2

Similar results were reported by Thomas et al., (2013), Kou and Poon (2012) and Olorunsogo and Padayachee (2002) have reported up to 70% increase in the absorption in concrete specimens made with up to 100% RCA replacement. The mixture made with 30% RCA-TSMA had the highest absorption results, which may be due to the higher air content in the fresh state.

A linear relationship exists between the permeable void volume and the RCPT results (Figure 5-14). This indicates that the permeable void could be an indication of resistance to chloride ion permeability for the tested concrete made with similar materials.

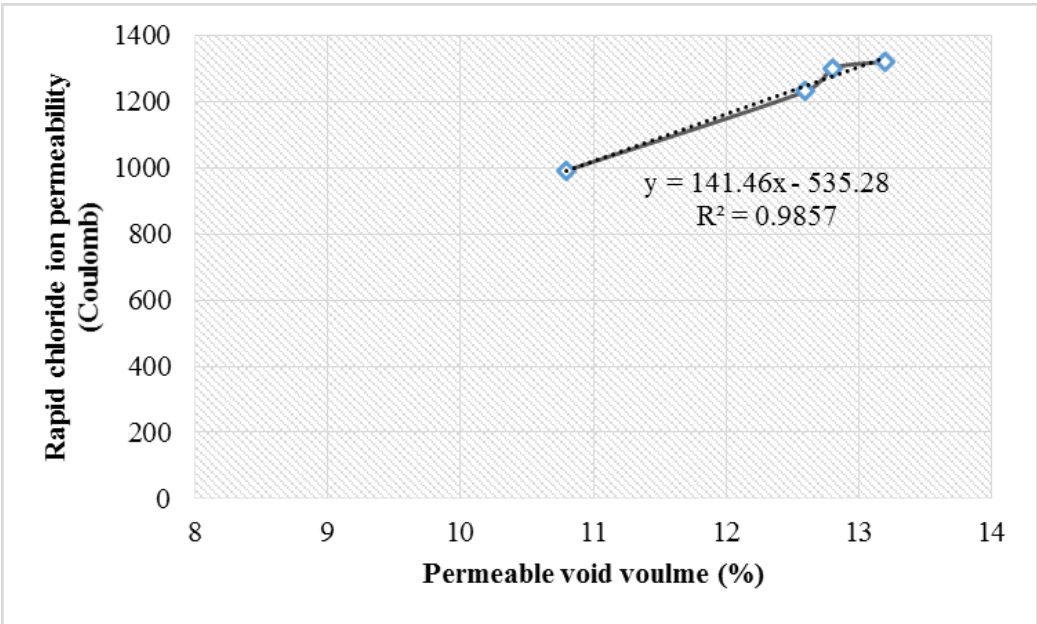


Figure 5-14. Correlation between the RCPT and the permeable void volume results

Freeze/thaw resistance. Prismatic specimens measuring 3×4×16 in. were used to perform the freeze/thaw testing according to ASTM C666, Procedure A (Missouri S&T). Another set of samples are tested by MoDOT to determine the freeze/thaw resistance according to ASTM C666, Procedure B. For procedure A, as in the case of the laboratory investigations in Chapter 4, specimens were cured in lime saturated water for four weeks before being subjected to freezing and thawing cycles. The curing period was 35 days in the case of the Procedure B.

Figure 5-15 plots the variations of the durability factor of specimens tested according to procedure A as a function of freeze/thaw cycle. The residual dynamic MOE (durability factor) was higher than 80% after 300 cycles of freezing and thawing, which reflects adequate frost durability for all tested mixtures. For procedure A, Reference concrete and that made with 40% RCA replacement exhibit slightly higher resistance to freezing and thawing than the other mixtures.

Table 5-12 presents the durability factors of the specimens of both the procedures A and B. Again, all concrete mixtures exhibited satisfactory freeze-thaw performance with durability factor values of $90\% \pm 3\%$.

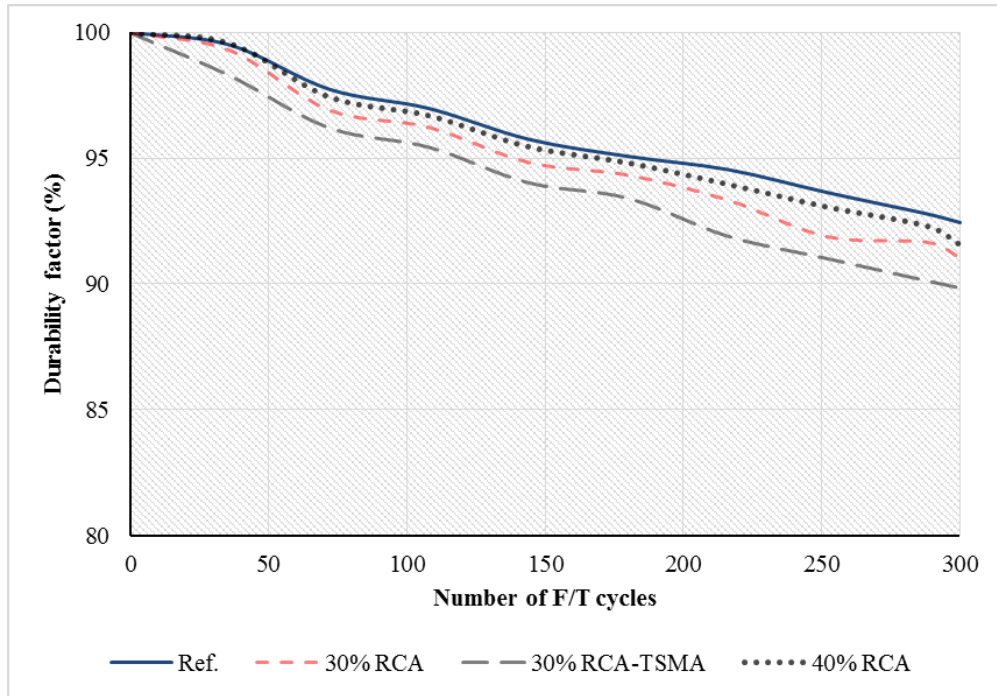


Figure 5-15. Variations in durability factor – Procedure A

Table 5-12. Durability factors after finishing the freeze/thaw testing (%)-ASTM C666

Mixture	Control	30% RCA	30% RCA-TSMA	40% RCA
Procedure A	92	92	90	91
Procedure B	90	92	88	87

Coefficient of thermal expansion. Coefficient of thermal expansion (CTE) affects deformation caused by seasonal variations in temperature. Higher CTE corresponds to larger slab deformations, joint openings, and more cracking potential due to warping, etc. Table 5-13 summarizes the CTE of concrete specimens determined according to AASHTO T336. The CTE values were used to determine the in-situ iso-thermal deformation.

The CTE is directly related to the CTE of the aggregate present in concrete mixture, type and content of aggregate. Higher MOE and smaller CTE of aggregate restrains the free deformation of the cement paste, which in turn decreases the CTE of the concrete. It is expected, in general,

to have higher CTE values in the case of RCA concrete (Opare 2008). This is due to the relatively lower stiffness of RCA particles compared to virgin coarse aggregate.

The data of this study indicated that the CTE increases as a function of RCA content. For the concrete made with 40% RCA, the CTE was 4.8 and 4.4 $\mu\epsilon/^\circ\text{F}$ compared to 4.4 and 4.2 $\mu\epsilon/^\circ\text{F}$ for the Reference mixture at 2 and 11 months, respectively.

Table 5-13. Coefficient of thermal expansion results- MoDOT lab

Mixture	Age (month)	Reference	30% RCA	30% RCA-TSMA	40% RCA
Coefficient of thermal expansion (E-6 in/in/ $^\circ\text{F}$)	2	4.4	4.6	4.6	4.8
	11	4.2	4.3	4.4	4.4

5.3.3. Core sampling

Several core samples were taken from all four mixture types to determine compressive strength, splitting tensile strength, modulus of elasticity, abrasion resistance, and preparing samples for scanning electron microscope (SEM) analysis. Figure 5-16 depicts the coring process that took place at 120 days of concrete placement. For each mixture type, seven cores of 4.0 in. diameter were taken as well as one core with 6.0 in. diameter. The latter was used for abrasion resistance test. It should be noted that after completion of the coring, the cores were surrounded by saturated sand to avoid any physical damages during transportation. The cores were then cured in lime saturated water in the laboratory until the age of testing. The core specimens were tested at 125 days of age after casting. The ends of the cores were grinded to ensure smooth, parallel, and uniform bearing surfaces. Test results of the core samples are summarized in Table 5-14.



Figure 5-16. Photos of core sampling at the job site (left) and grinding the test surface of the specimens (right)

Table 5-14. Properties of the core samples

Mix.	Compressive strength* (psi)	Ratio to 91 day laboratory results (%)	Splitting tensile strength (psi)	Ratio to 56 day laboratory results (%)	MOE (ksi)	Ratio to 56 day laboratory results (%)	Abrasion depth (in.)	
							Top	Bottom
Control	6030	97	535	111	4800	86	0.1	0.09
30% RCA	5750	99	550	110	4700	107	0.09	0.1
30% RCA-TSMA	4120	84	360	94	3900	99	0.1	0.1
40% RCA	4770	88	450	92	4900	102	0.09	0.09

*No adjustment factor for core results

The Reference mixture developed greater compressive and splitting tensile strength than the RCA mixtures, as presented in Table 5-14. An increase in the RCA content lead to a decrease in the mechanical properties of the concrete. However, all the mixtures had results higher than the required 28-day strength of 4,000 psi. The Reference and 30% concrete cores had results similar to that of 91 days. A slight decrease of 12% was observed in the case of 40% RCA cores compared to the 91-day results. In the case of the splitting tensile strength of the reference and the 30% RCA core samples, 10% increase was observed compared to the 56 day specimens,

which may be attributed to the hydration progress and pozzolanic reactions of fly ash. The 30% RCA-TSMA and the 40% RCA cores had 6% and 8% lower splitting tensile strength results compared to the 56-day results, respectively. MOE value obtained for reference concrete was 14% lower than the results obtained at 56 days, which may be due to the experimental errors or micro-cracks during the coring process. For other tested mixtures, slight increase (up to 7%) in MOE was observed, while comparing to 56-day results.

The 6.0-in. diameter core samples were used to determine the abrasion resistance in accordance with ASTM C 779-C. No difference in the abrasion depth was observed for the top and bottom surfaces of the cores. It should be noted that the top part of the cores were the tined surface of the pavement. The bottom parts were saw cut surfaces. No difference was observed in the abrasion resistance of the Reference and RCA mixtures.

Core samples taken from the pavement sections were also used to evaluate the micro-structural properties of the concrete. In particular, the interface between the residual mortar attached to the original virgin aggregate available in the RCA particles were investigated using a scanning electron microscope (SEM). Cracks were found in the mortar section of the RCA. Such cracks can be the result of the crushing process of the RCA. Some cracks also propagated through the interfacial transition zone (ITZ) of the RCA particles between the old virgin aggregate and the residual mortar, as shown in Figure 5-17 and Figure 5-18. Such micro-cracks are believed to be the main reason for some of the lower properties observed in RCA-made concrete.

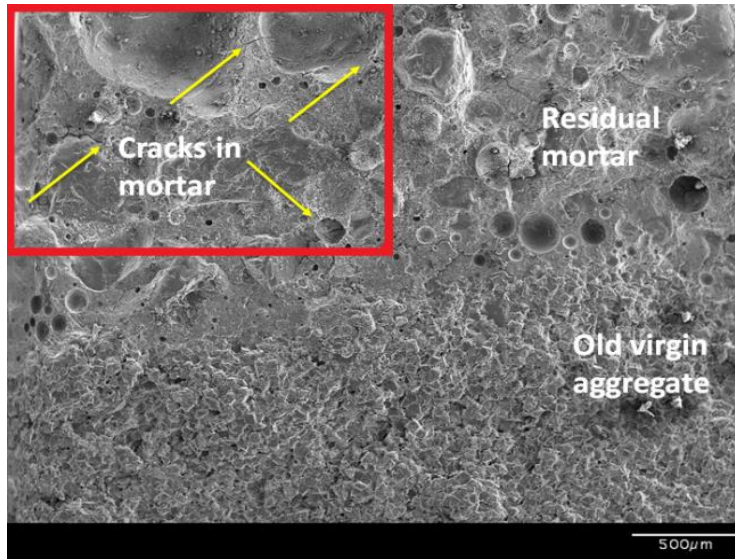


Figure 5-17 Cracks detected within the residual mortar attached to the RCA particles

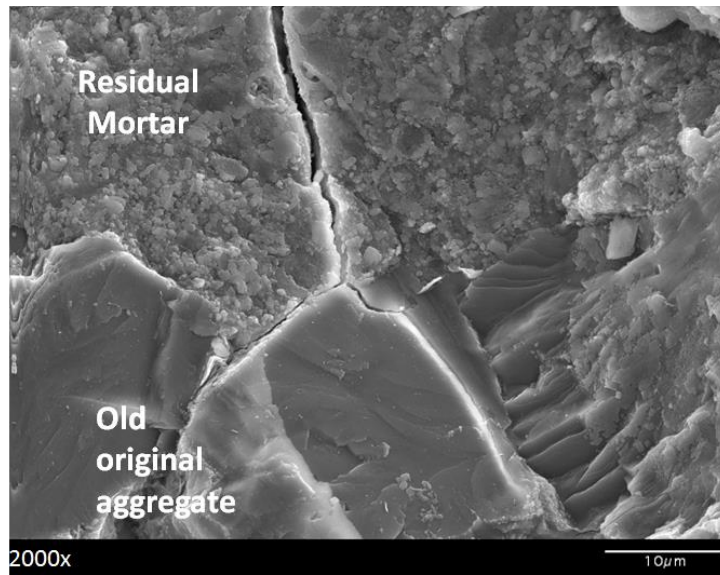


Figure 5-18. SEM image for the crack propagation through the old ITZ in RCA particles

Figure 5-19 shows the interface between new mortar surrounding the new virgin aggregate. Cracks and weakness points in mortar attached to RCA particles were not detected in the fresh mortar phase near the virgin aggregate.

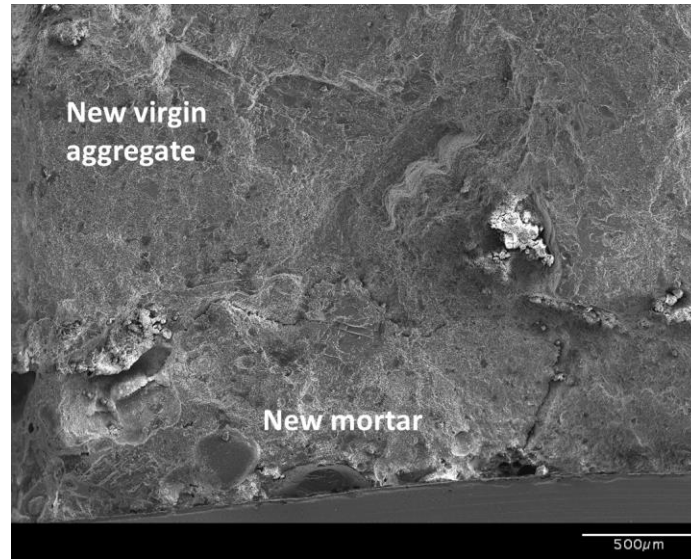


Figure 5-19. SEM image of the interface between the virgin aggregate and surrounding new mortar

5.3.4. Field instrumentation and monitoring of deformation

Vibrating wire strain gauges (VWSG) with length of 6.75 in. were placed in pavement sections constructed with the four concrete mixtures to monitor temperature and strain. The VWSG employed at the site is presented in Figure 5-20.

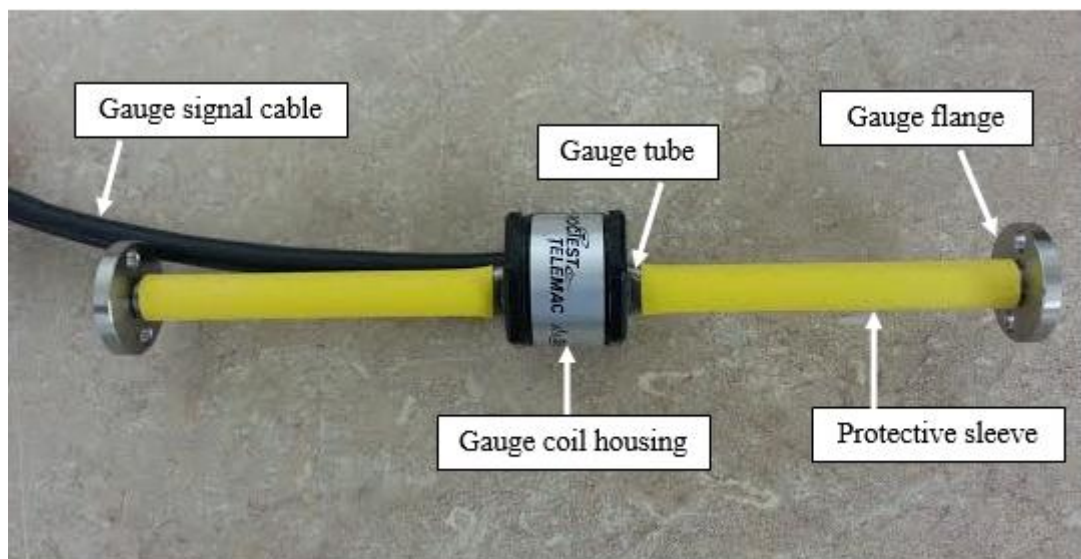


Figure 5-20. Vibrating wire strain gauge used to monitor temperature and strain in pavement

A VWSG consists of a tensioned steel wire anchored at both ends into flanges. The wire is enclosed in a stainless steel tube. Electromagnetic coils are located within the body close to the axis of the wire. When a brief voltage excitation, or swept frequency excitation is applied to the coils, a magnetic field is induced causing the wire to oscillate at its resonant frequency. The wire continues to oscillate for a short period through the ‘field’ of the permanent magnet, thus generating an alternating current (sinusoidal) output. The frequency of this current output is detected and processed by a vibrating wire readout unit, or by a data logger equipped with a vibrating wire interface, where it can be converted into units of Strain.

Data acquisition systems. Two solar powered data acquisition systems were placed at the site to record the data transformed from the VWSGs. The data are recorded in 5-minute intervals, and the data are retrieved at different time intervals. Sixteen VWSGs were logged into each of the data acquisition poles (Figure 5-21).



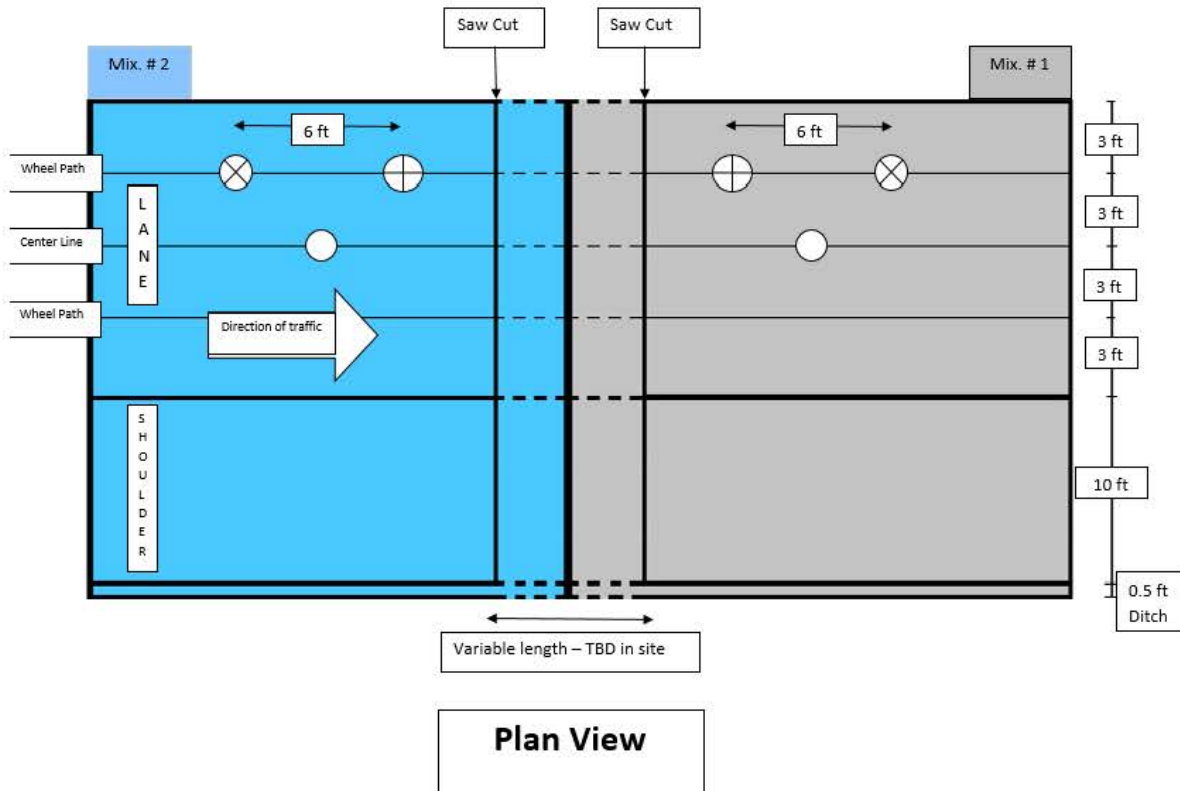
Figure 5-21. Solar powered data acquisition system and monthly data collection

Sensor placement. For each mixture, the VWSGs were located at three different locations. The sensors are used to determine the total strains in the pavement, including those caused by temperature variations, concrete shrinkage, warping, and curling (Figure 5-22).



Figure 5-22. Photos of placing the instrumentation and the data loggers at the job site

Figure 5-23 shows a schematic layout of the instrumentation plan. Three baskets of reinforcing bars were pre-fabricated to attach the VWSGs. Two baskets were placed along the wheel path of the pavement (sets A and B in Figure 5-23), and another set along the central line of the pavement (set C in Figure 5-23). As illustrated in Figure 5-23, clustering A of sensors has three VWSGs at 2-in. intervals along the height of the pavement aligned with the direction of traffic (A1, A2, and A4) in addition to a fourth gauge situated at the mid-section perpendicular to the direction of traffic (A3). Clustering B and C have two sensors each near the top and bottom of the pavement in the direction of traffic.



Point Name	Symbol	Location	Number of VWSG	Distribution of VWSGs in height	Depth of VWSG placement
A	⊕	Wheel path	4	Direction of traffic 	Top: one, parallel to traffic direction (A1)
					Middle: one, parallel to traffic direction (A2) and one perpendicular to direction of traffic (A3)
					Bottom: one, parallel to traffic direction (A4)
B	⊗	Wheel path	2	Direction of traffic 	Top: one, parallel to traffic direction (B1)
					Bottom: one, parallel to traffic direction (B2)
C	○	Center Line	2	Direction of traffic 	Top: one, parallel to traffic direction (C2)
					Bottom: one, parallel to traffic direction (C2)

Figure 5-23. Schematic of instrumentation plan

Iso-thermal deformation. Deformation recorded with a VWSG is affected by environmental conditions, including fluctuations in temperature. In order to express the iso-thermal deformation in concrete, it is required to subtract temperature-induced deformation of the concrete and the steel wire used in fabrication of the VWSGs according to the following equation:

$$\varepsilon_r = \varepsilon + (\alpha_c - \gamma\beta) \times (T_1 - T_0) \quad (5-1)$$

where:

ε : total strain reading, micro strain

ε_r : iso-thermal strain, micro strain

α_c : linear expansion coefficient of the EM-5 vibrating wire strain gauge = 6.4 $\mu\text{in/in}/^\circ\text{F}$

γ : freedom factor of the concrete structure in surrounding material ($0 \leq \gamma \leq 1$). For the incorporated VWSGs the value of γ is 1.0, denoting a full restraint of the concrete.

β : coefficient of thermal expansion of concrete, $\mu\text{in in/in}/^\circ\text{F}$, (see Table 5-13)

T_1 : temperature reading at a given time, $^\circ\text{F}$

T_0 : initial temperature, $^\circ\text{F}$ (usually 5 minutes after concrete placement)

Figure 5-24 compares the deformation in the reference concrete pavement read by the VWSG located at post A1 before and after taking into consideration the temperature fluctuations.

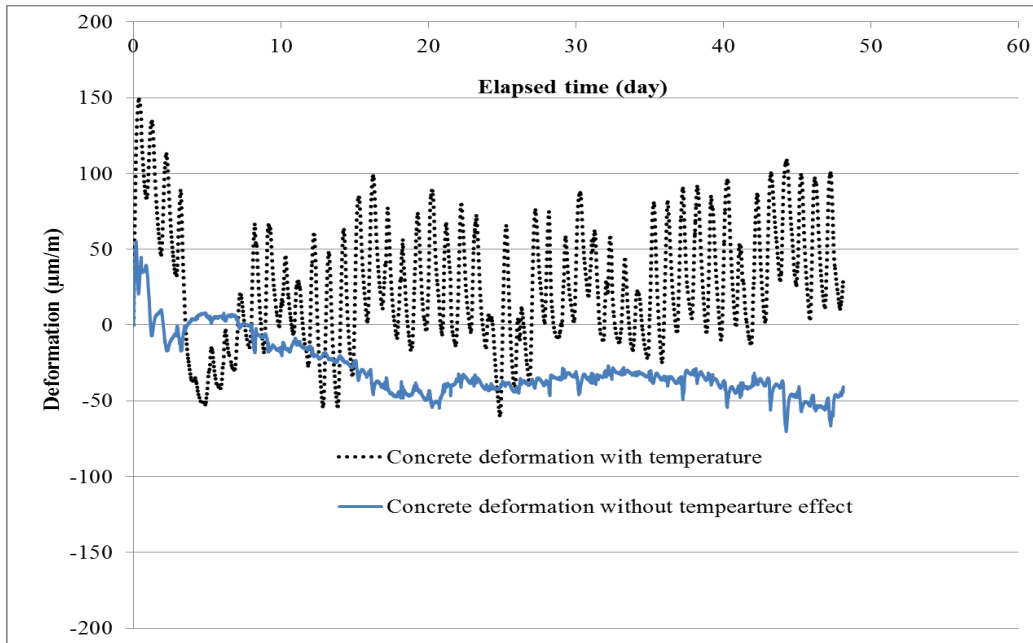


Figure 5-24. Total deformation and iso-thermal concrete deformation measured by A1 VWSG at 5-minute intervals (A1 sensor located at top surface of the pavement at the wheel path parallel to traffic)

A software package was developed to calculate the iso-thermal deformation based on the initial VWSG reading and laboratory results for coefficient of thermal expansion. The software was used for back-calculating the CTE based on daily cycles of temperature fluctuation and strain registered by the sensors, as presented in Figure 5-25.

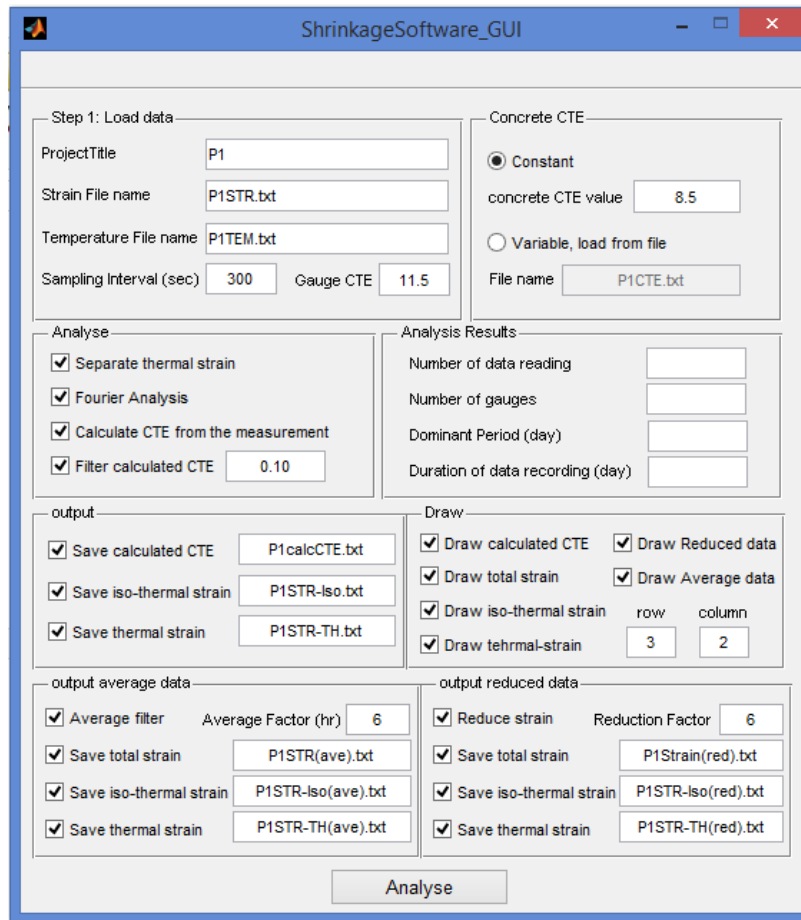


Figure 5-25. Deformation analyzer software interface

Table 5-15 includes the average CTE values calculated by the software as well as the measurements on 11 month cured specimens. The predicted CTE values are within the $\pm 5\%$ range of laboratory measurements.

Table 5-15. Comparing back-calculated CTE with laboratory measurements

Mixture	Reference	30% RCA	30% RCA-TSMA	40% RCA
Laboratory data ($\mu\text{in./in.}^\circ\text{F}$) - 11 months	4.21	4.32	4.44	4.38
Software calculation ($\mu\text{in./in.}^\circ\text{F}$)	4.37	4.29	4.62	4.42
Variation (%)	+3.6	-0.7	+4.1	+0.9

Pavement deformation behavior. The calculated total iso-thermal deformation is a combination of volume change during hydration, frictional stresses of the pavement, and autogenous concrete shrinkage followed by drying shrinkage deformations. Cyclic daily deformation caused by warping is another source of deformation that can be captured by the VWSGs. Warping by definition is the deformation in pavement due to temperature gradient through the pavement thickness. Temperature variations affects the pavement in two ways:

1. Uniform temperature changes that cause expansion and contraction of the whole slab
2. Temperature gradient between the top and bottom of the slab that causes a slab deformation called warping. Since the slab is restrained, the temperature-induced stresses are developed that may create cracks.

The temperature changes between day and night cause non-linear temperature differentials between the top and bottom of the slab. The stress-strain regime during the warping mechanism is illustrated in Figure 5-26. During night (or cold weather), the temperature at the top of the slab can be lower than that at the bottom. Thus, the top part of the slab tends to shrink compared to the bottom. However, the weight of the slab restrains the relative expansion and contraction, which can induce tensile stresses at the top of the slab and compressive stresses at the bottom. Similarly, during the day (or warm weather), the top of the slab tends to become warmer compared to the bottom results in lower bottom temperatures. Thus, the top tends to expand compared to the bottom. Again, the weight of the slab can restrain the relative expansion and contraction, which can induce tensile stresses at the bottom and compressive stresses at the top (Huang 2004).

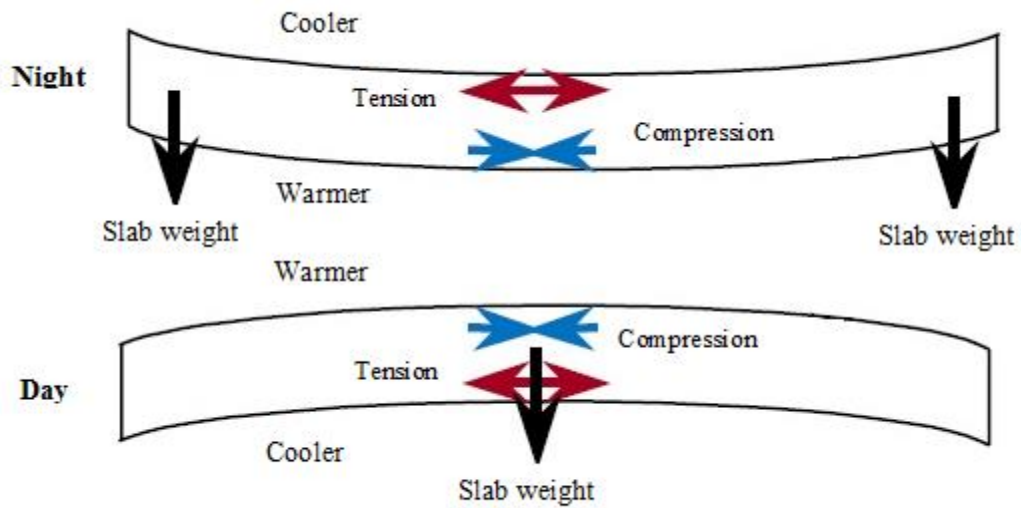


Figure 5-26. Warping mechanism by temperature gradient (Huang 2004)

Curling caused by moisture variation in slab depth is another source of deformation that can lead to cracking. The curling mechanism caused by moisture gradient and differential shrinkage through the slab thickness is illustrated in Figure 5-27.

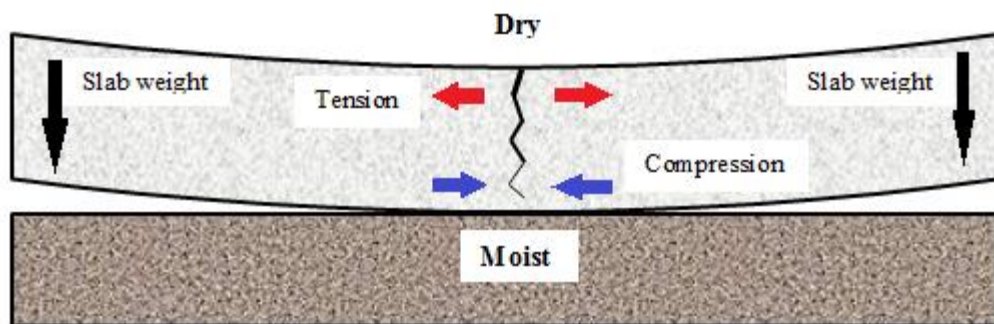


Figure 5-27. Curling caused by moisture gradient (Huang 2004)

It also should be noted that the cyclic deformation due to temperature (and moisture) variations are also detected in larger scale due to seasonal environmental variations. This is further discussed below.

Deformation analysis. The iso-thermal deformation determined at the top surface of the pavement at the wheel path parallel to traffic direction at sections corresponding to the four concrete mixtures in use (location A1) are presented in Figure 5-28. All deformation values are quite small. The total deformation is a combination of shrinkage deformation and environmental effects on pavement deformation behavior. All mixtures have similar deformation patterns during the first 140 days of the pavement life (mid-September 2013). The concrete exhibited initially an expansion of about 10 $\mu\text{m}/\text{m}$ before exhibiting some negative deformation caused by shrinkage and compressive stress (and strains) due to warping during the summer time. It should be noted that the sensor located at location A1 at 30% RCA-TSMA mixture was not functioning properly after about 200 days.

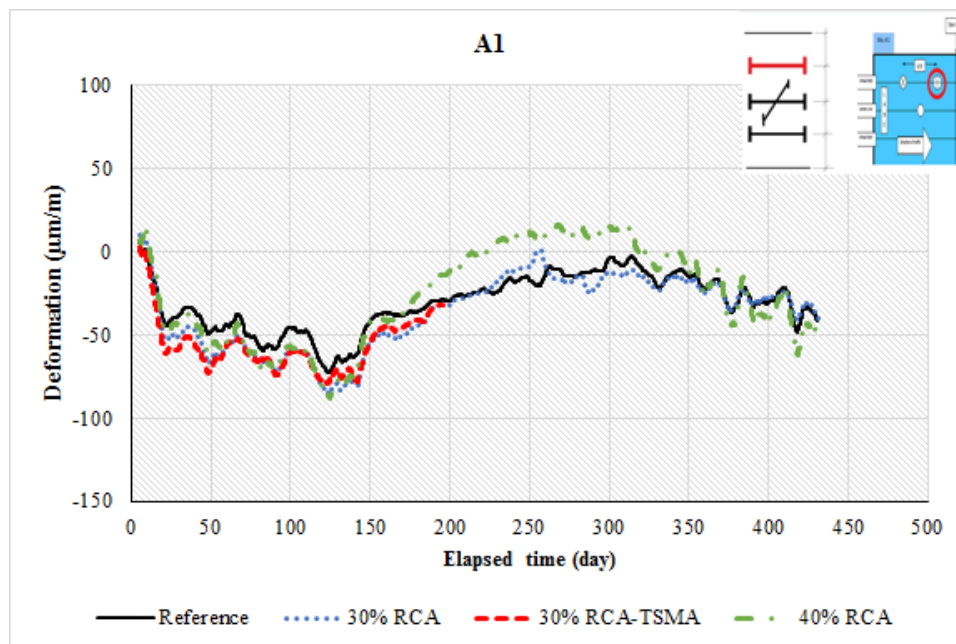


Figure 5-28. Iso-thermal strain of different mixtures at A1 location (top surface at wheel path parallel to traffic)

The deformation pattern is changed by the start of cold season (September). This indicates that the environmental effects (warping and curling) are the main factors governing the deformation characteristics as shown in Figure 5-28 where the negative deformations are changing to positive

strains caused by tensile stresses due to cold weather. This pattern, however, tends to be cyclic and repeating through the year, which can result in fatigue and cracking in pavement.

The highest variations in strain direction due to seasonal effects was observed in the case of 40% RCA mixture where an approximately 100 $\mu\text{m}/\text{m}$ ($\mu\text{in.}/\text{in.}$) was observed during the cold season up to 280 days, i.e. end of January 2014. The minimum value was about 60 $\mu\text{m}/\text{m}$ for the reference mixture. This might be due to the higher coefficient of thermal expansion and lower modulus of elasticity of the 40% RCA mixture compared to the reference and the 30% RCA mixture as demonstrated by the following equation (Huang 2004):

$$\delta_x = (C_x + \mu C_y)E\alpha(\Delta T)/2(1 - \mu^2) \quad (5-2)$$

where: δ_x is the warping stress in x direction, E is the modulus of elasticity of the concrete, α is the coefficient of thermal expansion, μ is the Poisson's ration, and C_x and C_y are the correction factors for infinite slab length. It is usually expected that a decrease in MOE and an increase in the CTE increase the warping stress and strain in rigid pavement.

Figure 5-29 presents the strains recorded at mid-height of the pavement parallel to the traffic direction (locations A2) at wheel path. The lowest deformation was observed in the case of 30% RCA mixture up to the start of cold season (140 days of age). The maximum variations in strain during the cold season was observed for the 30% RCA mixture with about 80 $\mu\text{m}/\text{m}$ change in strain direction. This was minimum in the case of the reference mixture with about 50 $\mu\text{m}/\text{m}$ variation.

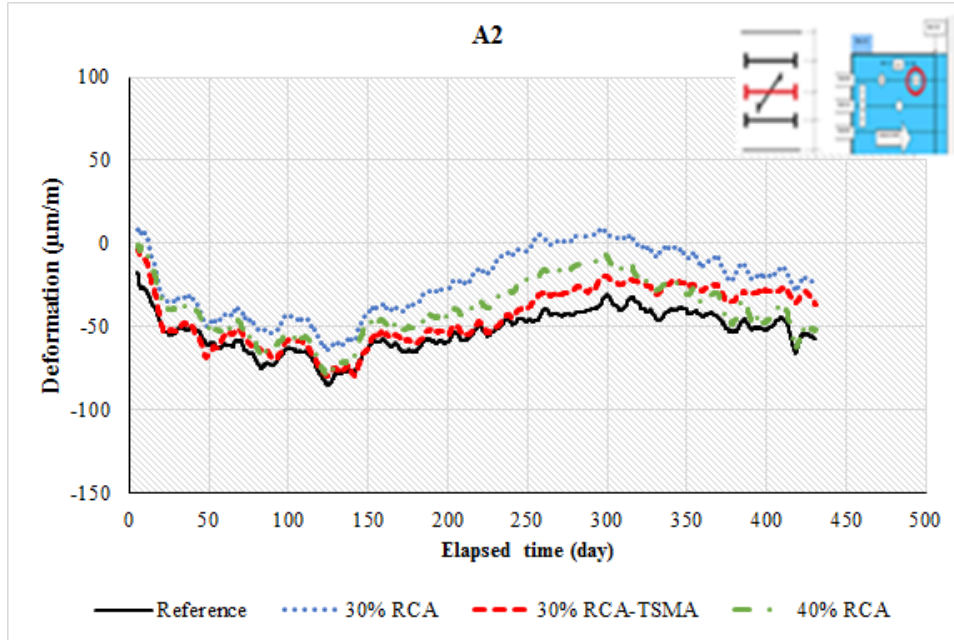


Figure 5-29. Iso-thermal strain of different mixtures at A2 location (mid-height at wheel path parallel to traffic)

Figure 5-30 shows the strains recorded at the mid-height of the pavement perpendicular to the traffic direction (locations A3) at the wheel path. The maximum deformation was registered in the 30% RCA-TSMA concrete up to 140 days. The minimum seasonal effect, i.e. change in strain direction due to reversed warping stress direction at cold season, was observed for the reference mixture. It seems that the variation in stress and strain direction after the peak in winter (about 300 days of age) tends to be slower compared to the A2 location (same location but parallel to the traffic flow).

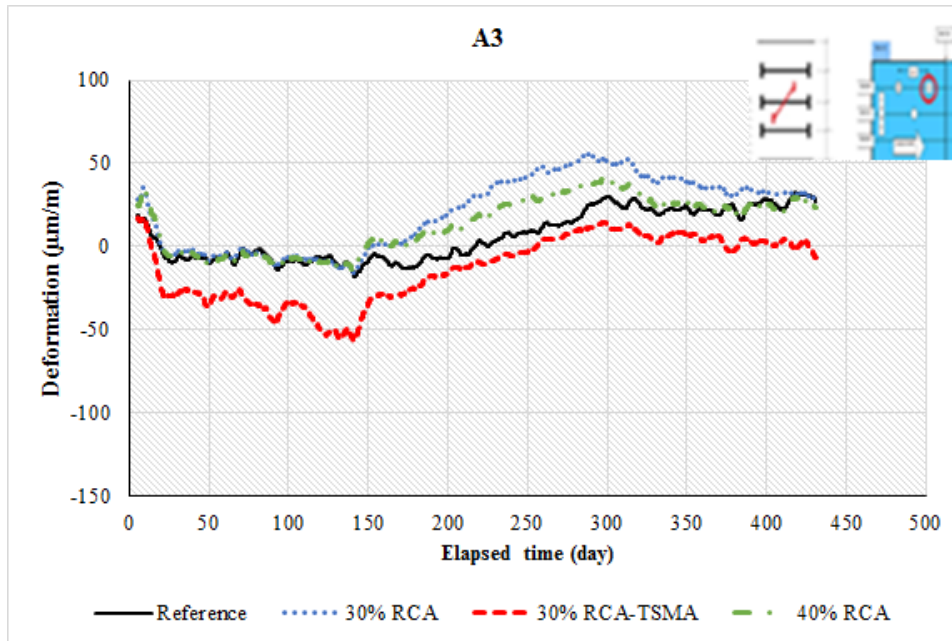


Figure 5-30. Iso-thermal strain measured at A3 for different mixtures (mid-height at wheel path perpendicular to traffic)

Figure 5-31 shows concrete iso-thermal deformations registered at location A4, which is the bottom part of the pavement at the wheel path parallel to the traffic direction. In the case of the deformations at the bottom part of the pavement, it was also observed that the reference concrete and the mixture with 40% RCA replacement had the highest deformation and that with 30% RCA had the minimum strain up to 140 days. Very slight seasonal effect was recorded for the reference mixture. This was maximum in the case of the 30% RCA-TSMA concrete.

In the case of VWSGs at the B1 location, shown in Figure 5-32, which is at the top of the paved surface, at the wheel path and parallel to the direction of traffic flow, it was observed that the mixture with 40% RCA replacement had the lowest strain, and that with 30%RCA-TSMA had the highest values up to 140 days, i.e. end of the summer. The maximum seasonal effect was observed for the 40% RCA mixture.

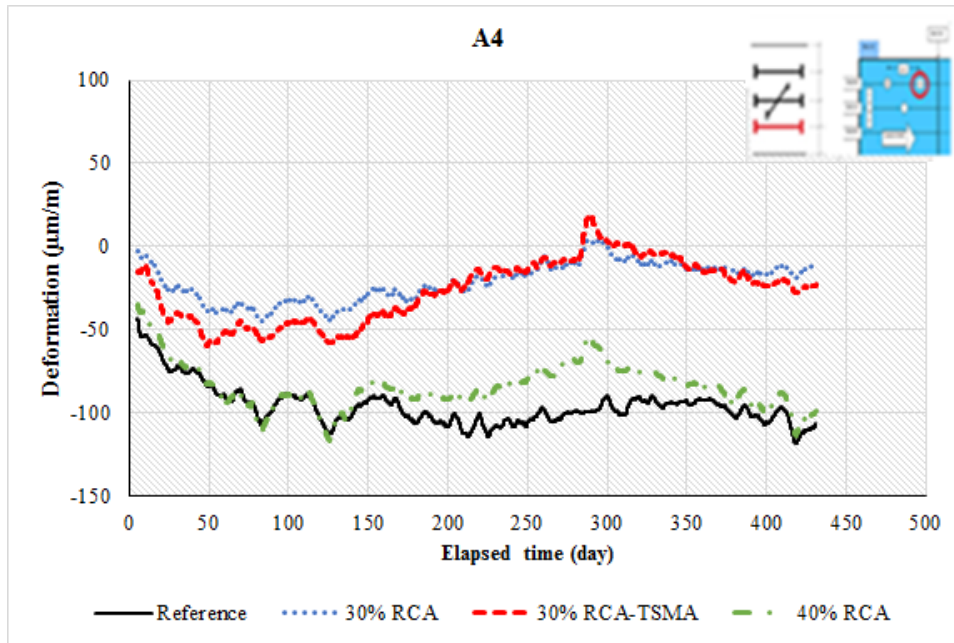


Figure 5-31. Iso-thermal strain at A4 for different mixtures (bottom part of pavement at wheel path parallel to traffic)

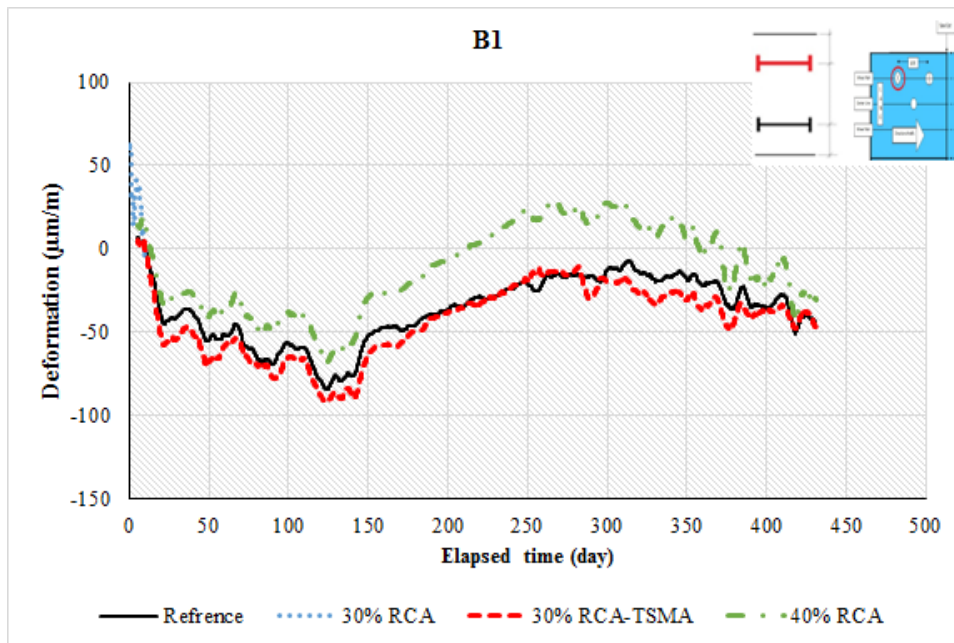


Figure 5-32. Iso-thermal strain at B1 for different mixtures (top surface of pavement at wheel path parallel to traffic)

Deformations in location B2 (bottom, wheel path, and parallel to traffic) are presented in

Figure 5-33. The mixture made with 40% RCA replacement had the maximum deformation

values compared to the minimum registered strains in mixture with 30% RCA-TSMA up to the end of summer. The minimum seasonal deformation was observed in the case of the 40% RCA mixture.

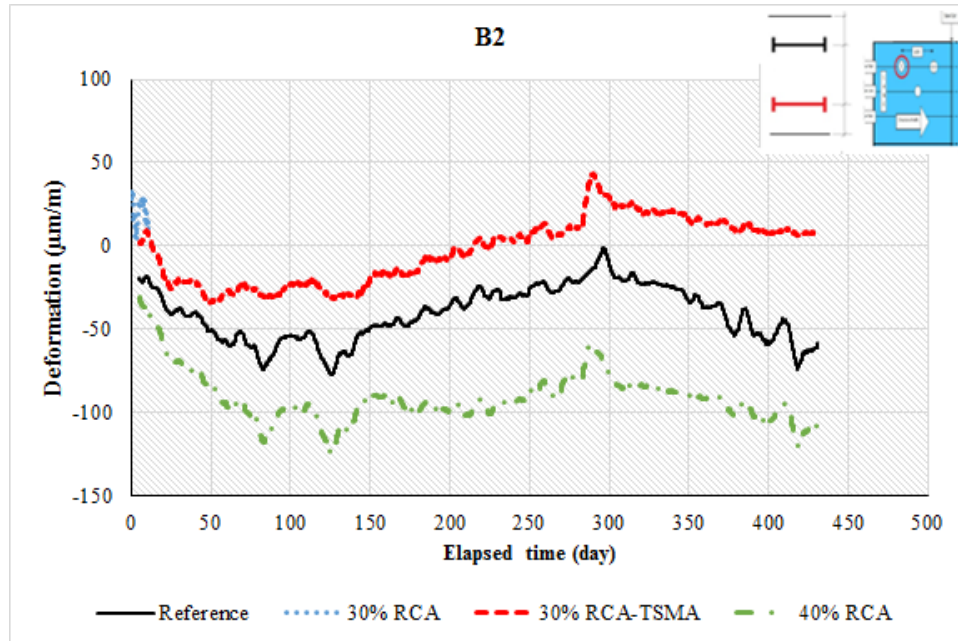


Figure 5-33. Iso-thermal strain at B2 for different mixtures (bottom pavement at wheel path parallel to traffic)

Recording data at the B1 location for mixture with 30% RCA replacement has encountered a problem, and therefore Figure 5-32 does not include the deformation of the 30% RCA-TSMA mixture. The same problem was found in the case of the 30% RCA replacement at B2 location which is at the bottom part of pavement, at the wheel path, parallel to traffic. The sensor cables in the B1 and B2 locations might be damaged during coring process.

Figure 5-34 shows the strains at C1, which is the top part of pavement at the center line of the lane and parallel to the traffic direction. The 40% RCA and Reference mixtures had the lowest deformation, and the 30% RCA mixtures had the highest strain up to 140 days. The minimum seasonal effect was observed for the 30% RCA mixture.

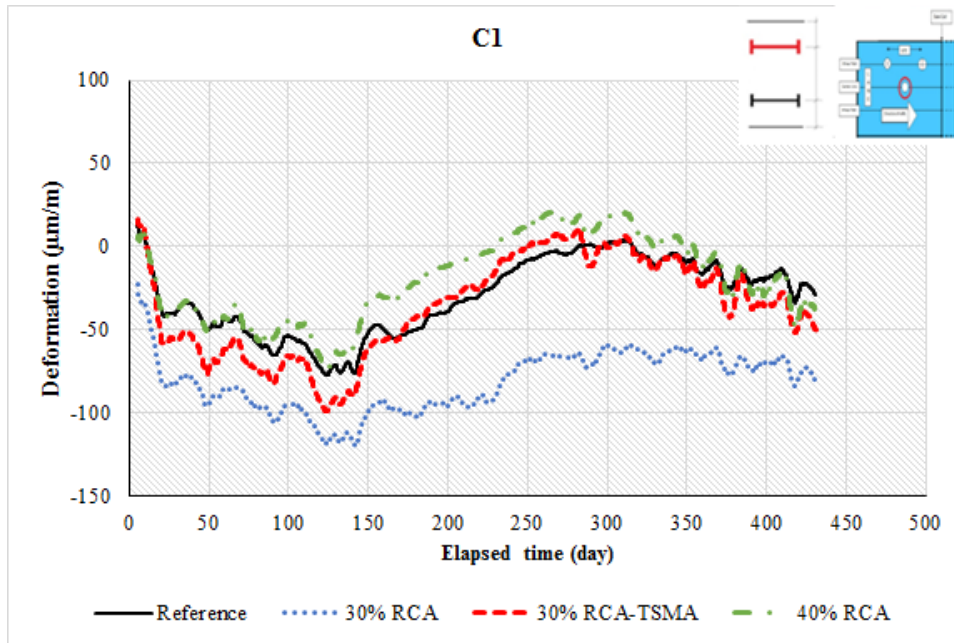


Figure 5-34. Iso-thermal strain at C1 for different mixtures (top surface of pavement at center line parallel to traffic)

Deformation at the C2 location, at centerline, at the bottom part of the pavement and parallel to the traffic are presented in Figure 5-35.

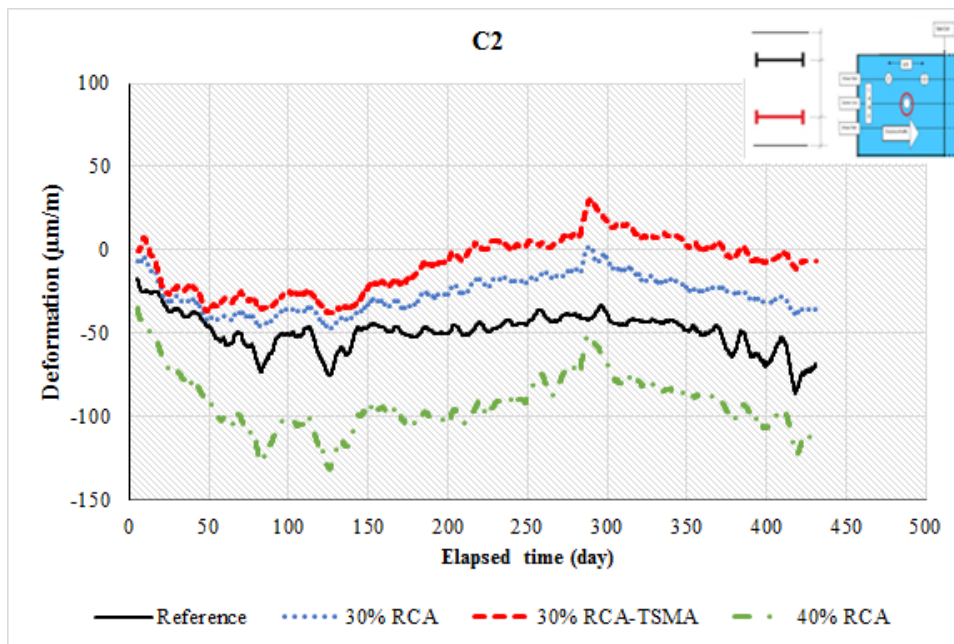


Figure 5-35. Iso-thermal strain at C2 for different mixtures (bottom part of pavement at center line parallel to traffic)

The maximum deformation was obtained with the 40% of RCA concrete by the end of the first summer. Very slight seasonal effect was observed in the case of the reference mixture. The maximum effect was proved to be for the 40% RCA concrete. Figure 5-36 up to Figure 5-39 plot the deformations registered at different locations (A1, A2, A3, and A4). It seems that the sensor located at bottom of the pavement are experiencing the lowest seasonal effect, while those at the top of the pavement reflected the largest seasonal deformation changes.

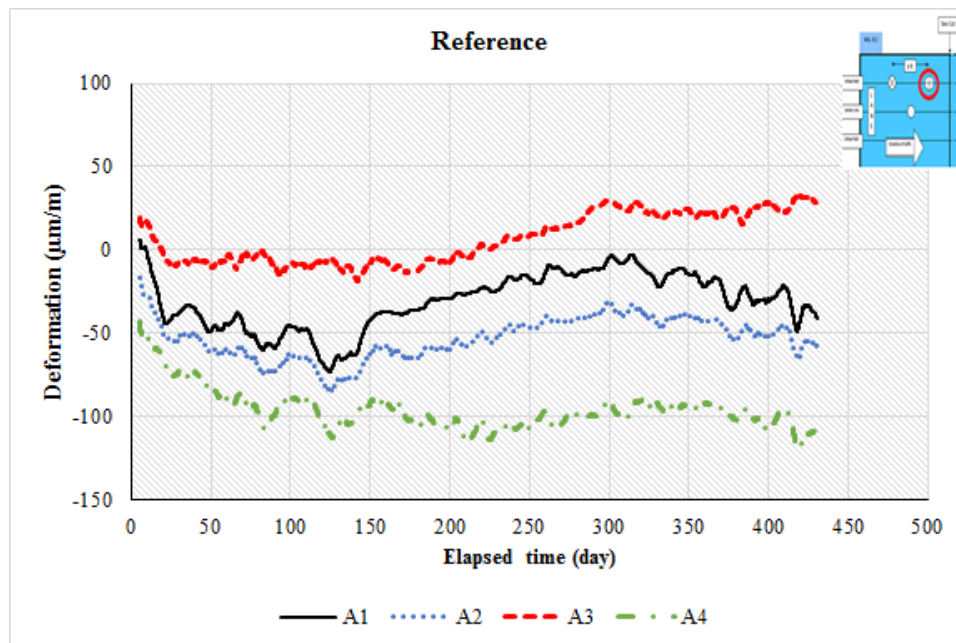


Figure 5-36. Iso-thermal strain measured by the VWSG at different depths at location A for the Reference mixture

For the reference and the 40% RCA mixtures, the iso-thermal deformation was shown to increase slightly up to 140 days with depth along the pavement for the A1, A2, and A4 that are positioned along the traffic direction. The highest strain was obtained by the A4 gage positioned at the bottom of the pavement, parallel to the direction of traffic flow. The lowest strain was observed at the A3 location, which is at mid-height of the pavement layer, perpendicular to traffic direction. Trends were different for the 30% RCA and the 30% RCA-TSMA mixtures. No special trend

was detected in these mixtures. However, the A3 location which is at mid-height of the pavement, perpendicular to the traffic direction had the minimum deformation up to 140 days.

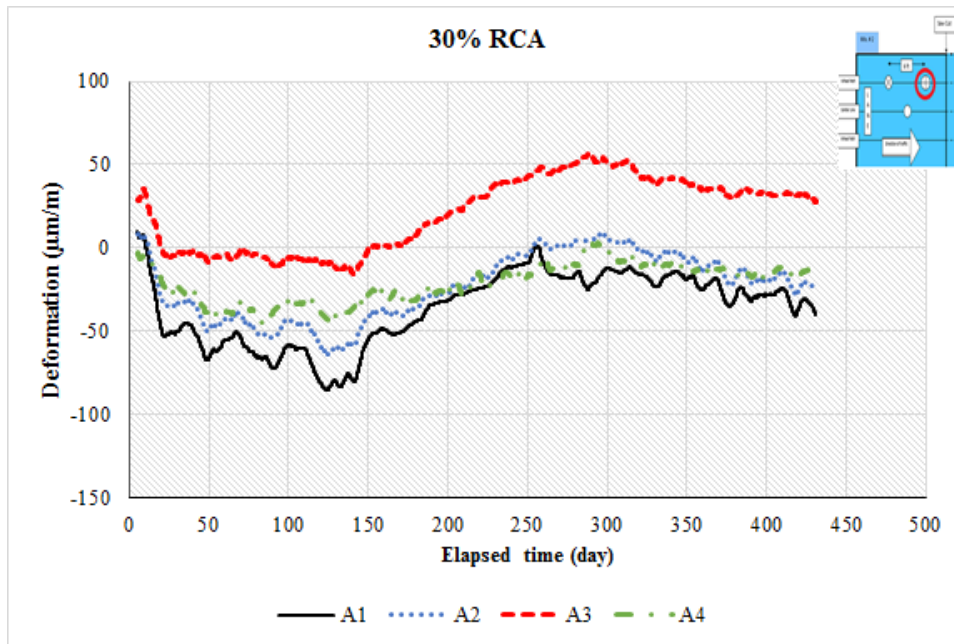


Figure 5-37. Iso-thermal strain measured by the VWSG at different depths at location A for the 30% RCA mixture

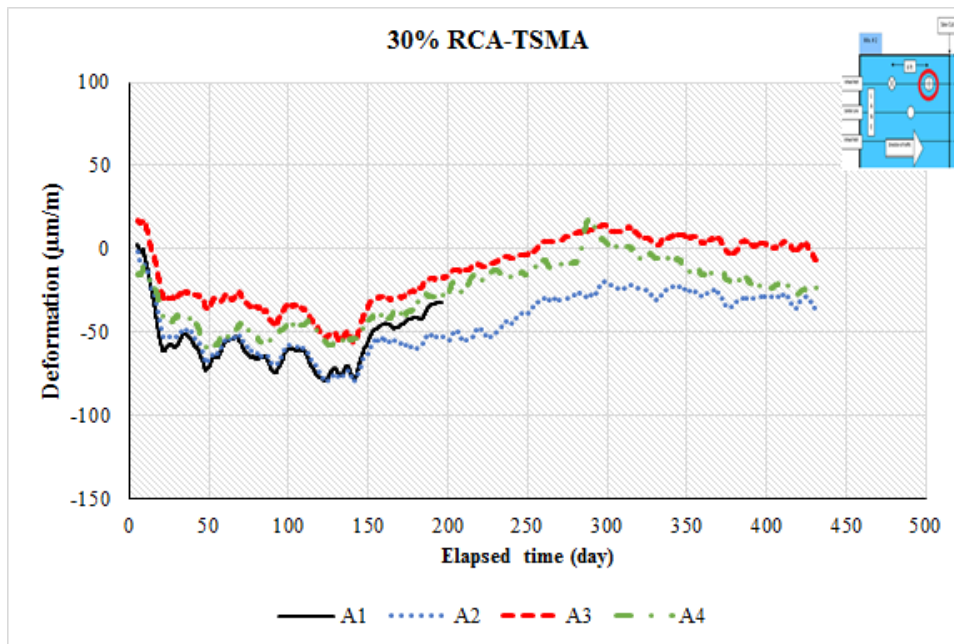


Figure 5-38. Iso-thermal strain measured by the VWSG at different depths at location A for the 30% RCA-TSMA mixture

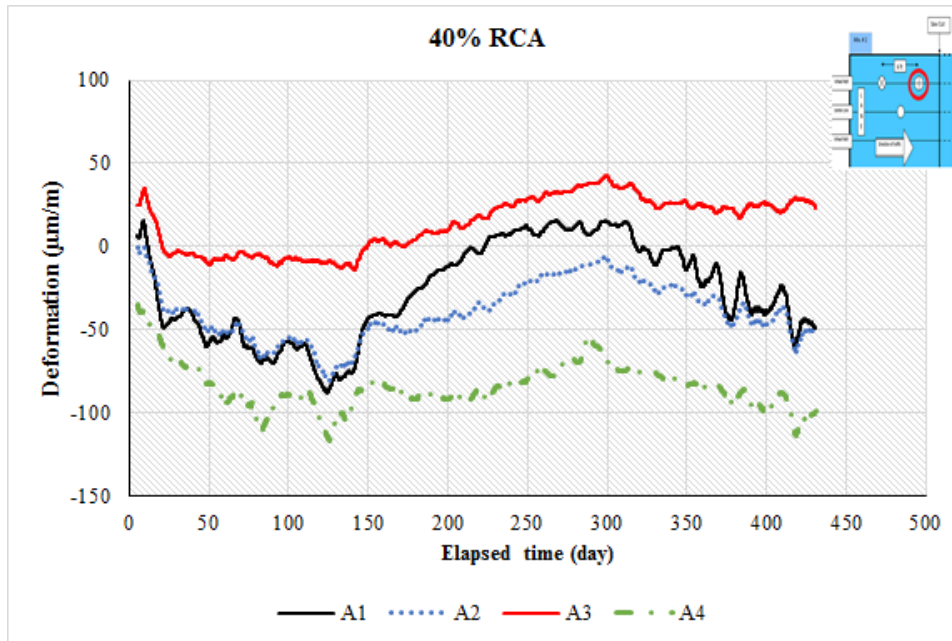


Figure 5-39. Iso-thermal strain measured by the VWSG at different depths at location A for the 40% RCA mixture

Figure 5-40 to Figure 5-46 depict the deformation at locations B1 and B2 (top and bottom at wheel path) and locations C1 and C2 (top and bottom at centerline) for all the employed mixtures. It was observed that for all the mixtures, except for the 40% RCA concrete, the sensors located at the pavement surface have registered higher deformations up to 140 days. This sensors are also reflecting larger seasonal effects for all the incorporated mixtures.

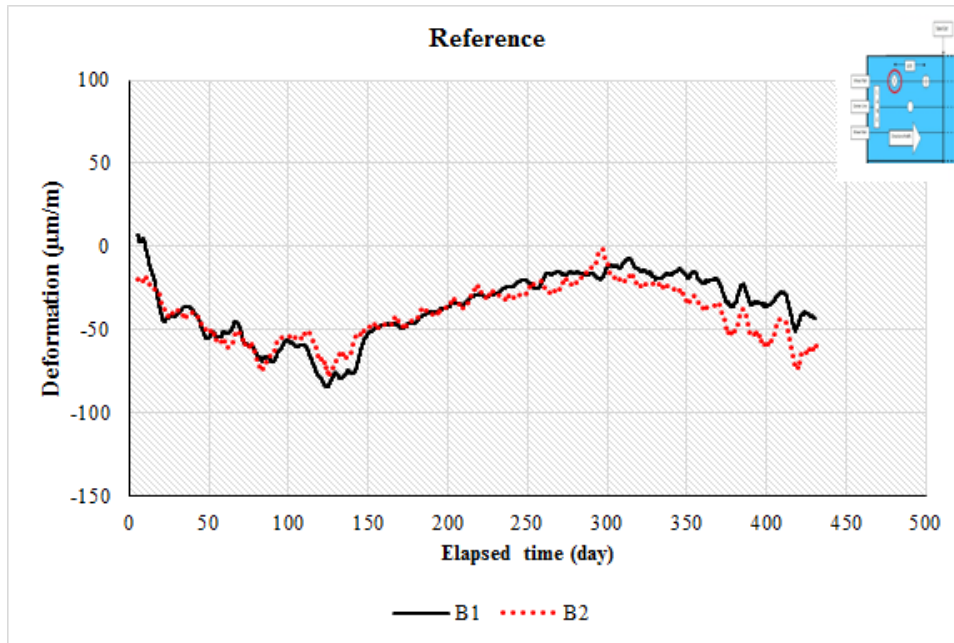


Figure 5-40. Iso-thermal strain measured by the VWSG at B1 and B2 locations for the Reference mixture

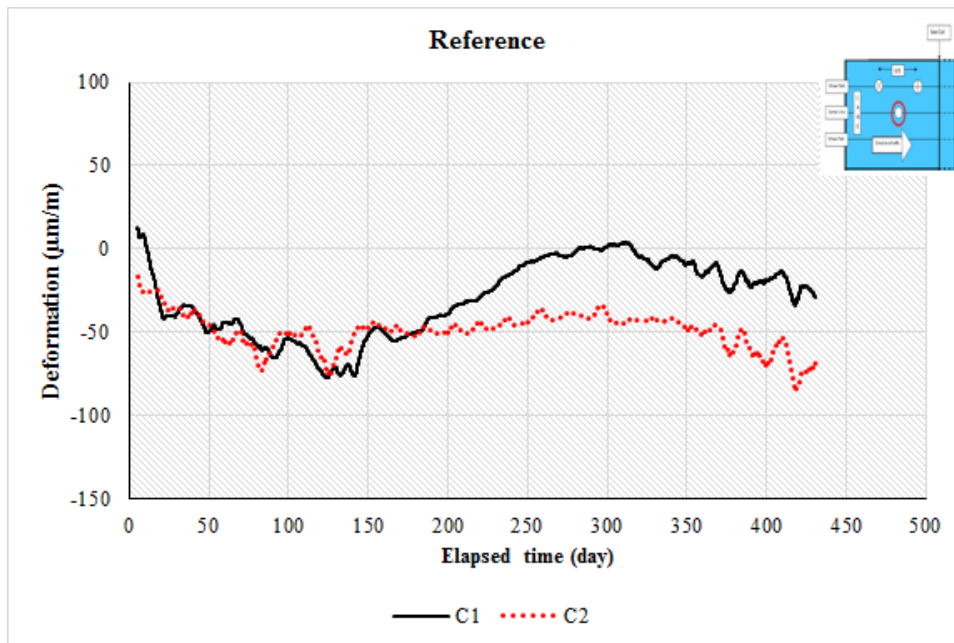


Figure 5-41. Iso-thermal strain measured by the VWSG at C1 and C2 locations for the Reference mixture

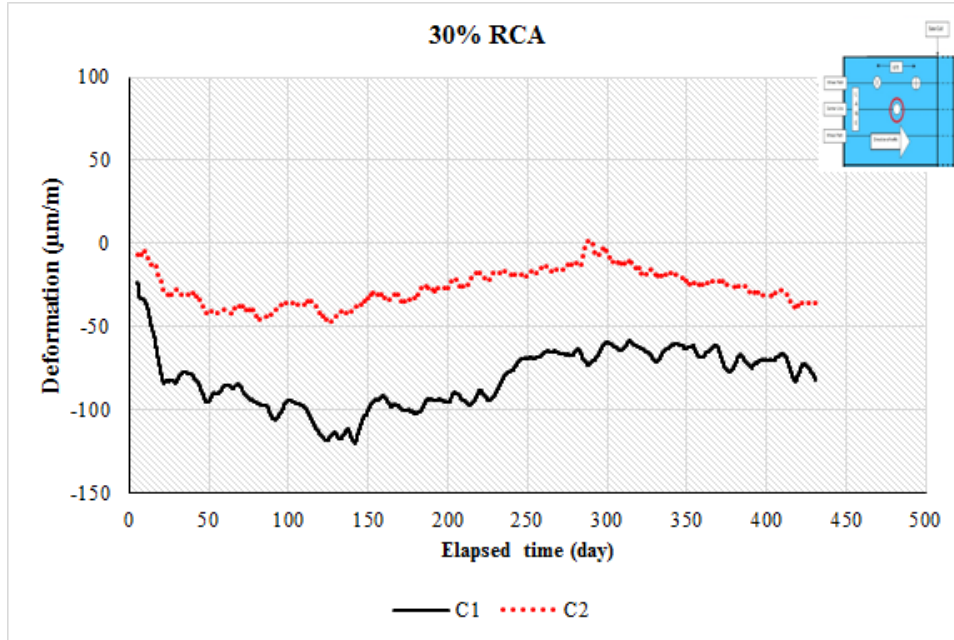


Figure 5-42. Iso-thermal strain measured by the VWSG at C1 and C2 locations for the 30% RCA mixture

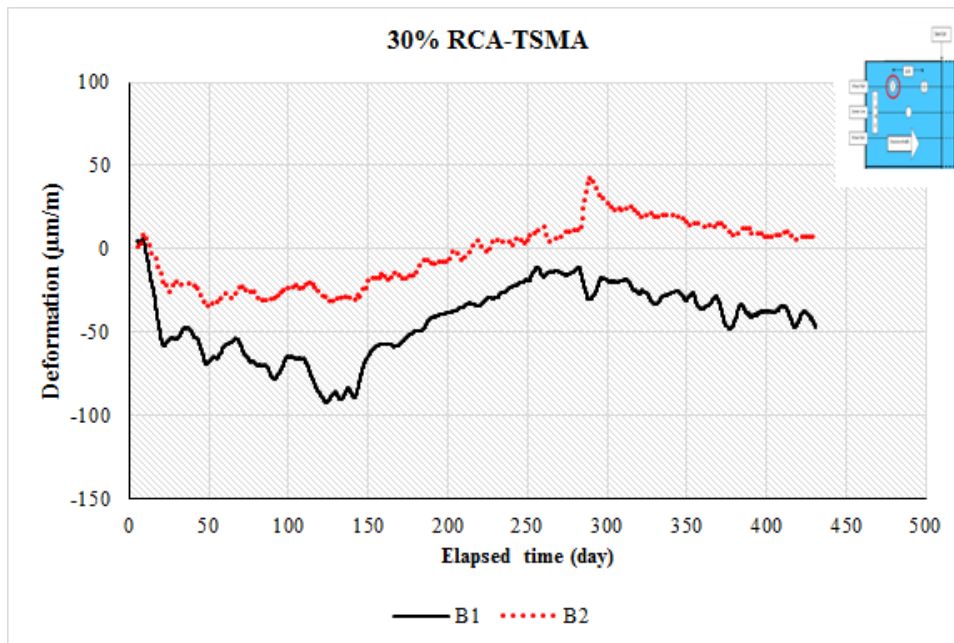


Figure 5-43. 40 Iso-thermal strain measured by the VWSG at B1 and B2 locations for the 30% RCA-TSMA mixture

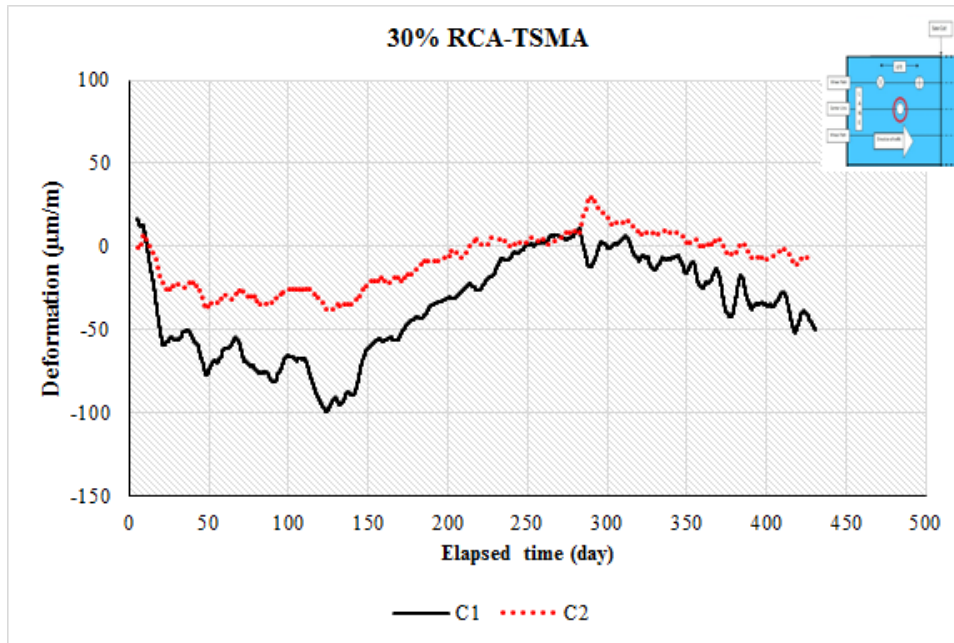


Figure 5-44. Iso-thermal strain measured by the VWSG at C1 and C2 locations for the 30% RCA-TSMA mixture

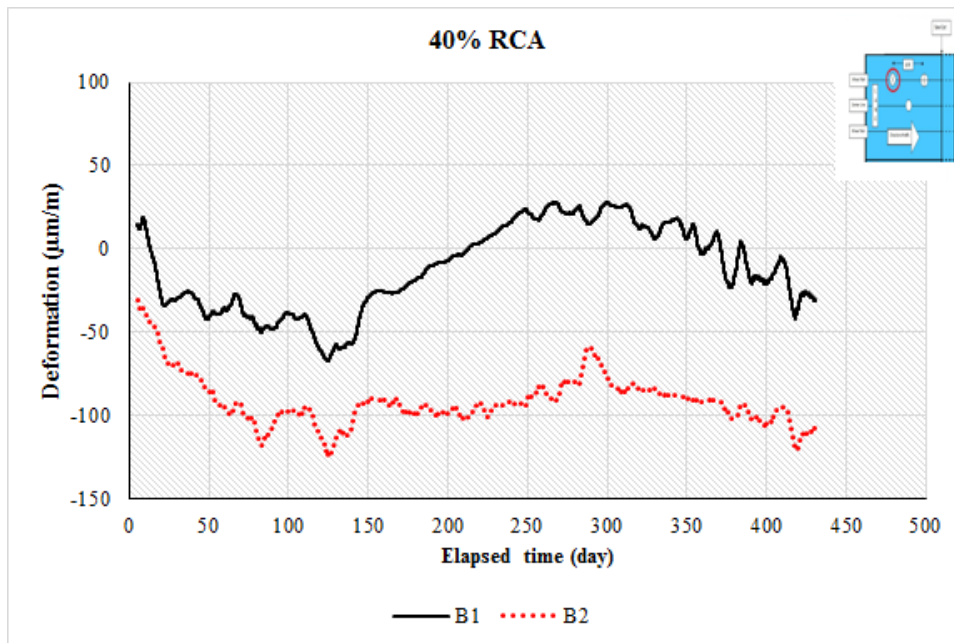


Figure 5-45. Iso-thermal strain measured by the VWSG at B1 and B2 locations for the 40% RCA mixture

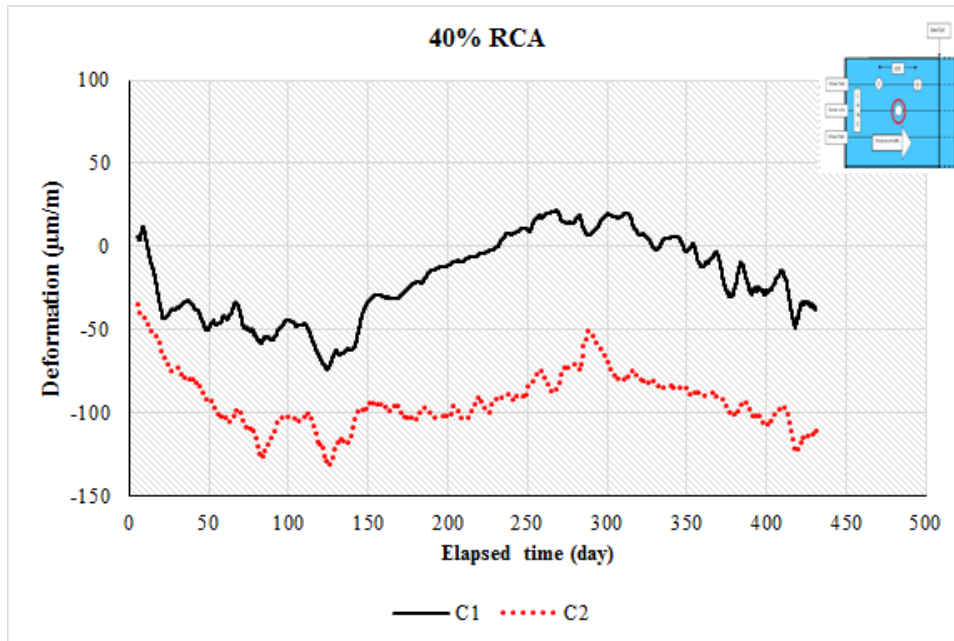


Figure 5-46. Iso-thermal strain measured by the VWSG at C1 and C2 locations for the 40% mixture

Figure 5-47 up to Figure 5-50 show the variations in strain recorded at the top surface of the pavement registered at different locations: at the wheel path (A1 and B1) and at the center line (C1) for the employed mixture. Results are consistent, and there is no considerable difference in the iso-thermal strain at the various locations, except for the 30% RCA concrete where slightly higher deformation value was obtained up to 140 days in the case of sensors located at the centerline. However, all the sensors have similar seasonal deformation values.

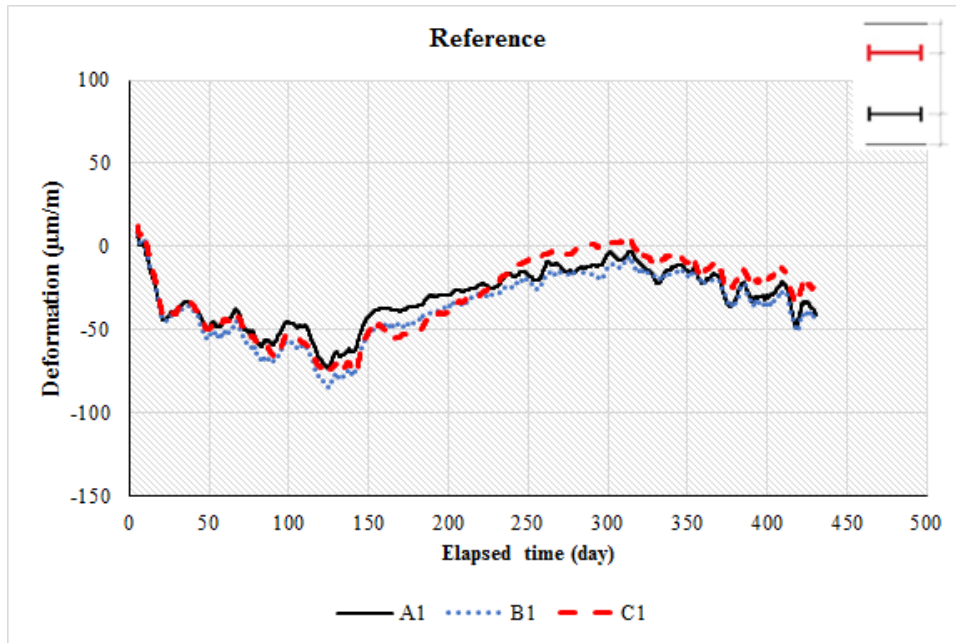


Figure 5-47. Iso-thermal strain of the Reference mixture near the top of the pavement (A1, B1, and C1)

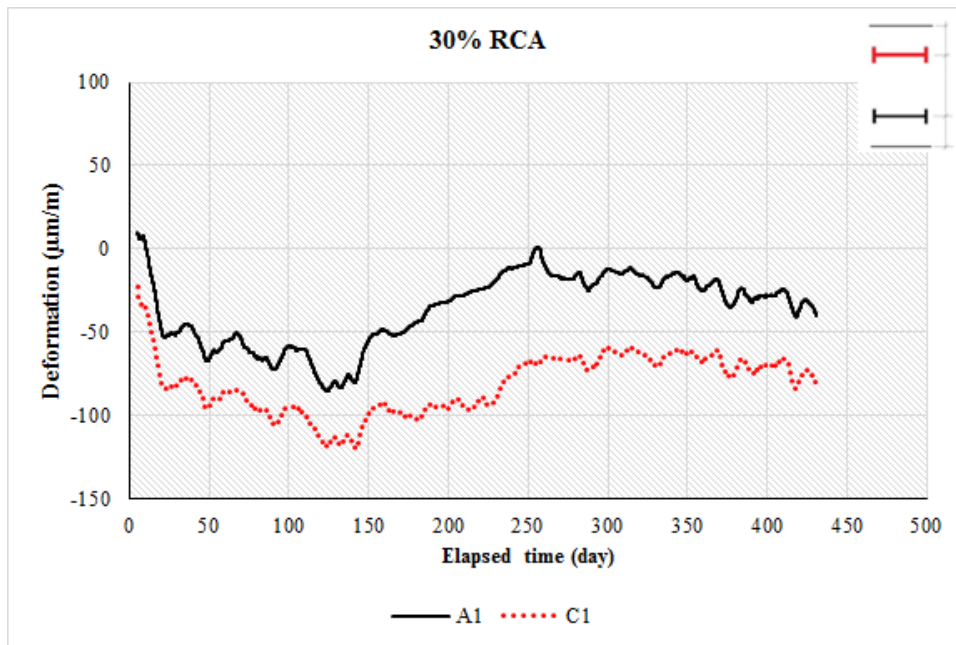


Figure 5-48. Iso-thermal strain of the 30% RCA mixture near the top of the pavement (A1 and C1)

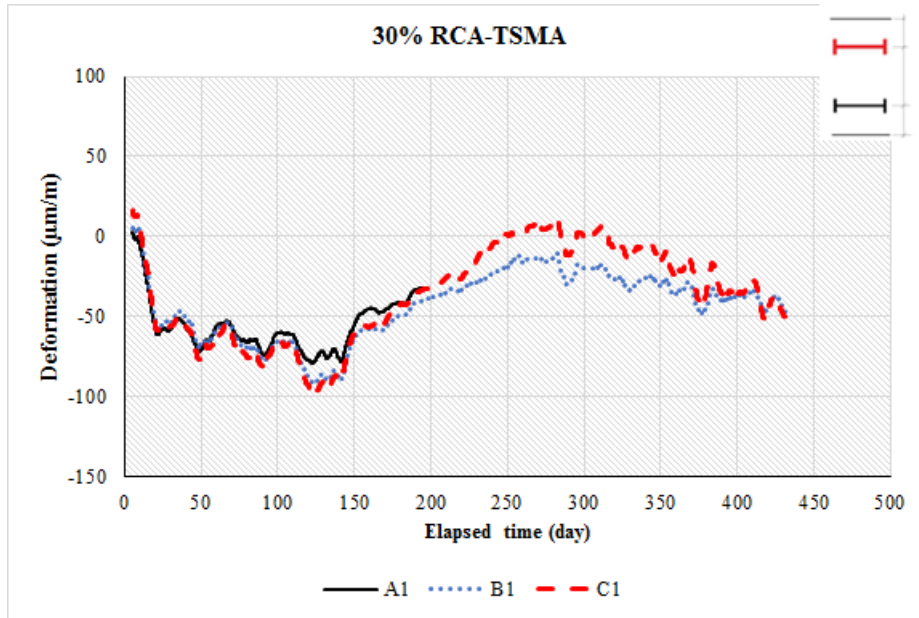


Figure 5-49. Iso-thermal strain of the 30% RCA-TSMA mixture near the top of the pavement (A1, B1, and C1)

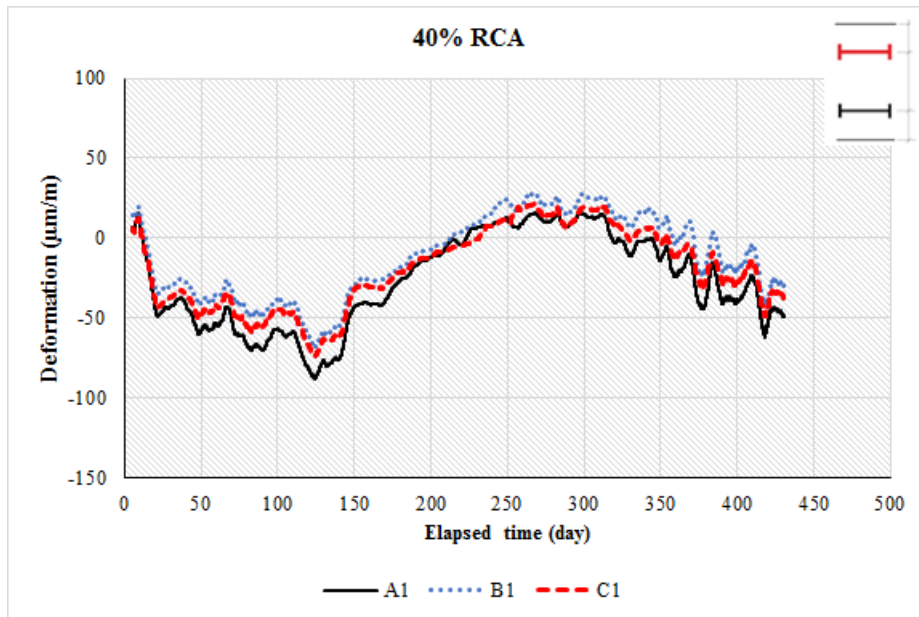


Figure 5-50. Iso-thermal strain of the 40% RCA mixture measured near the top of the pavement (A1, B1, and C1 sensors)

Deformation of the mixtures at the bottom of the pavement sections at the wheel path (A4 and B2) and at the center line (C2) are shown in Figure 5-51 up to Figure 5-54. In the case of Reference mixture, deformations at locations B2 and C2 are nearly identical. However, higher

deformation values are recorded at the A4 location. For the rest of concrete mixtures, all deformations at the bottom of the pavement layer are the same.

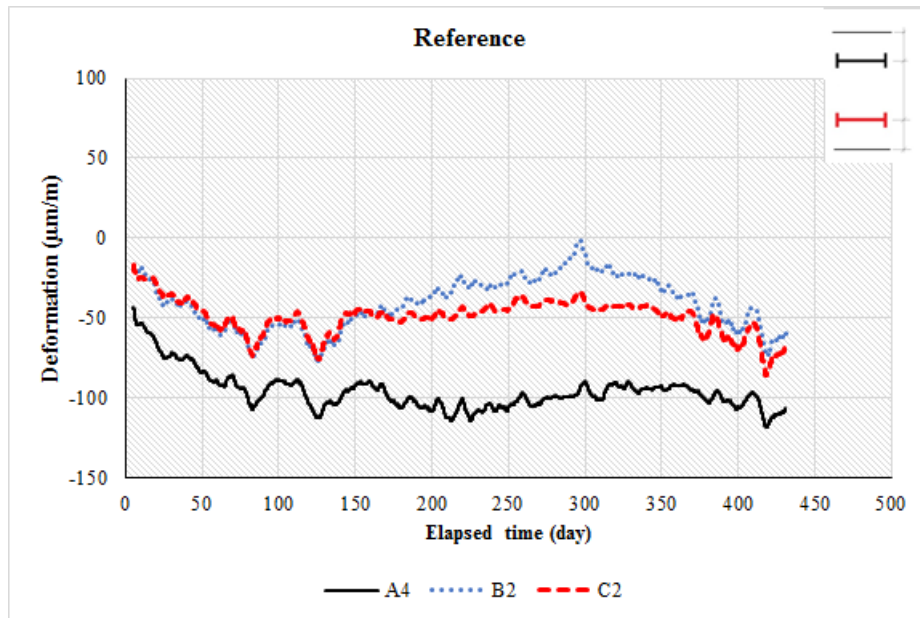


Figure 5-51. Iso-thermal strain measured at bottom part of pavement (A4, B2, and C2) for the Reference mixture

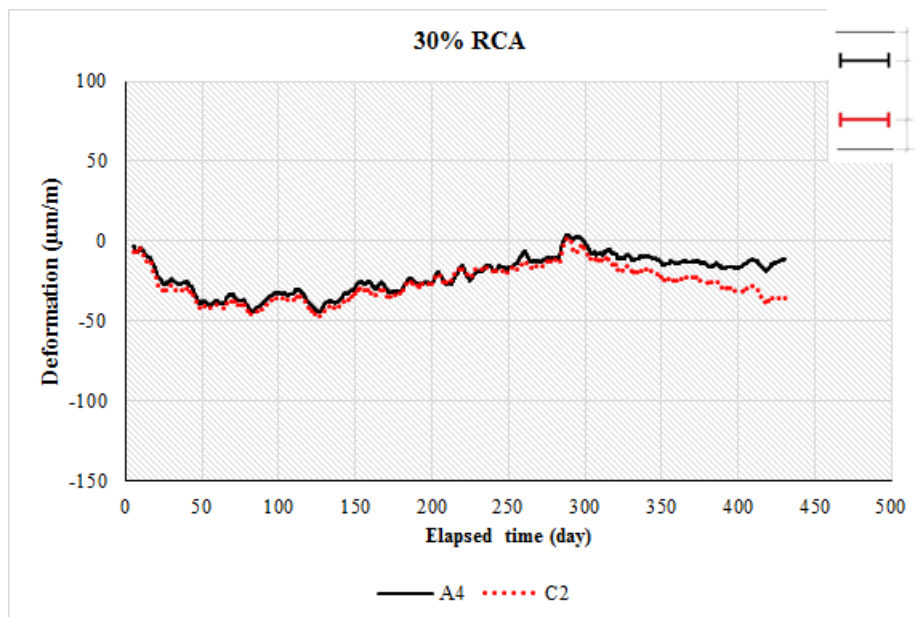


Figure 5-52. Iso-thermal strain measured at bottom part of pavement (A4 and C2) for the 30% RCA mixture

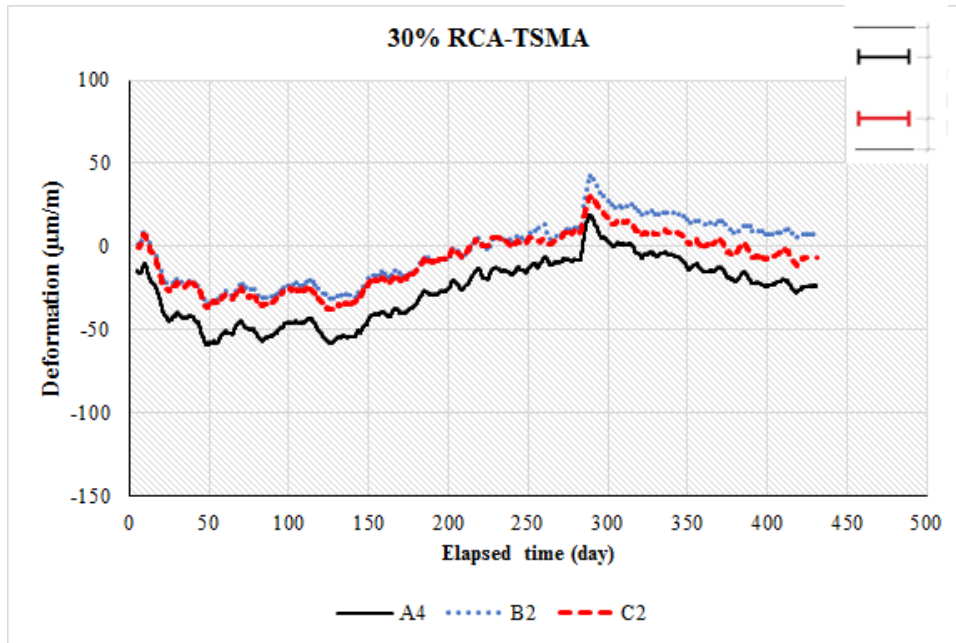


Figure 5-53. Iso-thermal strain measured at bottom part of pavement (A4, B2, and C2) for the 30% RCA-TSMA mixture

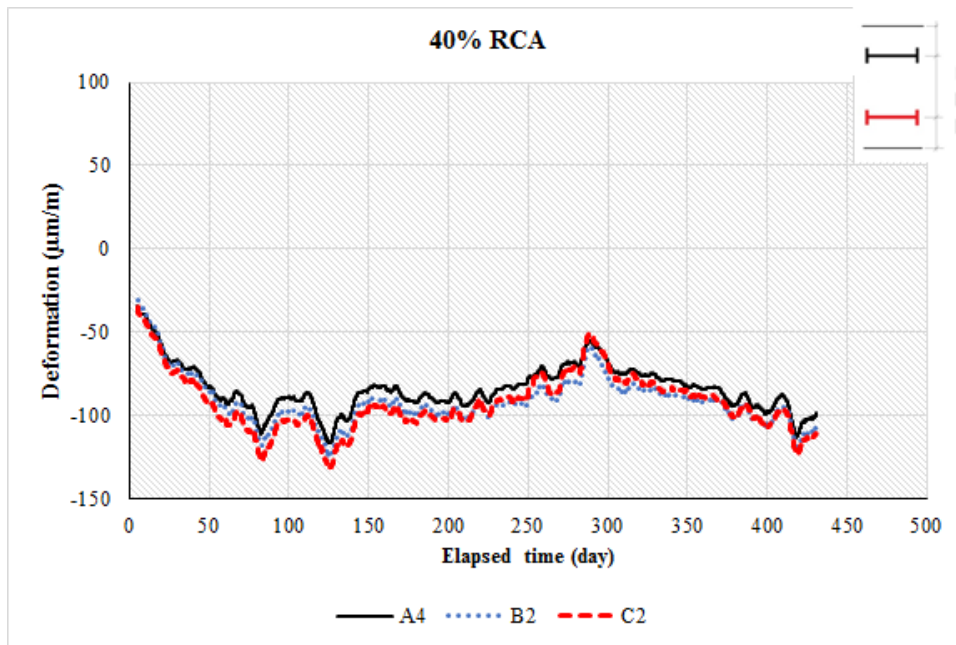


Figure 5-54. Iso-thermal strain near the bottom of the pavement (A4, B2, and C2) for the 40% RCA mixture

The above observations indicate that all four concrete pavements exhibited deformation less than $150 \mu\epsilon$ during the first summer season (140 days). This deformation is due to the synergic effect

of shrinkage, compressive strain caused by warping and tensile strains due to summer curling. By the beginning of the cold season that started September 2013, the strain direction changed from the initial negative values toward zero and then to positive values. This is believed to be due to the seasonal effects in terms of synergic effect of tensile stresses at the surface due to temperature drop and curling stresses. The seasonal effects are expected to be reverse in the case of the bottom sensors. Based on the observed data, this trend is not really reverse in the case of the sensors located at the bottom of the pavement. However, in the case of the bottom sensors, the seasonal effects on the strain direction was observed to be mostly less than the case of top sensors.

The reference mixture was proved to undergo the lowest seasonal effects, given its higher modulus of elasticity and lower coefficient of thermal expansion, as stated earlier. On the other hand, the mixtures made with 40% RCA and the concrete made with 30% RCA-TSMA had the highest deformations during the cold season. Still, it is important to note that all strain values were low and varied from +60 to -150 $\mu\epsilon$.

5.3.5. Summary and conclusion

Field implementation was conducted using four types of concrete mixtures. MoDOT's PCCP concrete mixtures was used as the reference mixture. In addition, three RCA-made concrete mixtures were employed to investigate performance of rigid concrete pavement made with coarse RCA. Up to 40% of the coarse aggregate was replaced by RCA. Several samples were taken to evaluate the performance of concrete mixtures in terms of fresh properties, mechanical properties, and durability. Pavement sections were also instrumented with vibrating wire strain gauges to monitor the long-term deformation of concrete mixtures. Based on the data presented in this chapter, the following conclusions are warranted:

- It can be stated that the RCA mixtures develop comparable performance to the Reference concrete made with the virgin aggregate in terms of mechanical properties, drying shrinkage, abrasion resistance, and durability properties.
- The 30% RCA-TSMA had lower properties compared to the rest of the concrete mixtures. This is believed to be due to the high air content (8%) of this mixture.
- A slight decrease in mechanical properties was observed due to the use of RCA. However, all the mixtures met the minimum compressive strength requirement of 4000 psi at 28 days.
- No significant difference was observed in the case of the splitting tensile strength and flexural strength of concrete made with up to 40% RCA compared to the Reference concrete made without any RCA.
- An average of 8% and 12% decrease in modulus of elasticity was observed in the case of 30% RCA and 40% RCA mixtures, respectively.
- No significant difference in 91-day rapid chloride-ion permeability was observed. A slight increase of 240 and 330 Coulomb was registered for the 30% and 40% RCA mixtures, respectively.
- All mixtures exhibited good frost durability with durability factors in range of $90\pm 3\%$ for both the ASTM C666, A and B procedures.
- 5% increase in coefficient of thermal expansion was observed in 11-month old 40% RCA concrete specimens.
- Core samples were taken to evaluate the in-situ properties of concrete mixtures. All mixtures had acceptable mechanical properties, in line with previous laboratory findings.
- Abrasion resistance of concrete mixtures was evaluated using the core samples. All mixtures had similar performance, with no spread due to the use of RCA.

- Scanning electron microscope analysis was conducted to investigate the micro-structural properties of RCA concrete. Higher concentration of micro-cracks was observed in the case of RCA mixtures, which may be attributed to the crushing process during RCA production.
- Based on the data obtained from the embedded sensors, all mixtures exhibited low isothermal deformation values varying from +60 to -150 $\mu\epsilon$.
- Based on the long-term deformation data obtained from embedded sensors, it was observed that pavement deformation pattern is changing through the year and is sensitive to variations in environmental conditions.
- Slightly higher seasonal effects are observed in the case of the RCA mixtures.
- Sensors located at the top part of the pavement sections are shown to be more sensitive to environmental effects.
- The coefficient of thermal expansion was back-calculated based on the deformation data and pavement temperature variations. Good correlation was observed between the laboratory measured values and calculations.

6. Truck loading testing

6.1. Introduction

Mechanistic-empirical design methods are used for pavement design by state agencies. There is a need to further understand the deformation characteristics of RCA concrete pavement as well as the typical virgin aggregate concrete (Immanuel 2006). Deformation induced by truck loading was used to investigate the behavior of the instrumented concrete pavement in this study. A truck loaded with aggregate was used for loading the instrumented pavement slabs. Deformation registered by the VWSGs during loading was determined and analyzed for further understanding of the structural response of the pavement sections under different loading conditions.

6.2. Pavement structure

The rigid pavement was cast on a 4.0 in. thick base layer made with a standard aggregate composition (Type 5 aggregate), complying with MoDOT specification Number 1007 (1999). The base was constructed on a compacted subgrade soil. A jointed plain concrete pavement (JPCP) system with uniform thickness of 8.5 in. was used for the construction of a 22.5 ft wide ramp approach (outside lane and shoulder). The pavement structure consisted a 12-ft lane limited to a 10-ft shoulder from one side and to the existing 12-ft wide lane from the other side. Longitudinal joints were saw-cut between the travel lane and shoulder. Transverse joints were also saw-cut at 15 ft spacing where dowel bars were pre-placed. This resulted in 12×15 ft pavement panels. Saw-cutting was performed about 6 to 8 hours after casting the concrete.

6.3. Re-examing the sensor locations

Displacement of reinforcement is one of the issues with slip-form paving. This is a great concern in the case of the dowel bars or reinforcing sheets that are not tied to the base correctly. The

same problem was probable in the case of sensor baskets embedded in the stiff concrete mixture used in the study. Therefore, a three step approach was used to ensure the exact location of the sensors relative to the loading point (tires of the truck), as described below:

1. The sensor locations were marked on the pavement surface based on the initial construction plans and project photos (Figure 6-1).



Figure 6-1. Photos of the location of the sensors

2. A deep metal scanner was used for detecting the marked area, as shown in Figure 6-2, to make sure that the sensors are located at the pre-determined locations.
3. Before the start of truck loading, the truck was positioned over the identified spots, and deformation was monitored. Based on the observed deformation patterns, maximum deflections registered at truck location positioned at the exact spots where the sensors are detected (Figure 6-2).



Figure 6-2. Deep metal scanner used for detecting sensor baskets (left) and simultaneous monitoring deformation to ensure exact location of sensors (right)

6.4. Data acquisition

The truck loading was conducted over two separate days. Different data acquisition systems were used for each day. The first testing was conducted on November 11, 2013. A data acquisition system capable of recording data with 2.5 Hz frequency was used for the first testing campaign. All embedded VWSGs were logged to the system, and time history deformations were monitored and registered during the loading. However, due to the low frequency of data recording, the signal to noise ratio was low, and the deformation values were not clear compared to the noise. The setup used for the first loading test, however, was useful to determine the exact location of the embedded sensors. As an example, deformation monitored at the top part of the 30% RCA concrete pavement for the first loading campaign is presented in Figure 6-3.

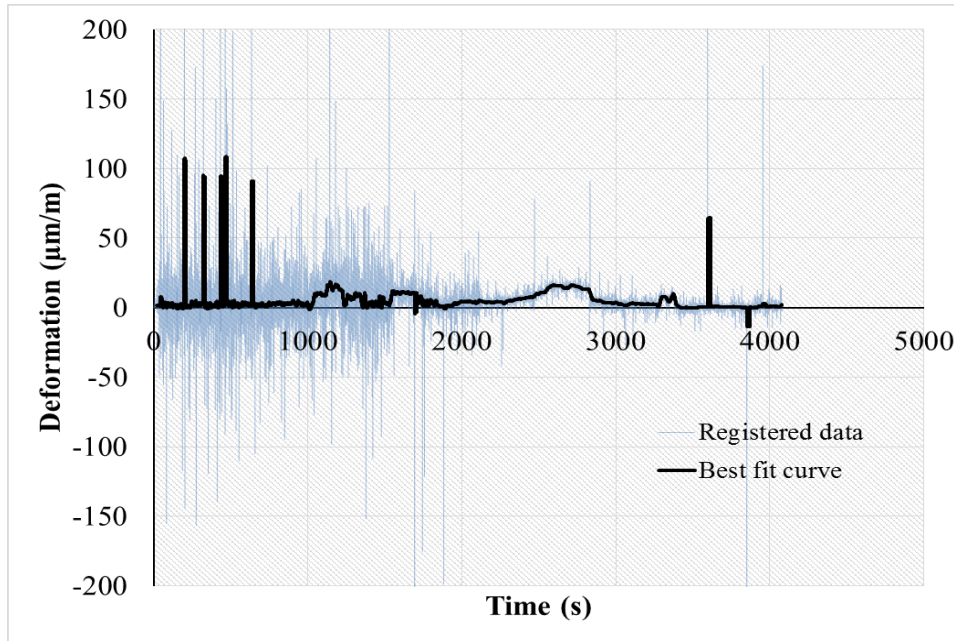


Figure 6-3. Time history deformation obtained during the first truck loading test campaign

The second test was conducted on December 17, 2013. This time, a high resolution data acquisition system capable of recording the data with high frequency up to 100 Hz was used. The 20Hz frequency was enough for registering smooth and noiseless deformation data, as presented in Figure 6-4.

Due to the limited number of input channels of the data acquisition system used in the second test campaign (eight sensors at the same time), mostly the VWSGs located at the wheel path located at top and bottom of the pavement section were used to monitor deformation caused by the truck loading. Therefore, four VWSGs were selected from each mixture and plugged into the data acquisition system.



Figure 6-4. Data logger used for the second truck loading test (Campbell Scientific Co. 2014)

Load frequency is calculated to be between 0 and 20 Hz based on the frame bending vibration mode frequency for trailers and tractors (Gillespie et al., 1993) and between 2 and 15 Hz based on the truck's suspension vibration frequency (Monismith et al., 1988). Gillespie et al., (1993) have reported that frequency is changing with the truck speed, varying from 4.6 HZ at 36 mph to 6.5 Hz at 51 mph. Similar trends were reported by Darestani et al., (2006), with frequency varying from 0.159 Hz at 1.2 mph to 8.724 Hz at 68 mph.

6.5. Truck and loading configuration

Figure 6-5 provides a schematic of the truck load configuration. For all loading scenarios, the wheel plane over sensors A and B correspond to that at the driver side were used for loading the sensors. In the case of the tandem axle, the tires at the driver side were placed on top of the sensors. The weights of both the driver and passenger sides of the front and the rear axles were determined in a weigh station. The loads of the axles and the contact pressure applied to the pavement surface based on the contact area beneath the tires are presented in Table 6-1.

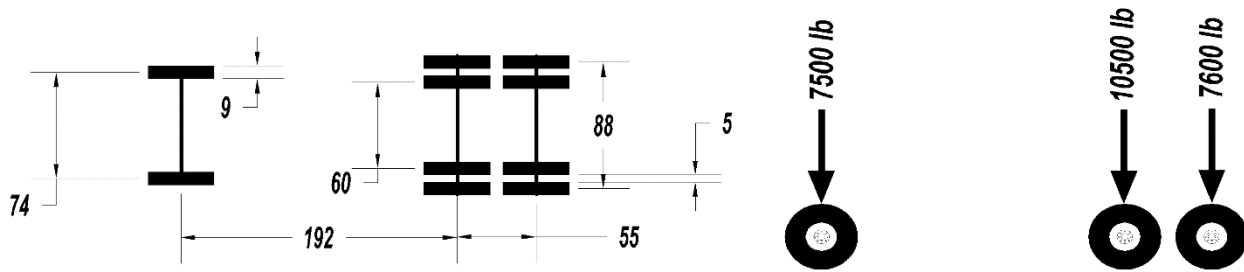


Figure 6-5. Schematic of truck load configuration, dimensions in in.

Table 6-1. Axle weights and pressure at tire-pavement contact area (driver side)

Axle type	Single	Tandem	
Tire position	Front tire	Front tires	Rear tires
Tire Load (lb)	7500	10500	7600
Contact pressure (psi)	83	146	106

The truck loading was conducted in a static, slow moving, and high speed mode. The static loading consisted of positioning the front wheel of the truck on top of the sensors to simulate the effect of static single axle loading. After the deformation was registered, the truck moved forward to have the tires of the rear tandem axle being positioned on sensor spots. In order to investigate the effect of speed on the pavement deformations, the truck was then passed over the marked sensor locations with different speeds varying from a slow crawling speed up to 21.5 mph for the sections made with 30% RCA and 30% RCA-TSMA. Two sensors were used for each depth (top and bottom) for both mixtures. The top and bottom sensors were located approximately 2.0 in. far from the top surface and bottom part of the pavement section, respectively. All sensors were aligned parallel to the traffic flow.

6.6. Results and discussion

6.6.1. General observations

All sensor readings were set to zero before the loading. Time history deformation was registered for all the loading scenarios, and the maximum deflection caused by the single and the tandem axle loadings was compared as suggested by Goulias et al., (2011). As an example, the deformations subjected to the slow moving load at top and bottom part of the pavement section cast with the 30% RCA mixture are presented in Figure 6-6.

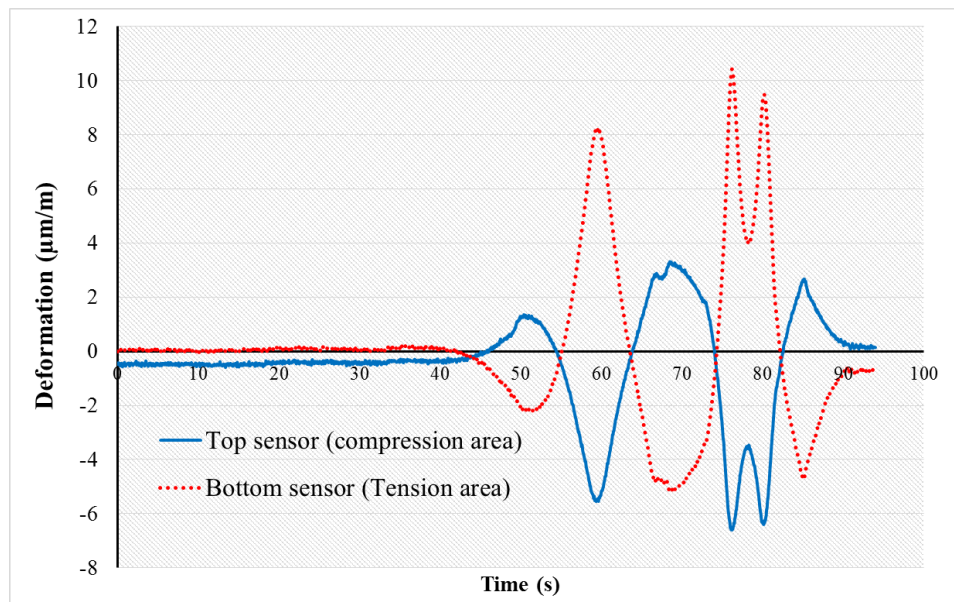


Figure 6-6. Sample deformations registered at top and bottom of the pavement due to slow moving truck

For every loading spot, it was found that for the tension areas, stresses are compressive just before the tire reaches the top of the sensor, and then the stresses change to tension and vice versa. Time needed for change stress between compression and tension varied with the speed of truck. An example for this behavior is presented in Figure 6-7 where the time history deformation of sensors located at the bottom part (tension zone) of the pavement cast with 30%

RCA for both the static and high speed loading. Similar patterns for the stress type during dynamic loading was also observed by Kumara (2005).

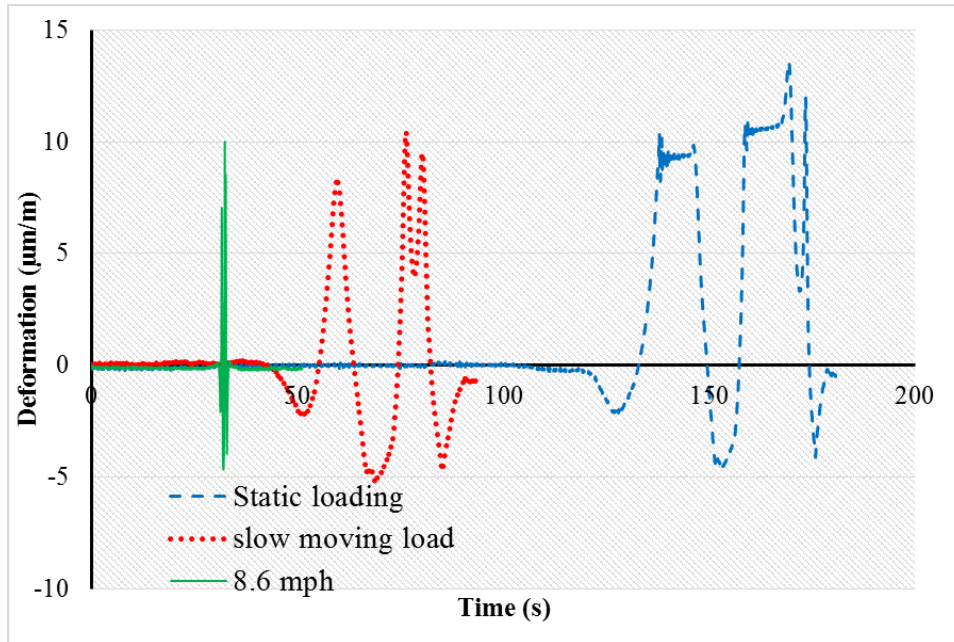


Figure 6-7. Variations in stress direction during the truck movement – bottom part of pavement

6.6.2. Peak deformation

The values of the maximum deformation at different sensor locations are summarized in Table 6-2 to Table 6-4 for different loading types. Negative values represent deformation in the compression zone (pavement surface), and positive data refer to the tensile strain measurements at the bottom part of pavement sections. Based on the data, it was clear that the deformation values registered at mid-height of the pavement section are significantly lower than those of the top or bottom parts. This is expected given the fact that the mid-height sensors are placed close to the neutral axis of the section, thus resulting in deformation values close to zero.

Table 6-2. Peak deformation registered through Static loading ($\mu\text{m/m}$)

- : compression, +: tension						
Axle type	Mixture type	Sensor location				
		Top 1	Bottom 1	Mid-height	Top 2	Bottom 2
Single	Ref	-3.2	5.3		-3.1	5.8
	30% RCA	-6.9	10.2	0.6	-	-
	30% RCA-TSMA	-	20.0		-10.3	17.5
	40% RCA	-6.4	10.6		-6.2	14.1
Tandem	Ref	-2.5	4.2		-4.1	7.5
	30% RCA	-7.7	13.6	1.8	-	-
	30% RCA-TSMA	-	20.3		-10.4	16.7
	40% RCA	-7.8	13.1		-6.1	13.9

Table 6-3. Peak deformation registered for slow moving load ($\mu\text{m/m}$)

- : compression, +: tension						
Axle type	Mixture type	Sensor location				
		Top 1	Bottom 1	Mid-height	Top 2	Bottom 2
Single	Ref	-3.1	4.9		-3.0	5.7
	30% RCA	-5.1	8.0	0.4	-	-
	30% RCA-TSMA	-	15.7		-8.9	13.8
	40% RCA	-4.4	6.7		-4.3	7.9
Tandem	Ref	-3.0	4.7		-3.7	6.9
	30% RCA	-6.1	10.4	0.7	-	-
	30% RCA-TSMA	-	18.3		-10.0	16.3
	40% RCA	-6.0	10.5		-4.6	9.2

Table 6-4. Peak deformation registered for high speed moving load ($\mu\text{m}/\text{m}$)

-: compression, +: tension

Speed (mph)	Axle type	Mixture	Sensor location				
			Top 1	Bottom 1	Mid-height	Top 2	Bottom 2
8.6	Single	30% RCA	-4.4	7.7	0.4	-	-
		30% RCA-TSMA	-	13.2	-	-7.1	11.3
	Tandem	30% RCA	-5.7	10.1	0.6	-	-
		30% RCA-TSMA	-	15.3	-	-8.6	13.7
14.3	Single	30% RCA	-3.9	7.1	0.5	-	-
		30% RCA-TSMA	-	11.7	-	-6.8	10.7
	Tandem	30% RCA	-6.0	10.1	0.4	-	-
		30% RCA-TSMA	-	15.3	-	-8.8	14.2
21.5	Single	30% RCA	-3.5	5.9	0.3	-	-
		30% RCA-TSMA	-	11.1	-	-6.6	10.2
	Tandem	30% RCA	-4.9	8.1	0.3	-	-
		30% RCA-TSMA	-	12.9	-	-8.8	12.2

6.6.3. Verification of peak deformation

The mechanistic approach for calculating the stress at interior parts of rigid pavement proposed by Huang (2004) was used to verify deformation data from the truck loading test. The 56-day modulus of elasticity and Poisson's ratio was used as the model input. Linear stress distribution through the pavement thickness were used to calculate and convert to the stress and corresponding strain at each sensor depth (Equation 6-1). The average tensile strain caused by single axle during static loading is compared to the strain values estimated by equation 6-1 in

Figure 6-8. The model estimations are similar for all mixtures. Measurements are up to 10 $\mu\epsilon$ smaller than the estimated values except for the 30% RCA-TSMA mixture.

$$\delta = \frac{3(1 + \nu)P}{2\pi h^2} \left(\ln \frac{l}{b} + 0.6159 \right) \quad (6-1)$$

where ν is the Poisson's ratio, h is the slab thickness (in.), P is the load (lb), l is the radius of relative stiffness, and b is a function of P and h.

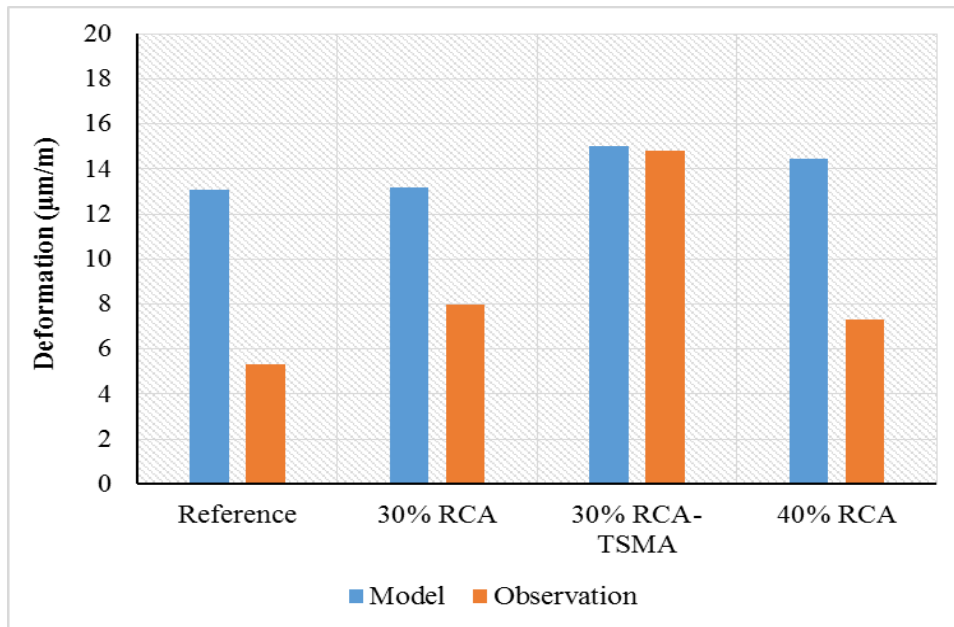


Figure 6-8. Comparisons of measured deformation to strain values estimated using Equation 6-1. As stated earlier, VWSGs were used to monitor the long-term deformation of the concrete sections due to shrinkage and environmental effects. Figure 6-9 shows typical deformation registered over time for a sensor embedded at the bottom part of the reference concrete, in the wheel path, parallel to the direction of traffic. The deformation caused by shrinkage and environmental effects are much higher than those caused by truck loading.

Peak deformation values measured for different concrete mixtures are presented in Figure 6-10 and Figure 6-11. The lowest deformation was observed in the case of the reference concrete.

Concrete mixtures made with 30% and 40% RCA replacement had similar performance for all loading scenarios. The highest deformation values were recorded for the mixture made with 30%RCA-TSMA. However, all the registered deformation values are very small.

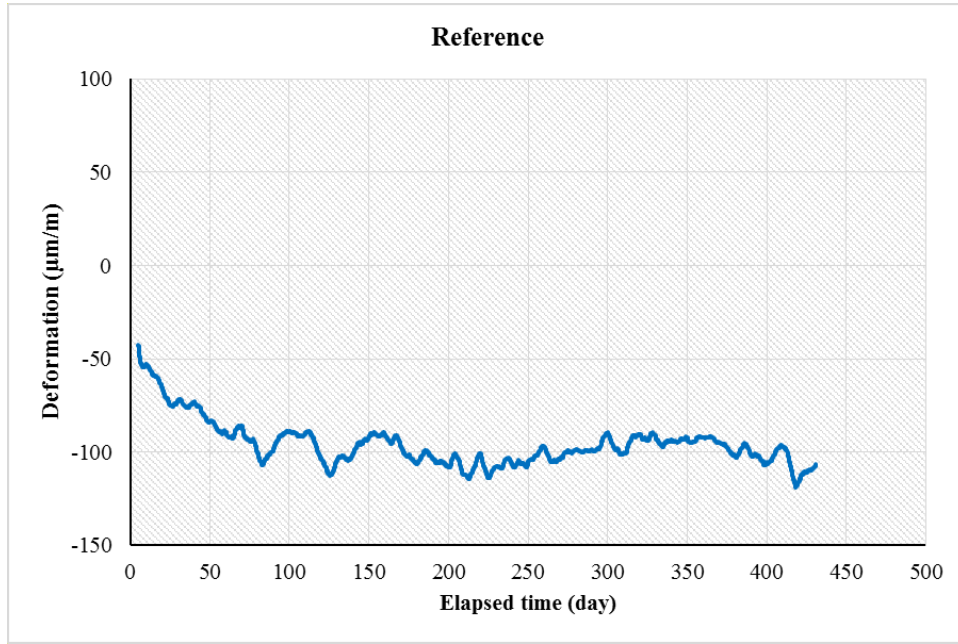


Figure 6-9. Total deformation registered at the bottom part of the reference concrete at wheel path

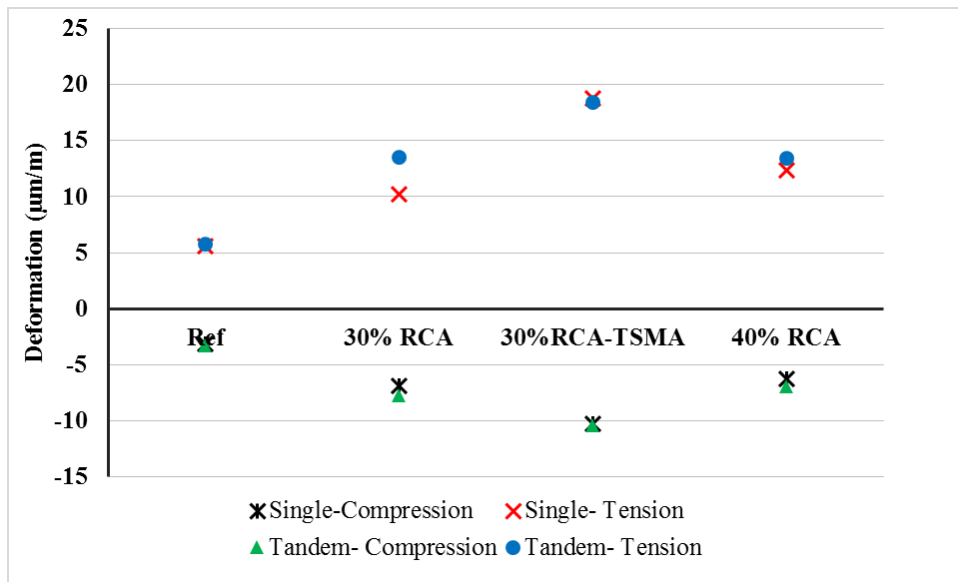


Figure 6-10. Maximum strain recorded during static loading

The variations in deformation with respect to the speed of loading from static to high speed of 21.5 mph are presented in Figure 6-12. The static loading led to the highest peak deformation values among the various loading types. The increase in the speed of truck results in a decrease in the peak deformation as presented in Figure 6-12.

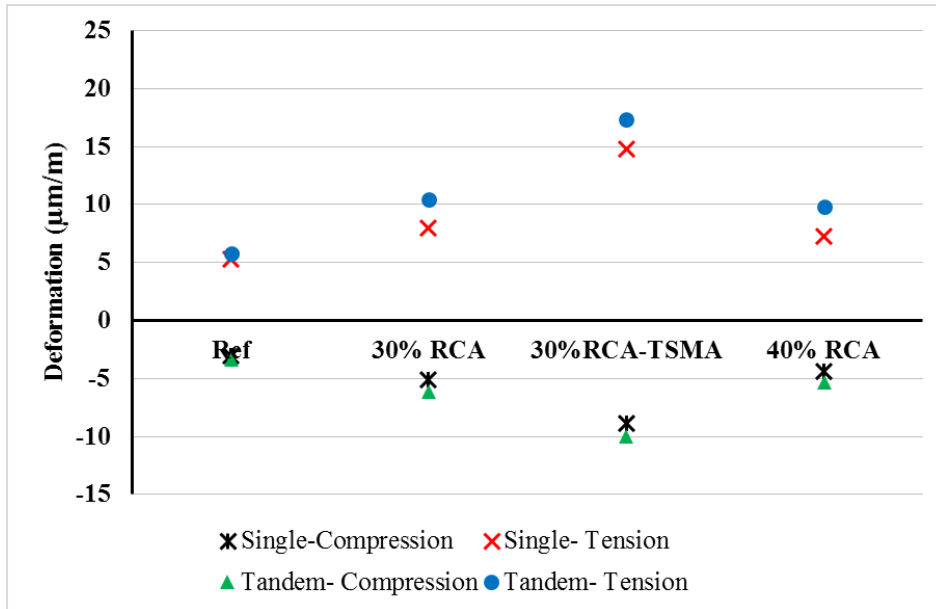


Figure 6-11. Maximum strain recorded during the low speed loading

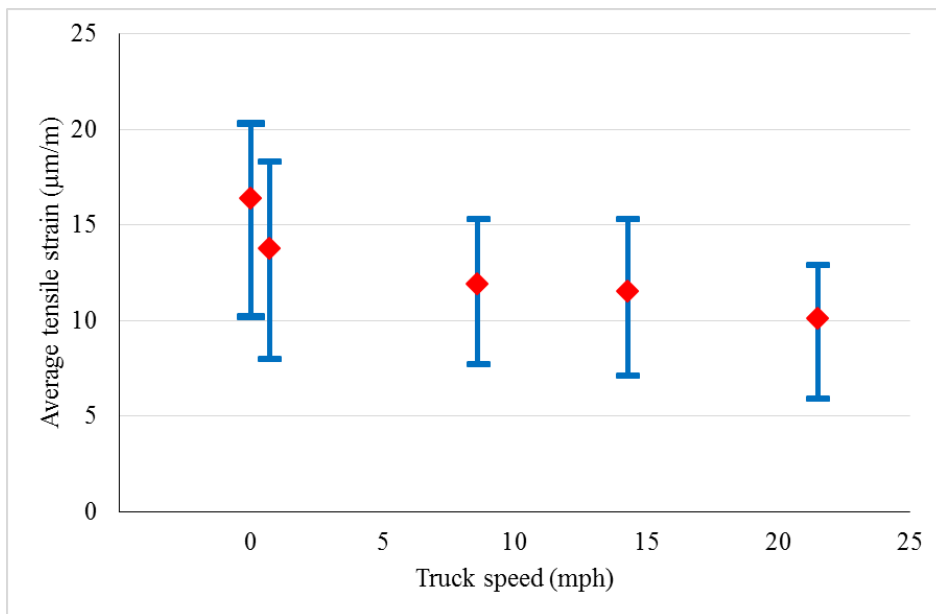


Figure 6-12. Average tensile strains recorded during the loading with different speeds

6.6.4. Statistical data analysis

A statistical analysis software package (SAS 9.3) was used to test the following hypothesis at 95% confidence level ($\alpha=0.05$ significance level) (Montgomery 2001):

H_{0-1} : there is no significant difference in deformation for different concrete types

H_{a-1} : the assumption of H_{0-1} is not correct

H_{0-2} : there is no significant difference in deformation at different speeds of passing

H_{a-2} : the assumption of H_{0-2} is not correct

H_{0-3} : there is no significant difference in deformation by different axle types

H_{a-3} : the assumption of H_{0-3} is not correct

Initially, a four-way experimental design was used for the data analysis. The factors that were taken into consideration were: concrete type (four levels), loading speed (two levels), truck axle type (two levels), and sensor location (two levels). In each case, the response consisted of determining the deformation registered by each sensor. Two replications were assumed for each location. However, as mentioned earlier, not all the sensors were responding reliably on the test day. Therefore, a Type III sum of square approach was used for analyzing the software output in order to compensate for the missing data points (Montgomery 2001). Considering the symmetric behavior of the sensors located at the tensile and compression zones, most of the mean deformation values calculated by the software were close to zero. This results in misleading comparison with no significant difference in the mean values for different treatment combinations, i.e., combinations of different levels of different factors. Therefore, the structure of the analysis was modified to a three-way analysis that was conducted on the data set obtained only from the bottom sensors located in the tension area where more observations were registered.

Statistical analysis relies on the fact that the calculated P-value less than the significance level ($\alpha=0.05$) means that the factor or the interaction between factors will be statistically significant, while P-values greater than $\alpha=0.05$ threshold reveal the fact that such particular factor or interaction will not be statistically significant (Montgomery 2001).

Effect of concrete mixture and axle type on deformation. A summary of the analysis of variance (ANOVA) results is presented in Table 6-5.

Table 6-5. Three-way ANOVA results at 0.05 significance level

Source	DF	Type III SS	Mean Square	F Value	Pr > F
Concrete	3	551.9642857	183.9880952	74.26	<.0001
Speed	1	38.4160000	38.4160000	15.51	0.0020
Concrete*Speed	3	17.8985714	5.9661905	2.41	0.1179
Axle	1	15.8760000	15.8760000	6.41	0.0264
Concrete*Axle	3	4.7785714	1.5928571	0.64	0.6020
Speed*Axle	1	1.1560000	1.1560000	0.47	0.5075
Concrete*Speed*Axle	3	2.9971429	0.9990476	0.40	0.7533

Although the magnitude of the deformation registered at sensor locations is relatively small, given the analytical results presented in Table 6-5 it was concluded that all the studied factors, including concrete type, speed, and axle type will have significant effect on deformation values. None of the two-way or three-way interactions between the factors were significant at 0.05 significance level as presented in Table 6-5.

Several sets of contrast vectors were used for comparing the deformations registered for different levels of factors in the SAS software. Based on the contrast data presented in Table 6-6, it was concluded that the reference mixture had the lowest deformation comparing to the RCA mixtures. No significant difference was observed between the 30%RCA and 40%RCA mixtures.

However, the 30%RCA-TSMA mixture had significantly higher deformation compared to other RCA-made mixtures. This might be attributed to the inferior mechanical properties of this mixture which is believed to be mostly due to higher air content of the concrete.

Table 6-6. Contrast results at 0.05 significance level

Contrast	DF	Contrast SS	Mean Square	F Value	Pr > F
Ref. vs RCA	1	386.1553846	386.1553846	155.86	<.0001
Ref. vs RCA30	1	122.4016667	122.4016667	49.41	<.0001
RCA30 vs RCA40	1	0.1066667	0.1066667	0.04	0.8391
RCA30 vs TSMA	1	64.6816667	64.6816667	26.11	0.0003
static vs slow	1	38.4160000	38.4160000	15.51	0.0020
single tandem	1	15.8760000	15.8760000	6.41	0.0264

Axle type was also shown to have significant effect on deformation. Higher deformation was registered in the case of tandem axle compared to the single axle load.

Effect of speed on deformation. Another three-way experimental design was also used for investigating the effect of speed on deformations registered by the sensors. This time, only the mixtures made with 30% RCA and 30%RCA-TSMA were used along with three more speed levels varying from 15 to 21.5 mph. Experimental design included two levels of concrete type, two levels of axle type, and five levels of speed as the factors. Only deformations registered at the tension zone were considered for the response. Two replications were assumed for the treatment combinations.

A summary of the ANOVA results from SAS outputs is presented in Table 6-7. None of the interactions between the main effects were significant at 0.05 significance level (P-values higher than 0.05). Effect of concrete type, axle type, and speed on deformation were found to be significant at 0.05 significance level.

Table 6-7. Second set of three-way ANOVA results at 0.05 significance level

Source	DF	Type III SS	Mean Square	F value	Pr>F
Concrete	1	194.4000000	194.4000000	106.52	<.0001
Speed	4	108.5926667	27.1481667	14.88	0.0003
Concrete*Speed	4	8.4433333	2.1108333	1.16	0.3856
Axle	1	36.5040000	36.5040000	20.00	0.0012
Concrete*Axle	1	0.7706667	0.7706667	0.42	0.5304
Speed*Axle	4	2.0826667	0.5206667	0.29	0.8809
Concrete*Speed*Axle	4	3.8160000	0.9540000	0.52	0.7216

Again it was concluded that the mixture made with 30% RCA had lower deformation values compared to the mixture made with 30%RCA-TSMA. Deformation caused by tandem axle loading proved to be more than that registered for the single axle loading. Table 6-8 includes the results of comparisons between the deformation means registered for different speed levels. It should be noted that the means marked with the same letter are not significantly different.

Table 6-8. Grouping the means of speed levels

Tukey grouping	Mean deformation ($\mu\epsilon$)	N	Speed (mph)
A	16.4	6	0
B	13.8	6	0.7
B	11.9	6	8.6
C	11.5	6	14.3
C	10.1	6	21.5

Increasing the loading speed from a static mode to 0.7 mph resulted in 16% decrease in the average deformation at the bottom sensors. The increase in speed from static to slow moving

condition can therefore reduce deformation. Similar effects were reported by the American Association of State Highway Officials (AASHO 1962) where the increase in loading speed from 3.2 to 95.6 km/h can decrease the value of pavement response by 29%. Izquierdo et al., (1997) studied the stress-strain behavior of plain concrete pavement constructed over a low stiffness subbase under heavy truck load. Their study proved that the increase in speed can noticeably reduce slab deflection and stress level. Studies reported by Stoner et al., (1990) and Gillespie et al., (1993) also concluded that the increase in the speed of loading can have an inverse effect on the magnitude of deformation and slab deflection. On the other hand, Liu and Gazis (1999) reported that in presence of substantial surface roughness in the pavement, greater tensile stress can be obtained under dynamic loading rather than static loading.

6.7. Conclusion

Four types of concrete mixtures were studied in this study to determine the effect of using RCA on stress-strain behavior of JPCP systems. The following conclusions are made based on the obtained results:

- Deformation of the pavement cast with concrete made with RCA was higher than that of the reference pavement with no RCA. This might be due to the lower mechanical properties, especially the lower modulus of elasticity of the RCA-made concrete mixtures.
- No significant difference in deformation under truck loading was found between the mixtures made with 30% and 40% RCA. However, the concrete made with 30% RCA-TSMA had higher deformation compared to the other mixtures. This can be due to the lower mechanical properties of this mixture that had 2.5% higher air content (fresh concrete) than the other mixtures.

- Deformation caused by the tandem axle is significantly higher than values recorded for single axle loading (up to 50%).
- Increase in the truck's passing speed results in a decrease in deformation. The static loading yielded significantly greater deformation than the slow moving load. It should be noted that however, the speed effect seems to be negligible beyond the speed of and slow moving load. However, the speed effect on the deformation reduces with the increase in the speed.
- Mechanistic approach for calculating the traffic induced stress and corresponding strain was used to verify the measurements. The model estimations are similar for all mixtures. Measurements are up to $10 \mu\epsilon$ smaller than the estimated values except for the 30% RCA-TSMA mixture. All the measured and estimated values are much smaller than the long-term deformation values registered by the VWSGs ($20 \mu\epsilon$ vs. $100\mu\epsilon$).

7. Summary and Conclusion

The main objective of this research study was to evaluate the feasibility of using RCA in concrete production for rigid pavement applications. The research was focused on Class PCCP MoDOT concrete. Fresh properties, mechanical properties, and durability of concrete made with fine and coarse RCA was investigated in the laboratory. Several mixtures made with various amounts of fine RCA ranging between 0 to 20%, up to 30% coarse RCA replacement, different amounts of Class C fly ash replacement ranging from 25% to 40%, and different w/cm of 0.37 to 0.42 were investigated in the laboratory.

Based on the previous MoDOT experiences and initial laboratory data, three RCA mixtures were proposed for field implementation. Pavement sections in St. Louis area were constructed using RCA. Fresh properties of the mixtures were monitored both at the batching plant and job site. Variety of samples were extracted for further investigation on mechanical properties and durability of the mixtures.

VWSGs were employed to investigate the long-term deformation of the pavement sections. Sensors were embedded in different depths and locations in all mixtures. In-situ data acquisition systems recorded the data every five minutes. Data was retrieved and analyzed on a monthly basis.

Core samples were extracted from different sections. In-situ mechanical properties of the concrete mixtures were investigated. Samples were prepared for investigating the microstructural properties of the mixtures using SEM.

Dynamic truck load testing was conducted to evaluate the structural response of the pavement sections to controlled traffic loading. Statistical data analysis was employed to rate the performance of the pavement sections.

Based on the findings presented in this study, the following conclusions are warranted:

- Using up to 40% coarse RCA in pavement application will not lead to significant decrease in performance of the mixtures.
- Increasing the fine RCA content to 20% does not have a significant effect on mechanical properties of the concrete mixtures. However, durability might be an issue of concern especially in the case of the de-icing salt scaling.
- Incorporation of up to 40% Class C fly ash does not have a significant effect on properties of RCA-made concrete mixtures.
- Variations in w/cm can significantly affect both the mechanical properties and durability of the concrete mixtures. Decreasing the w/cm will be helpful in enhancing the properties of RCA-made concrete.
- The TSMA was employed for producing concrete mixtures at both the laboratory and field investigations. The effect of TSMA was not significant in enhancing the properties of RCA concrete.
- The EMV method was successfully employed to produce RCA-made concrete mixtures during the laboratory investigations. Given the reduced amount of the cementitious materials in this mixture, the overall performance of the EMV mixture was satisfactory.
- Micro-cracks and defects can be found in RCA particles due to crushing process. This leads to lower performance of the RCA mixtures compared to the virgin aggregate specimens.

- Based on the long-term deformation data obtained from embedded sensors, it was observed that pavement deformation pattern is changing through the year and is sensitive to variations in environmental conditions.
- Slightly higher seasonal effects are observed in the case of the RCA mixtures.
- Sensors located at the top part of the pavement sections are shown to be more sensitive to environmental effects.
- The coefficient of thermal expansion was back-calculated based on the deformation data and pavement temperature variations. Good correlation was observed between the laboratory measured values and calculations.
- Increasing the RCA content results in increased deformation under traffic loading.
- Deformation caused by the tandem axle is significantly higher than values recorded for single axle loading (up to 50%).
- Increase in the truck's passing speed results in a decrease in deformation. The static loading yielded significantly greater deformation than the slow moving load. It should be noted that however, the speed effect seems to be negligible beyond the speed of and slow moving load. However, the speed effect on the deformation reduces with the increase in the speed.
- Mechanistic approach for calculating the traffic induced stress and corresponding strain was used to verify the measurements. The model estimations are similar for all mixtures. Measurements are up to 10 $\mu\epsilon$ smaller than the estimated values except for the 30% RCA-TSMA mixture. All the measured and estimated values are much smaller than the long-term deformation values registered by the VWSGs (20 $\mu\epsilon$ vs. 100 $\mu\epsilon$).

References

- AASHO, (1962), “The AASHO road test, Highway Research Board of the NAS-NRC division of engineering and industrial research. Report 5, Special Rep. 61E,” *American Association of State Highway Officials (AASHO), Washington, D.C.*
- AASHTO TP 95, (2011), “Standard Method of Test for Surface Resistivity Indication of Concrete’s Ability to Resist Chloride Ion Penetration.”
- Abbas A., Fathifazl G., Fathifazl G., Isgor O. B., Razaqpur A. G., Fournier B., and Foo S., (2009), “Durability of recycled aggregate concrete designed with equivalent mortar volume method”, *Cement and Concrete Composites*, Vol. 31, Issue 8, 555-563.
- Abbas A., Fathifazl G., Isgor O. B., Razaqpur A. G., Fournier B., and Foo S., (2008), “Proposed method for determining the residual mortar content of recycled concrete aggregates”, *Journal of ASTM International*, Vol. 5, No. 1, 12.
- Abbas A., Fathifazl G., Fournier B., Isgor O.B., Zavadil R., Razaqpur A.G., Foo S., “Quantification of the residual mortar content in recycled concrete aggregates by image analysis”, *Material Characterization* 60 (2009), 716-728.
- Abd Elhakam A., Mohamed A., and Awad E., (2012), “Influence of self-healing, mixing method and adding silica fume on mechanical properties of recycled aggregates concrete”, *Construction and Building Materials*, Volume 35, 421–427.
- ACPA (2009), “Recycling concrete pavement”, *American concrete pavement association*, Skokie, Illinois.
- Ajdukiewicz A., and Kliszczewicz A. (2002), “Influence of recycled aggregates on mechanical properties of HS/HPC”, *Cement and Concrete Composites*, Volume 24, Issue 2, 269–279.
- American Association of State Highway Officials (AASHO), (1962) “The AASHO road test, Highway Research Board of the NAS-NRC division of engineering and industrial research.” *Rep. 5, Special Rep. 61E, AASHO, Washington, D.C.*
- ASTM C 1760, (2012), Standard Test Method for Bulk Electrical Conductivity of Hardened Concrete.

ASTM C127, (2012), Standard Test Method for Density, Relative Density (Specific Gravity), and Absorption of Coarse Aggregate.

ASTM C138/C138M, (2012) Standard Test Method for Density (Unit Weight), Yield, and Air Content (Gravimetric) of Concrete.

ASTM C143/C143M, (2012), Standard Test Method for Slump of Hydraulic-Cement Concrete.

ASTM C157/C157M, (2008), Standard Test Method for Length Change of Hardened Hydraulic-Cement Mortar and Concrete.

ASTM C192 / C192M, (2013), Standard Practice for Making and Curing Concrete Test Specimens in the Laboratory.

ASTM C231/C231M, (2010), Standard Test Method for Air Content of Freshly Mixed Concrete by the Pressure Method.

ASTM C232/C232M, (2012), Standard Test Methods for Bleeding of Concrete.

ASTM C29/C29M, (2010), Standard Test Method for Bulk Density (“Unit Weight”) and Voids in Aggregate.

ASTM C33/C33M, (2013), Standard Specification for Concrete Aggregates.

ASTM C39/C39M, (2012), Standard Test Method for Compressive Strength of Cylindrical Concrete Specimens.

ASTM C469/C469M, (2010), Standard Test Method for Static Modulus of Elasticity and Poisson’s Ratio of Concrete in Compression.

ASTM C496/C496M, (2011), Standard Test Method for Splitting Tensile Strength of Cylindrical Concrete Specimens.

ASTM C535, (2012), Standard Test Method for Resistance to Degradation of Large-Size Coarse Aggregate by Abrasion and Impact in the Los Angeles Machine.

ASTM C642, (2006), Standard Test Method for Density, Absorption, and Voids in Hardened Concrete.

ASTM C666/C666M, (2003), (Reapproved 2008) Standard Test Method for Resistance of Concrete to Rapid Freezing and Thawing.

- ASTM C672 / C672M, (2012), Standard Test Method for Scaling Resistance of Concrete Surfaces Exposed to Deicing Chemicals.
- ASTM C78/C78M, (2010), Standard Test Method for Flexural Strength of Concrete (Using Simple Beam with Third-Point Loading).
- Bagragi N. K., Vidyahara H. S., and Ravandeh K., (1990), “Mix Design Procedure for Recycled Aggregate Concrete”, *Construction and Building Materials*, Vol 4, No 4, 188-193.
- Bhatti, M. A., and Stoner, J. W. (1998). “Nonlinear pavement distress model using dynamic vehicle loads.” *Journal of Computing in Civil Engineering*. 4(2), 71– 78.
- Building Code Requirements for Structural Concrete (ACI 318), (2011), An ACI Standard and Commentary Reported by ACI Committee 318.
- César Medina. C., Isabel S. R. M., and Frías. M., (2013), “Freeze-thaw durability of recycled concrete containing ceramic aggregate”, *Journal of Cleaner Production*, Volume 40, 151–160.
- Chatti, K., Lysmer, J., and Monismith, C. L. (1994). “Dynamic finite element analysis of jointed concrete pavements.” Transportation Research Record. 1449, *Transportation Research Board, Washington, D.C.*, 79–90.
- Cheng GY. (2005), “Experimental study on the basic performance of recycled aggregate concrete with different displacement ratio”, *Chinese Concrete Journal*, 11, 67–70 [only available in Chinese].
- Chini, A.R., Muszynski, L.C., and Hicks, J., (2003), “Determination of acceptance permeability characteristics for performance-related specifications for portland cement concrete”, final report submitted to Florida Department of Transportation, 116-118.
- Choi S., Won M., (2009), “Performance of continuously reinforced concrete pavement containing recycled concrete aggregate”, *GeoHunan international conference on new technologies in construction and rehabilitation of Portland cement concrete pavement and bridge deck pavement, ASCE*.
- Cuttel D., Snyder M., Vandenbossche J., Wade M., (1997), “Performance of rigid pavements containing recycled concrete aggregates”, *Transportation research record 1574, Transportation research board, Washington D.C.*

- Darestani M.Y., Thambiratnam D.P., Nataatmadja A., Baweja D., (2007), “Structural response of concrete pavement under moving truck loads”, *Journal of transportation engineering*, 133, 670-676.
- Darestani, M. Y., Thambiratnam, D. P., Baweja, D., and Nataatmadja, A. (2006a). “Dynamic response of concrete pavements under vehicular loads.” Proc., *IABSE Symp. Responding to Tomorrow’s Challenges in Structural Engineering, Budapest, Hungary*.
- Domingo-Cabo A., Lázaro C., López-Gayarre F., Serrano-López M. A., Serna P., and Castaño-Tabares J.O., (2009), “Creep and shrinkage of recycled aggregate concrete”, *Construction and Building Materials* 23, 2545–2553.
- Englesen C., Mehus J., Pade C., Saether D., (2005), “Carbon dioxide uptake in demolished and crushed concrete”, Project report 395-2005, *Norwegian building research Institute, Oslo, Norway*.
- Fathifazl G., Abbas A., Razaqpur A. G., Isgor O. B., Fournier B., and Foo S., (2009), “New mixture proportioning method for concrete made with coarse recycled concrete aggregate”, *Journal of Materials in Civil Engineering*, Vol 10, Issue 21, 601-611.
- Fathifazl. G., Razaqpur. A.G., Isgor. O. B., Abbas. A., Fournier. B., and Foo. S., (2011), “Creep and drying shrinkage characteristics of concrete produced with coarse recycled concrete aggregate”, *Cement and Concrete Composites*, 33, 1026–1037.
- Gabr A. R. and D.A. Cameron, (2012), “Properties of recycled concrete aggregate for unbound pavement construction”, *Journal of Materials in Civil Engineering*, 24, 754-764.
- Garber S., Rasmussen R., Cackler T., Taylor P., Harrington D., Fick G., Snyder M., Van Dam T., Lobo C., (2011), “A technology development plan for the use of recycled concrete aggregates in concrete paving mixtures”, *National Concrete Pavement Technology Center*.
- Gillespie T.D., Karamlhas, S. M., Cebon, D., Sayers, M. W., Nasim, M. A., Hansen, W., and Ehsan, N., (1993), “Effects of heavy vehicle characteristics on pavement response and performance, Final Report, Prepared for National Cooperative Highway Research Program”, *Transportation Research Board–National Research Council, The University of Michigan Transportation Research Institute, Ann Arbor, Mich.*

- Gillespie, T. D., Karamlhas, S. M., Cebon, D., Sayers, M. W., Nasim, M. A., Hansen, W., and Ehsan, N. (1993). "Effects of heavy vehicle characteristics on pavement response and performance." Final Rep., Prepared for National Cooperative Highway Research Program– *Transportation Research Board*–National Research Council, The Univ. of Michigan Transportation Research Institute, Ann Arbor, Mich.
- Gómez-Soberón J. M. V., (2002), "Porosity of recycled concrete with substitution of recycled concrete aggregate: An experimental study", *Cement and Concrete Research*, Volume 32, Issue 8, 1301-1311
- Goulias D.G., Kim H., Scharz C.W., (2011), "Evaluation of in situ pavement material properties and behavior through field instrumentation and load testing", *Journal of Transportation Engineering*, vol. 137, 466-473.
- Goulias D.G., Kim H., Scharz C.W., (2011), "Evaluation of in situ pavement material properties and behavior through field instrumentation and load testing", *Journal of Transportation Engineering, ASCE*, 137: 466-473.
- Hansen T.C., and Boegh E., (1985), "Elasticity and drying shrinkage of recycled aggregate concrete", *ACI Journal* 82(5), 648-652.
- Hansen. T.C., (1986), "Recycled aggregate and recycled aggregate concrete, second state of- the-art report, developments from 1945–1985". *Materials and Structures*, 19(3), 201–246.
- Hoffmann. C., Schubert. S., Leemann. A., and Motavalli. M., (2012), "Recycled concrete and mixed rubble as aggregates: Influence of variations in composition on the concrete properties and their use as structural material", *Construction and Building Materials*, 35, 701–709.
- Hu J., Wang Z., and Kim Y., (2013), "Feasibility study of using fine recycled concrete aggregate in producing self-consolidating concrete", *Journal of Sustainable Cement Based Materials*, Vol. 2, No. 1, 20-34.

- Hu MP. (2007), “Mechanical properties of concrete prepared with different recycled coarse aggregates replacement rate”. Chinese Concrete Journal, 2:52–4 [only available in Chinese].
- ICAR rheometer manual (2013), Germann Instrumens, Inc., www.germann.org.
- Immanuel S., Timm D.H., (2006), “Measured and theoretical pressures in base and subgrade layers under dynamic truck loading”, *Airfield and Highway Pavement Specialty Conference*, 155-166.
- Immanuel S., Timm D.H., (2006), “Measured and theoretical pressures in base and subgrade layers under dynamic truck loading”, *Airfield and Highway Pavement Specialty Conference*, 155-166.
- Izquierdo J. T., Rodrigues, L., and Rios, B. C., (1997), “Structural evaluation and analysis of instrumented in-service concrete pavements subjected to heavy dynamic loads” *Transportation Research Record. 1568, Transportation Research Board, Washington D.C.*, 24-34.
- Izquierdo, J. T., Rodrigues, L., and Rios, B. C. (1997). “Structural evaluation and analysis of instrumented in-service concrete pavements subjected to heavy dynamic loads.” *Transportation Research Record. 1568, Transportation Research Board, Washington D.C.*, 24–34.
- Kim H., and Bentz D., (2008), “Internal curing with crushed returned concrete aggregates for high performance concrete”. NRMCA concrete technology forum: Focus on sustainable development, Denver, United States, 1-12.
- Kim, S. M., Won, M. C., and McCullough, B. F. (2002). “Dynamic stress response of concrete pavements to moving tandem-axle loads.” *Transportation Research Record. 1809, Transportation Research Board, Washington D.C.*, 32–41.
- Kim. K., Shin. M., and Soowon Cha, (2013), “Combined effects of recycled aggregate and fly ash towards concrete sustainability”, *Construction and Building Materials*, Volume 48, Pages 499–507
- Kou SC, Poon, C.S., and Chan, D., (2007), “Influence of fly ash as cement replacement on the properties of recycled aggregate concrete”, *Journal of Materials in Civil Engineering*, 19(9), 709-717.
- Kou. S., Poon. C., and Wan. H., (2012), “Properties of concrete prepared with low-grade recycled aggregates”, *Construction and Building Materials*, 36, 881–889.

- Kou. S.C., and Poon. C.S., (2012), “Enhancing the durability properties of concrete prepared with coarse recycled aggregate”, *Construction and Building Materials*, Volume 35, 69-76.
- Kumara M. A. W., (2005), “Analysis and verification of stress and strains and their relationship to failure in concrete pavements under heavy vehicle simulator loading”, Ph.D. thesis, Graduate school of the University of Florida, p.96.
- Li. W., Xiao. J., Sun. Z., Kawashima. S., and Shah. S.P., (2012), “Interfacial transition zones in recycled aggregate concrete with different mixing approaches”, *Construction and Building Materials*, 35, 1045–1055.
- Limbachiya M. C., Leelaware, T., and Dhir R.K., (2000), “Use of recycled concrete aggregate in high-strength concrete”, *Materials and Structures*, 33(10), 574-580.
- Limbachiya M. C., Marrocchino E., and Koulouris A., (2007), “Chemical–mineralogical characterization of coarse recycled concrete aggregate”, *Waste Management*, 27, 201–208.
- Limbachiya. M., Seddik. M., and Ouchangur, Y., (2012), “Performance of Portland/silica fume cement concrete produced with recycled concrete aggregate”, *ACI Materials Journal*, 109 (1), 91-100.
- Liu C., Gazis, D., (1999), “Surface roughness effect on dynamic response of pavements”, *Journal of Transportation Engineering*, vol. 125(4), 332–337.
- Liu, C., and Gazis, D. (1999). “Surface roughness effect on dynamic response of pavements.” *Journal of Transportation engineering*, 125(4), 332–337.
- Mc Neil K., Kang T., (2012), “recycled concrete aggregate: a review”, *International Journal of Concrete Structures and Materials*, Vol. 7, 61-69.
- McIntyre. J., Spatari. S., and MacLean. H.L., (2009), “Energy and greenhouse gas emissions trade-offs of recycled concrete aggregate use in nonstructural concrete: A north American case study”, *Journal of Infrastructure Systems*, 15, 361-370.

- Mehta P. K. and Monteiro P. J. M. (2006), “Concrete, microstructure, properties, and materials, 3rd Edition”, McGraw-Hill.
- Missouri standard specifications for highway construction (1999), *Missouri Highways and Transportation Commission Jefferson City, Missouri, Section 1007, Aggregate for Base*, 582-586.
- Monismith C.L., Lysmer J., Sousa J., and Hedrick J.K., “Truck pavement interaction: requisite research”, (1988), University of California transportation center, *SAE technical paper series 48, Berkely*.
- Montgomery. D.C., (2001), “Design and analysis of experiments- 5th Edn”, *John Wiley and Sons*.
- Movassaghi R., (2006), “Durability of reinforced concrete incorporating recycled concrete aggregate (RCA)”, *A thesis presented to the University of Waterloo in fulfilment of the requirements for Master of Applied Science in mechanical engineering, University of Waterloo, Canada*, 115-119.
- Nagataki S., Gokce A., and Saeki T., (2000), “Effects of recycled aggregate characteristics on performance parameters of recycled aggregate concrete”, *Proceedings of Fifth CANMET/ACI International Conference on Durability of Concrete*, Barcelona, Spain, 51-71.
- Nassar, R. U. D., and Soroushian, P., (2012), “Use of milled waste glass in recycled aggregate concrete”, *Proceeding of the ICE Construction materials*, 165(5), 304-315.
- NCHRP synthesis 435, (2013), “ Recycled materials and byproducts in highway applications, volume 6, reclaimed asphalt pavement, recycled concrete aggregate, and construction demolition waste”, *Transportation research Board*.
- Nixon. P. J., (1978), “Recycled concrete as an aggregate for concrete—a review”, *Materials and Structures*, 11(5), 371–8.
- Olorunsogo. F. T., and Padayachee. N., (2002), “Performance of recycled aggregate concrete monitored by durability indexes”, *Cement and Concrete Research*, Volume 32, Issue 2, 179-185.

- Opare K., (2008), "Assessment of the coefficient of thermal expansion of Alabama concrete", *A thesis submitted to the graduate faculty of Auburn University in partial fulfilment of the requirements for the degree of Master of science, Alabama, USA.*
- Otsuki. N., Miyazato. S., and Yodsudjai. W., "Influence of Recycled Aggregate on Interfacial Transition Zone, Strength, Chloride Penetration and Carbonation of Concrete", *Journal of Materials in Civil Engineering*. 2003.15:443-451.
- Padmini. A.K., Ramamurthy.K. , Mathews. M.S., (2009), "Influence of parent concrete on the properties of recycled aggregate concrete", *Construction and Building Materials*, Volume 23, Issue 2, 829–836.
- Proceq (2013), Resipod Family Operating instructions, concrete durability testing, Proceq SA. www.proceq.com.
- Ravindrarajah S. R., and Tam C.T., (1985), "Properties of concrete made with crushed concrete as coarse aggregate". *Magazine of Concrete Research*, 37(130), 29–38.
- Research Report Cement Concrete and Aggregates Australia, Chloride Resistance of Concrete, (2009), 3-34. <http://www.concrete.net.au/publications/publication>.
- Richardson. A., Coventry. K., and Bacon. J., (2011), "Freeze/thaw durability of concrete with recycled demolition aggregate compared to virgin aggregate concrete", *Journal of Cleaner Production*, Volume 19, Issues 2–3, Pages 272–277.
- Ryu. J.S., (2002), "Improvement on strength and impermeability of recycled concrete made from crushed concrete coarse aggregate", *Journal of Materials science Letter* 21, 1565-1567.
- Sagoe-Crentsil k., Brown T., and Taylor A. H., (2001), "Performance of Concrete made with commercially produced coarse recycled concrete aggregate", *Cement and Concrete Research*, 31, 707-712.

- Salas A., Lange D., Roesler J., (2010), “Batching effects on properties of recycled aggregate concrete for airfield rigid pavements”, *FAA Technology Transfer Conference and Exposition*, Atlantic city, NJ, USA.
- Shayan. A., and Xu. A., (2003), “Performance and Properties of Structural Concrete Made with Recycled Concrete Aggregate”, *ACI Materials Journal*, V. 100, No. 5, 371-380.
- Shoukry, S. N., and Fahmy, M. R. (2002). “Optimization of concrete slab geometry for enhanced rigid pavement performance and service life.” *WVDOT Research Project No. 140, West Virginia Univ., Morgantown, W.V.*
- Sim J., and Park C., (2011), “Compressive strength and resistance to chloride ion penetration and carbonation of recycled aggregate concrete with varying amount of fly ash and fine recycled aggregate”, *Waste Management* 31, 2352–2360.
- Speare, P.R., Ben-Othman, B. (1993), “Recycled concrete coarse aggregates and their influence on durability”, *Concrete 2000; Economic and durable construction through excellence: Proceedings of the international conference held at the University of Dundee, Scotland, UK*, 419-432.
- Stoner J.W., Bhatti, M. A., Kim, S. S., Koo, J. K., Molinas-Vega, I., and Amhof, B., (1990), “Dynamic simulation methods for evaluating motor vehicle and roadway design and resolving policy issues”, *MIDWEST Transportation Center, U.S. Transportation System and Iowa Department of Transportation, Ames, Iowa*.
- Surya M., Rao K. V., and Lakshmy P., (2013), “Recycled aggregate concrete for transportation infrastructure”, *Procedia - Social and Behavioral Sciences*, V. 104, 1158–1167.
- Tabsh S. W., and Abdelfatah A. S., (2009), “Influence of recycled concrete aggregates on strength properties of concrete”, *Construction and Building Materials* 23, 1163–1167.

- Tam V. W. Y., and C.M. Tam, (2008), “Diversifying two-stage mixing approach (TSMA) for recycled aggregate concrete: TSMAs and TSMAsc”, *Construction and Building Materials*, 22, 2068–2077
- Tam V. W. Y., Gao X.F., and Tam C.M., (2005), “Microstructural analysis of recycled aggregate concrete produced from two-stage mixing approach”, *Cement and Concrete Research*, 35, 1195– 1203.
- Tam V. W. Y., Gao X.F., C.M. Tam, and Ng K.M., (2009), “Physio-chemical reactions in recycle aggregate concrete”, *Journal of Hazardous Materials*, 163, 823–828.
- Tam V. W. Y., Tam C.M., and Wang Y., (2007), “Optimization on proportion for recycled aggregate in concrete using two-stage mixing approach”, *Construction and Building Materials* 21, 1928–1939.
- Thomas. C., Setién. J., Polanco. J.A., Alaejos. P., and Sánchez de Juan. M., (2013), “Durability of recycled aggregate concrete”, *Construction and Building Materials*, Volume 40, 1054-1065.
- Topçu IB, and Sengel S. (2004), “Properties of concretes produced with waste concrete aggregate”, *Cement and Concrete Research*, 34(8), 1307–1312.
- United Nations General Assembly (1987) Report of the World Commission on Environment and Development: Our Common Future. Transmitted to the General Assembly as an Annex to document A/42/427 - Development and International Co-operation: Environment. Retrieved on: 2009-02-15.
- Volz J., Khayat K., Arezoumandi M., Drury J., Sadati S., Smith A., Steele A., (2014), “Recycled concrete aggregate (RCA) for infrastructural elements”, *Final report, prepared for Missouri Department of Transportation*, 69-72.
- Wolfe M. H., (2011), “Bond strength of high-volume fly ash concrete”, *a thesis presented to the faculty of the graduate school of the Missouri University Of Science And Technology in partial fulfillment of the requirements for the degree master of science in civil engineering., Missouri, USA*, 18-19.

- Xiao JZ, and Li JB. (2005), “Study on relationships between strength indexes of recycled concrete”.
Chinese Journal of Building Materials, 9(2):197–201 [only available in Chinese].
- Xiao. J., Li. W., Fan. Y., and Huang. X., (2012), “An overview of study on recycled aggregate concrete in China (1996–2011)”, *Construction and Building Materials*, 31, 364–383.
- Yong, P. C. and Teo, D.C.L., (2009), “Utilization of recycled aggregate as coarse aggregate in concrete”,
UNIMAS E-Journal of Civil Engineering, 1(1), 1-6.
- Zaghloul, S., and White, T. (1993). “Nonlinear dynamic analysis of concrete pavements.” *Proc. 5th Int. Conf. on Concrete Pavement Design and Rehabilitation, Purdue Univ.*, 277–292.
- Zhang W., Ingham J., (2010), “Using recycled concrete aggregate in New Zealand ready-mix concrete production”, *Journal of Materials in Civil Engineering, ASCE*, Vol 22, N0. 5.
- Zollinger, D. G., Tang, T., and Xin, D. (1994). “Saw cut depth considerations for jointed concrete pavement based on fracture mechanics analysis.” *Transportation Research Record. 1449, Transportation Research Board, Washington D.C.*, 91–100.